AN ABSTRACT OF THE DISSERTATION OF

Gregory Watson for the degree of Doctor of Philosophy in Molecular and Cellular Biology presented on June 8, 2015.

Title: The Response to Sulforaphane in Metastatic Prostate Cancer Cells.

Abstract approved:

_____

Emily Ho

Sulforaphane is an isothiocyanate derived from cruciferous vegetables and has been under investigation as a cancer chemopreventive agent for over two decades. The compound is well tolerated and has been shown to slow cancer progression in several different pre-clinical models of carcinogenesis, such as of the lung, breast and colon. Recent work has suggested that sulforaphane may also slow cancer growth and progression in a pre-clinical model of prostate carcinogenesis. Prostate cancer accounted for approximately 14% of all new cancer diagnoses in 2014, making it the most commonly diagnosed type of cancer. Developing sulforaphane as a cancer therapeutic agent could provide an inexpensive and safe new treatment option to delay prostate cancer onset and to reduce the number of new diagnoses for this

common cancer. In addition, gaining a mechanistic understanding of how sulforaphane slows prostate cancer progression could identify new protein targets for therapeutic development.

Previous work utilizing human prostate cancer cell lines has identified many proteins and signaling pathways that respond to sulforaphane and have subsequently been proposed as contributors to prostate cancer suppression by sulforaphane (i.e. mechanistic targets). However, a majority of previous investigations charactering the response to sulforaphane in prostate cancer cells utilize sulforaphane at concentrations above what any prostate cancer cell will experience *in vivo* and/or for treatment periods that are not consistent with what we know about sulforaphane pharmacokinetics, tissue distribution and elimination. There is therefore a critical need to characterize the response to sulforaphane in prostate cancer cells under conditions that adhere to *in vivo* concentration and pharmacokinetics if we are to understand how sulforaphane may slow prostate cancer progression. To address this issue we carried out a series of *in vitro* investigations under conditions to mimic an *in vivo* exposure and explored the potential contribution of two cellular processes on sulforaphane-mediated suppression, chromatin regulation and autophagy.

Previous research has suggested that sulforaphane stimulates the turnover of the chromatin-modifying enzymes class I histone deacetylase 3 and DNA-methyltransferases. These enzymes modify chromatin in protein complexes that include the enzymes that control histone methylation, suggesting that changes in histone deacetylase and DNA-methyltransferase protein levels may influence histone methylation levels. We therefore tested whether sulforaphane treatment leads to changes in global histone methylation levels. We found that sulforaphane leads to a transient decrease in histone H3 lysine 9 trimethylation levels, a mark that is controlled by the enzyme SUV39H1. Sulforaphane treatment led to posttranslational modification of SUV39H1 that coincided with its dissociation from chromatin. These novel findings suggest histone methylation may have a role in the cellular response to sulforaphane.

Several investigations have suggested that autophagy is involved in influencing the cellular response to sulforaphane in prostate cancer cells *in vitro* and *in vivo*; however, previous work has not specifically addressed autophagic flux. In addition, sulforaphane has been proposed to decrease the level of histone deacetylase 6 (HDAC6) and HDAC6 has recently be shown to be required for efficient autophagic flux in mouse embryonic fibroblasts. We therefore tested whether sulforaphane or HDAC6-inhibition decreases autophagic flux in prostate cancer cells. We found that sulforaphane stimulates autophagic flux in metastatic prostate cancer cells at high concentrations. An assessment of HDAC6-interacting proteins in LNCaP metastatic prostate cancer cells showed HDAC6 interacts with proteins associated with autophagy. However, HDAC6-inhibition with the small molecule tubacin did not influence autophagic flux, suggesting metastatic prostate cancer cells do not require HDAC6 activity for autophagy.

Changes in gene transcription in response to sulforaphane have been used to infer the outcome of sulforaphane treatment. However, sulforaphane can lead to a rapid decrease in global protein synthesis in some prostate cancer cell lines. This suggests that using gene transcription to infer the outcome of sulforaphane treatment may be misleading if transcripts are not efficiently translated into proteins. To address this issue we applied proteomics to directly assess the global protein profile of LNCaP cells in response to sulforaphane. We found that sulforaphane does not lead to a global remodeling of the proteome following sulforaphane treatment in this cell type. Proteomics did, however, identify proteins that have not previously been implicated in LNCaP cell maintenance (e.g. TRIAP1). We show that TRIAP1 influences LNCaP cell proliferation, and thus show that proteomics can be used to identify novel candidate therapeutic targets in metastatic prostate cancer cells.

The central findings from this dissertation work suggest that sulforaphane does not directly influence key outcomes (e.g. apoptosis, autophagy) that have been associated with sulforaphane treatment in metastatic prostate cancer cells

when treatment concentrations and exposure times are made to conform to *in vivo* sulforaphane pharmacokinetics. This is important in understanding how sulforaphane may lead to prostate cancer suppression because it suggests the involvement of important *in vivo* factors that mediate suppressive activity. Future *in vivo* work that builds off the results presented in this dissertation will be important for the further development of sulforaphane as a prostate cancer therapeutic agent.

The Response to Sulforaphane in Metastatic Prostate Cancer Cells

by

Gregory Watson

A DISSERTATION

submitted to

Oregon State University

in partial fulfillment of

the requirements for the

degree of

Doctor of Philosophy

Presented June 8, 2015

Commencement June 2015

Doctor of Philosophy dissertation of Gregory Watson presented on June 8,2015

APPROVED:

Major Professor, representing Molecular and Cellular Biology

Director of Molecular and Cellular Biology Program

Dean of the Graduate School

I understand that my thesis will become part of the permanent collection of Oregon State University libraries. My signature below authorizes release of my thesis to any reader upon request.

Gregory Watson, Author

ACKNOWLEDGEMENTS

I would like to thank my thesis advisor Dr. Emily Ho for allowing me to receive my doctoral training in her laboratory. I am grateful for her patience and the opportunity to gain an exposure to a wide variety of scientific ideas and techniques. I thank her for the opportunity to collaborate with others and I truly appreciate the freedom to explore my scientific ideas and hypotheses as I worked through my dissertation projects. I also value her support in career development through conference attendance and speaking opportunities that will serve me well in the future.

I would like to thank my thesis committee members, Dr. Rod Dashwood, Dr. Michael Freitag, Dr. Jean Hall, Dr. Siva Kolluri, and Dr. Dave Williams, for contributing to my work throughout my graduate career. Thank you for always making yourselves available to discuss my work and for offering advice and valuable criticism that improved my work and helped me grow as a scientist.

Thank you to the Ho Lab members for creating a great research environment. I would especially like to thank Dr. Carmen Wong for always taking time out of her schedule to evaluate and provide feedback on everything I have written over the last four years. I would also like to thank her for acting as a sounding board for ideas throughout my time in the Ho Lab. She made a large contribution to my success over the last several years.

I would like to acknowledge Dr. Samanthi Wickramasekara and Dr. Claudia Maier for their contribution to my dissertation work. I am very thankful that they were willing to collaborate on my dissertation projects and for taking the time to work with me and provide their expertise. Their support played a large role in advancing and completing all of my research.

Thank you to the faculty and staff of the Department of Biological and Population Health Science (formerly Nutrition) for creating a great place to work over the last few years. I would particularly like to thank Dr. Don Jump and Dr. Urszula Iwaniec for contributing to my growth over the last several years. Your

advice, insights and contributions regarding both scientific matters and professional development is greatly appreciated.

Last, but certainly not least, I would like to express my great appreciation for all the wonderful people in the Molecular and Cellular Biology Program. I've truly enjoyed my interaction with the faculty, staff and students associated with the MCB Program. I would particularly like to thank my rotation mentors, Dr. Ling Jin and Dr. Martin Schuster, and my coursework professors for providing a strong scientific foundation for me to build on throughout the rest of my career. I would also like to thank Dr. Barbara Taylor, the MCB Director for most of my graduate career, for her strong support over the past several years.

CONTRIBUTION OF AUTHORS

Chapter 1. Written by Gregory Watson. Laura Beaver, David Williams, Roderick Dashwood and Emily Ho evaluated and approved the final manuscript.

Chapter 2. Gregory Watson, Samanthi Wickramasekara, Zoraya Palomera-Sanchez, Chelsea Black, Claudia S Maier, David E Williams, Roderick H Dashwood and Emily Ho contributed to overall research design, evaluation and reporting. Gregory Watson designed, conducted or oversaw all experiments. Samanthi Wickramasekara generated the mass spectrometry data. Zoraya Palomera-Sanchez generated immunofluorescence images. Chelsea Black prepared samples for Western blot analysis.

Chapter 3. Gregory Watson, Samanthi Wickramasekara, Yufeng Fang, Zoraya Palomera-Sanchez, Claudia S Maier, David E Williams, Roderick H Dashwood, Viviana I Perez and Emily Ho contributed to overall research design, evaluation and reporting. Gregory Watson designed, conducted or oversaw all experiments. Yufeng Fang generated confocal images.

Chapter 4. Gregory Watson, Samanthi Wickramasekara, Yufeng Fang, Claudia S Maier, David E Williams, Roderick H Dashwood, Viviana I Perez and Emily Ho contributed to overall research design, evaluation and reporting. Gregory Watson designed, conducted or oversaw all experiments. Samanthi Wickramasekara generated the mass spectrometry data. Yufeng Fang generated confocal images.

Chapter 5. Gregory Watson, Samanthi Wickramasekara, Claudia S Maier, David E Williams, Roderick H Dashwood and Emily Ho contributed to overall research design, evaluation and reporting. Gregory Watson designed, conducted or

oversaw all experiments. Samanthi Wickramasekara generated the mass spectrometry data.

Chapter 6. Written by Gregory Watson.

TABLE OF CONTENTS

TABLE OF CONTENTS (Continued)

TABLE OF CONTENTS (Continued)

TABLE OF CONTENTS (Continued)

TABLE OF CONTENTS (Continued)

TABLE OF CONTENTS (Continued)

LIST OF FIGURES

LIST OF FIGURES (Continued)

LIST OF FIGURES (Continued)

LIST OF TABLES

Page

Chapter 1

Introduction: Phytochemicals from cruciferous vegetables, epigenetics, and prostate cancer prevention

Gregory Watson, Laura Beaver, David Williams, Roderick Dashwood, Emily Ho

Published in The AAPS Journal

Spring Street 233

New York, NY 10013

USA

Issue 4 October 2013

Watson, Gregory W., et al. "Phytochemicals from cruciferous vegetables, epigenetics, and prostate cancer prevention." *The AAPS journal* 15.4 (2013): 951-961.

1.1 Abstract

Epidemiological evidence has demonstrated a reduced risk of prostate cancer associated with cruciferous vegetable intake. Follow-up studies have attributed this protective activity to the metabolic products of glucosinolates, a class of secondary metabolites produced by crucifers. The metabolic products of glucoraphanin and glucobrassicin, sulforaphane and indole-3-carbinol respectively, have been the subject of intense investigation by cancer researchers. Sulforaphane and indole-3-carbinol inhibit prostate cancer by both blocking initiation and suppressing prostate cancer progression *in vitro* and *in vivo*. Research has largely focused on the anti-initiation and cytoprotective effects of sulforaphane and indole-3-carbinol through induction of Phase I and Phase II detoxification pathways. With regards to suppressive activity, research has focused on the ability of sulforaphane and indole-3-carbinol to antagonize cell signaling pathways known to be dysregulated in prostate cancer. More recent investigations have characterized the ability of sulforaphane and indole-3-carbinol derivatives to modulate the activity of enzymes controlling the epigenetic status of prostate cancer cells. In this review we will summarize the well-established, “classic” non-epigenetic targets of sulforaphane and indole-3-carbinol, and highlight more recent evidence supporting these phytochemicals as epigenetic modulators for prostate cancer chemoprevention.

1.2 Introduction

Global cancer diagnoses are predicted to increase for the foreseeable future, with a key contributor being an aging world population. Although age is a strong risk factor for cancer, many other variables also influence the relative risk of disease development. Lifestyle and dietary choices are two factors that have a prominent role in cancer risk; however, given the combination of individual genetic variation and variability in lifestyle and dietary choices, it is extremely difficult to identify discrete factors that have a consequential role in disease risk.

Population-wide study of individuals whose characteristics vary can provide correlative data that can then be used to develop testable hypotheses. This strategy has proven useful in identifying dietary components associated with decreased cancer risk. A growing number of epidemiological studies have drawn an association between cruciferous vegetable intake and decreased prostate cancer risk (1, 2). Further epidemiological analysis stratifying specifically on glucosinolate intake (a class of natural compounds produced by crucifers) identified a significant inverse trend with prostate cancer risk (3). Controlled experimentation with glucosinolate derivatives, such as sulforaphane and indole-3-carbinol (I3C), has characterized inhibitory and cytotoxic activity in prostate cancer cells and animal model systems and has provided a mechanistic explanation for how crucifers are causative in lowering cancer risk.

Prostate cancer is the second most commonly diagnosed cancer in men worldwide. However, clinical prostate cancer incidence by nation shows considerable variability. In general, Western nations tend to have a high incidence of prostate cancer, while Asian nations are characterized by a low incidence. In the United States, prostate cancer is predicted to account for 28.5% of all male cancer diagnoses in 2012, affecting over 240,000 men (154 per 100,000) (4), whereas the rate in Asian nations can be up to ten fold lower (5). Diet and lifestyle are thought to be primary contributors to the difference in prostate cancer rates between Western and Asian nations. The proposed influence of diet on prostate cancer rate is supported by studies showing convergence with Western prostate cancer rates in Asian immigrant communities in the United States (6, 7). With regard to cruciferous vegetable intake, Asian nations tend to consume much higher amounts per person than Western nations (8), suggesting crucifer intake may be an important diet and lifestyle factor contributing to differences in prostate cancer risk.

The cruciferous vegetable family (Brassicaceae) includes many vegetables that are found in the diet – from broccoli, Brussels sprouts, and

cauliflower, that are common in the Western diet, to daikon, watercress, and bok choy that are more common in Asian cuisine. Cruciferous vegetables contain a number of glucosinolates whose presence and relative abundance are specific to each species and even to specific cultivars (9). Glucosinolates are the natural plant chemicals (phytochemicals) that give rise to bioactive species. They are cleaved by the endogenous plant enzyme myrosinase to yield active phytochemicals that possess varying degrees of anti-cancer activity. Two phytochemicals that have drawn a significant amount of attention are sulforaphane and I3C. In this review, we will highlight the ability of these phytochemicals to inhibit prostate cancer, focusing on their post-initiation suppressive activity. Finally, we will discuss more recent data characterizing activity as epigenetic modulators.

1.3 Metabolism and Bioactivity of Sulforaphane and Indole-3-Carbinol

Following consumption, glucosinolates are cleaved by plant-derived myrosinase when the plant wall is disrupted by chewing, and, to a lesser extent, by gut microbial myrosinases to release sulforaphane and I3C from their precursors. Sulforaphane and I3C then undergo further post-consumption modification, with sulforaphane undergoing enzymatic metabolism via the mercapturic acid pathway, and I3C undergoing spontaneous self-condensation and polymerization in the gut and possibly in the plasma (Figure 1.1). It is the post-consumption products of these glucosinolates that possess anti-cancer activity. Experimentation has demonstrated multi-targeted inhibitory effects that both block cancer formation and suppress prostate cancer growth.

1.3.1 Sulforaphane

Sulforaphane and its metabolites are the principal bioactive phytochemicals derived from broccoli and broccoli sprouts. Sulforaphane is present as the glucosinolate glucoraphanin in cruciferous vegetables.

Glucoraphanin is cleaved by the endogenous plant enzyme myrosinase into sulforaphane and glucose when the enzyme and glucosinolate are brought into contact (Figure 1.1A). Once released, sulforaphane is available for uptake in the human gut. Sulforaphane is then metabolized through the mercapturic acid pathway, producing several metabolic products (Figure 1.1B).

Human feeding studies have determined the absorption and kinetics of sulforaphane metabolism *in vivo*. Sulforaphane is rapidly taken up and metabolized by the body, reaching a plasma concentration peak within ~ 2 hours of consumption (10). Absorption and kinetics in animal models is consistent with the human data; both human and animal feeding studies have shown clearance of sulforaphane and its metabolites from the plasma within 24 hours of ingestion, and evidence in animal models suggests tissue accumulation may be possible following repeated ingestion (10-12).

Although post-consumption sulforaphane levels in human prostate tissue have not yet been evaluated, there are several lines of evidence that suggest sulforaphane does reach the prostate and causes changes in cellular processes. Work in rodent models has demonstrated that sulforaphane and its metabolites reach prostate tissue after oral administration. Clarke *et al.* showed the presence of sulforaphane metabolites in the prostates of mice 2 and 6 hours after ingesting 20 µmol sulforaphane (13). Similarly, Veeranki *et al.* showed an increase in sulforaphane metabolites in rat prostate tissue 1.5 hours after ingesting 150 µmol/kg sulforaphane (12). In both the transgenic adenocarcinoma of mouse prostate (TRAMP) mouse model (transformed prostate tissue) and a prostate specific PTEN deletion mouse model, broccoli sprout or sulforaphane treatment caused prostate specific changes in gene expression, suggesting sulforaphane or its metabolites reach the prostate (14-16). In the TRAMP model, supplementation with broccoli sprouts stimulated nuclear factor E2-related factor 2 (nrf2) controlled gene expression and decreased Akt signaling in prostate

tissue, whereas in the PTEN deletion model sulforaphane treatment reversed gene expression changes caused by PTEN loss in the prostate.

Importantly, oral administration of broccoli sprouts and sulforaphane inhibited prostate tumor progression in the TRAMP and PTEN-null mouse models, demonstrating the therapeutic potential of the natural product sulforaphane in the prostate. These mouse models are currently the closest simulation of human prostate cancer progression and provide strong pre-clinical evidence of sulforaphane bioactivity against prostate cancer progression.

In one human feeding study, men with high grade prostatic intraepithelial neoplasia (PIN), a pre-cancerous condition characterized by foci of abnormal prostate epithelial cell proliferation, supplemented their diets with broccoli or peas for twelve months and then submitted prostate tissue samples for analysis during routine tissue biopsy (16). The analysis found changes in gene expression related to TGFβ, insulin signaling, and EGF signaling, suggesting broccoli (*i.e.* sulforaphane) supplementation can affect signaling pathways related to cell growth in prostate tissue. Further work in human subjects quantifying sulforaphane metabolite levels in the prostate after acute versus long term exposure will help guide both dietary recommendations and the development of sulforaphane as a natural agent for prostate health.

1.3.2 Indole-3-Carbinol

I3C is released from its glucosinolate precursor glucobrassicin when brought into contact with myrosinase. Like glucoraphanin, glucobrassicin is found in cruciferous vegetables, with exceptionally high concentrations in Brussels sprouts and garden cress. In an acidic environment like the human stomach, I3C is rapidly converted into an array of acid condensation products and modified derivatives (17).

In vivo assessment of I3C and its products suggest that diindolylmethane (DIM), an I3C acid-condensation product, is one of the major bioactive

compounds responsible for the benefits associated with I3C. I3C undergoes condensation and modification after oral administration in mice, with the parent compound undetectable in plasma within one hour (18). A separate human feeding study did not detect I3C in the plasma of study participants administered the pure indole, but instead detected only DIM (19). Because DIM was the only acid condensation product detected in human plasma after oral administration of I3C, these data support the dimer DIM as the key mediator of prostate protection.

It is important to note that *in vitro* and *in vivo* studies have shown an anti-cancer effect associated with I3C. These studies utilize pure I3C as the treatment compound *in vitro* by dosing cultured prostate cancer cell lines, or *in vivo* by direct injection (20). Relatively few of these investigations assess the post-treatment derivatives of I3C, making it difficult to determine whether treatment effects are in response to I3C or specific condensation products. One study has found significant spontaneous conversion of I3C to DIM in culture media and simulated peritoneal fluid (21), which supports a model where I3C is converted to DIM or other condensation products after *in vitro* dosing or intraperitoneal (IP) administration. Our discussion will therefore focus on the mechanisms through which DIM may block or suppress prostate cancer. Discussion involving purified I3C as treatment will also be presented, but we will be working under the assumption that it is converted to DIM [For further reading supporting I3C conversion see Bradlow Review (22)].

In vivo work in mouse models supports DIM as an inhibitor of prostate cancer progression. Dietary supplementation of DIM significantly inhibited the progression of prostate cancer in the TRAMP model (23). DIM decreased tumor growth (as measured by genitourinary weight), decreased proliferating cell markers, and increased cell death effectors. The authors also note that DIM supplementation had no significant effect on cell markers in normal mice. Though DIM supplementation did not lead to complete eradication of transformed

cells and prostate tumors in the TRAMP model, there is clear evidence that dietary intervention with the natural product DIM is a strategy worth pursuing.

1.3.3 Application of *in vitro* and *in vivo* Exposure to Dietary Intake

Pharmacokinetic studies suggest peak plasma concentrations of sulforaphane and DIM may be below those achieved in controlled pre-clinical experiments. Plasma sulforaphane level reached over 7 μM in subjects eating "SuperBroccoli" soup (24), and a Phase I clinical dose escalation study found DIM to reach levels just over 1 μM in men supplemented with 300 mg of an enhanced-bioavailability formulation of DIM (BR-DIM) (25). Neither study suggests these are maximum achievable plasma concentrations, and no (or very limited) adverse effects were noted, suggesting higher plasma levels are reachable and tolerable. The effects of long term, low-level dietary exposure are not as well understood, but there is some evidence of tissue-specific sulforaphane accumulation over time in rats (12). In humans, few studies have characterized bioavailability and concentrations of sulforaphane, DIM, or their metabolites in tissues. Further work characterizing tissue specific acute versus repeated exposure is needed to fully understand the effects of these phytochemicals when attained from the diet.

1.4 Chemoprevention mechanisms

1.4.1 Pre-Initiation Blocking Activity

1.4.1.1 Sulforaphane

Sulforaphane has been extensively investigated as a cancer blocking agent due its ability to induce Phase II enzymes (26, 27). The expression of these enzymes is controlled by transcription factor nrf2. Under basal conditions, nrf2 is sequestered in the cytoplasm by redox-sensitive protein Kelch-like ECH-associated protein 1 (KEAP1). However, under redox stress, KEAP1 releases nrf2 which then translocates to the nucleus and binds antioxidant response

elements (ARE) in the promoters of target genes, stimulating their expression. Up-regulation of Phase II enzymes, such as heme oxygenase I (HO-1) or NADPH quinone oxidoreductase 1 (NQO1), greatly increases a cell's detoxification capacity. Phase II enzymes conjugate moieties to reactive molecules, thus decreasing their ability to cause cellular damage and enhancing their solubility for excretion. Sulforaphane is a strong glutathione-S-transferase (GST) inducer, which conjugates glutathione to electrophiles and neutralizes their reactivity. The first step in sulforaphane metabolism also involves glutathione conjugation, followed by enzymatic reactions in the mercapturic acid pathway (Figure 1.1B). For more thorough reviews of sulforaphane and Phase II blocking activity see Fahey and Talalay (27), and Guerrero-Beltran et al (28).

1.4.1.2 Indole-3-Carbinol

DIM can also be considered a prostate cancer blocking agent through its ability to stimulate cellular detoxification pathways. DIM is a reported aryl-hydrocarbon receptor (Ahr) agonist in multiple cell lines (29). Ahr is a nuclear receptor transcription factor that stimulates the expression of detoxification enzymes in the cytochrome P450 (CYP) family (Phase I) and increases the capacity of cells to deal with xenobiotic stress. DIM treatment also stimulates the nrf2 mediated Phase II response, which enhances reactive molecule metabolism and excretion of genotoxic agents (29-31). Through the activation of Ahr and nrf2 signaling pathways, DIM effectively increases the cells detoxification potential and blocks what otherwise could be tumor initiating events.

An ancillary benefit to enhanced Phase I expression also seems to be changes in steroid hormone profile (32). Because hormones are extensively processed and modified through oxidation / reduction reactions, changes in Phase I enzyme levels could alter hormone profiles. Sex hormones have a large role in prostate cancer progression and have been found to be altered with I3C or DIM supplementation in men and women (33-36). Hormone-sensitive prostate

cancer responds to estradiol (E2) *in vitro* (37), and I3C can reduce E2 levels in men (34). Though these studies have not yet looked at male hormones that drive hormone-sensitive prostate cancer, changes in estrogen hormone levels raises the possibility that male sex hormone levels are also altered and could therefore influence the growth of transformed cells early in the process of prostate cancer development.

1.4.2 Post-Initiation Suppressive Activity

Aside from their blocking activity, sulforaphane and DIM are also able to suppress cancer growth post-initiation (Figure 1.2). This effect has been demonstrated in prostate cancer cell lines and in the TRAMP model. The ability to inhibit growth and stimulate apoptosis of transformed cells is suggestive that sulforaphane and DIM have activity outside of the Phase I / Phase II response. These findings are particularly interesting with respect to prostate cancer because a majority of men will develop hyperplasia and localized neoplasia as a natural part of the aging process. Any treatment that can keep these growths localized and inhibited could substantially decrease the number of advanced prostate cancer cases. Thus, sulforaphane and I3C effects outside the Phase I / Phase II response have been an area of great interest to prostate cancer researchers. Recent investigations have attributed suppressive activity to antagonism of signaling pathways known to be important for prostate cancer progression, such as the Akt signaling axis, as well as modulation of epigenetic enzymes, both of which contribute to growth arrest and induction of apoptosis.

1.4.2.1 Sulforaphane

1.4.2.1.1 Attenuation of Akt / NFkB Signaling and Induction of Apoptosis

Enhanced Akt signaling is a common acquisition in transformed prostate tissue (38-40), and inhibiting the Akt signaling axis is potentially a good therapeutic target for suppressing prostate cancer growth and survival (41, 42).

Traka *et al.,* were able to show that Akt signaling was attenuated in prostate tissue of human subjects in response to long term dietary consumption of sulforaphane rich broccoli (15). Studies in animal models and cultured prostate cancer cells using purified sulforaphane have also shown attenuated Akt signaling. In the TRAMP mouse model, Keum *et al.* showed a decrease in Akt activation in transformed prostate tissue, while Traka *et al.* showed an attenuation of induced gene expression pursuant to the loss of the Akt suppressor PTEN (14, 15). *In vitro* analysis of PC3 prostate cancer cells treated with purified D,L-sulforaphane showed a decrease in Akt phosphorylation, decreased phosphorylation of mTOR target proteins, and a decrease in cellular protein translation (43), supporting a specific activity for sulforaphane in inhibiting the Akt signaling pathway.

Akt signaling is involved in many cellular processes (44-47) and could explain how sulforaphane treatment leads to decreases in the expression of multiple pathways known to support cancer growth. A decrease in NFkB transcriptional activity has been noted in prostate cancer cell lines in response to sulforaphane treatment (46, 48, 49). Sulforaphane caused the observed decrease by inhibiting NFkB translocation from the cytoplasm to the nucleus. Inhibition of the Akt signaling pathway could lead to sequestration of NFkB in the cytoplasm by decreasing mTOR complex activity and IKK activity (50), a signaling pathway delineated in PTEN null prostate cancer cells.

The net effect of decreased Akt / NFkB signaling could be to tip the cell fate scales toward apoptosis in prostate cancer cells. A decrease in NFkB-dependent inhibitor of apoptosis (IAP) proteins by sulforaphane may provide the stimulus for transformed cells to undergo intrinsic, mitochondrial mediated apoptosis (51-53). A decrease in IAP by antisense RNA is able to increase basal apoptosis in prostate cancer cells (54). The observation that mitochondria are necessary for at least a portion of sulforaphane induced cell death supports a model of stimulation of intrinsic apoptosis as an important process in prostate

cancer cell killing (55). Indeed, sulforaphane treatment *in vitro* and in the TRAMP model increases the Bax/Bcl-2 protein ratio and triggers a caspase cleavage cascade that results in cell death (56, 57).

Inhibition of Akt signaling and stimulation of growth arrest and apoptosis are two key sulforaphane effects in transformed prostate tissue. This is not to say that sulforaphane does not influence many other signaling pathways in prostate cancer cells. In fact, it is likely that other known sulforaphane effects contribute to suppression. For information detailing sulforaphane effects outside of those mentioned here, see Clarke *et al.,* (58) and Juge *et al.,* (59).

1.4.2.2 Indole-3-Carbinol

1.4.2.2.1 Induction of Apoptosis

Initial experiments investigating the potential of I3C to inhibit prostate cancer growth focused on controlled *in vitro* experimentation using the advanced prostate cancer cell line PC3 (60). I3C treatment led to cell cycle arrest and induction of apoptosis. I3C treatment was able to cause this inhibition by decreasing the expression / activity of pro-cell cycle progression kinase CDK6 and by upregulating the expression of cell cycle inhibitors p21 and p27 independent of p53 (Figure 1.2). Intrinsic apoptosis was triggered by a shift in Bax and Bcl2 expression toward a ratio favoring cell death, and was evidenced by PARP cleavage and DNA laddering. A decrease in NFkB activation was also noted (60). Further investigation using a range of representative androgen-dependent and independent prostate cancer cell lines (LNCaP, DU145, and PC3) confirmed a decrease in cell growth and induction of apoptosis in response to I3C and DIM treatment (61, 62); however, there are conflicting reports concerning the mechanism responsible for induction of apoptosis (63). Further work characterizing cell death in response to I3C and DIM at physiologically relevant doses will be necessary to understand how these phytochemicals inhibit prostate cancer growth *in vivo*.

1.4.2.2.2 Attenuation of Akt / NFkB Signaling

Subsequent studies in androgen-independent DU145 cells using equimolar I3C and DIM treatment characterized G1 cell cycle arrest and a decrease in Akt and PI3K proteins associated only with DIM treatment (64). DIM also decreases phophorylated (activated) Akt, as well as nuclear NFkB, NFkB DNA binding, and NFkB transcription activity (65-68). DIM may decrease Akt signaling by activating upstream regulator AMPK: a recent report showed DIM activated AMPK both *in vitro* and *in vivo* and was associated with mTOR and androgen receptor (AR) inhibition (Figure 1.2) (69).

1.4.2.2.3 Inhibition of Androgen Receptor Signaling

A comparison of prostate cancer cell I3C/DIM sensitivity between studies and within studies utilizing different prostate cancer cell lines has shown decreased sensitivity of more advanced, AR negative PC3 cells, and, importantly, prostate cancer cells seem to be much more sensitive to DIM treatment than non-transformed cells (68). DIM may specifically interfere with prostate cancer growth at the initial stages by suppressing the androgen signaling pathway (70), which would explain increased sensitivity of AR positive cancers. DIM treatment decreased AR controlled gene expression in prostate cancer cells *in vitro* by inhibiting translocation of AR to the nucleus (70). Bhuiyan *et al.,* also found decreased androgen signaling in response to DIM treatment, but showed this effect was the result of not only a failure of AR to translocate to the nucleus, but also due to a decrease in AR expression (65). This is an important inhibitory activity since hyperactive androgen receptor is one of the most common and early events in prostate cancer development.

1.4.3 Epigenetic Activity

Prostate cancer cells – and cancer cells in general – display epigenetic abnormalities that are thought to enhance the cancer phenotype. Transformed cells show global DNA hypomethylation, site specific DNA hypermethylation, altered cellular histone deacetylase (HDAC) activity, and altered miRNA expression (71, 72). Genes that inhibit cancer cell growth, such as cell cycle inhibitors or pro-apoptotic genes, are frequently silenced epigenetically. DNA methyltransferases (DNMTs) (enzymes that methylate DNA cytosine residues) and HDACs often work together in larger protein complexes to strip chromatin of active acetylation marks and lay down DNA methylation for stable gene repression. Targeting the enzymes that regulate the epigenetic signature of prostate cancer cells has proven to be a viable target in cancer prevention and cancer therapeutic research. Currently, there are several clinical trials aimed at determining the tolerance and efficacy of HDAC and DNMT inhibitors in human subjects (73). Importantly, sulforaphane and DIM have been characterized as diet-based modulators of epigenetic enzymes (Figure 1.3).

1.4.3.1 Sulforaphane

Sulforaphane metabolites sulforaphane-GSH and sulforaphane-Cys have been characterized as HDAC inhibitors (Figure 1.1) (74). HDAC overexpression is frequently observed in prostate cancer (75), and knockdown of HDAC enzymes with small RNAs leads to decreased cancer cell growth and alterations in the expression of genes associated with prostate cancer progression (76, 77). Treatment of prostate cancer cells with sulforaphane leads to a decrease in cellular HDAC activity and a global increase in histone acetylation (78, 79). Increases in histone acetylation also occur within the promoters of silenced tumor suppressor genes and are accompanied by increased gene expression. Tumor suppressor gene p21 is often silenced in prostate cancer cells. Treatment with sulforaphane leads to an increase in promoter acetylation and an increase in p21

expression. This effect was even observed in the p53 null prostate cancer cell line PC3 (80) and suggests epigenetic reactivation.

Sulforaphane also decreases DNMT protein levels in prostate cancer cells by decreasing DNMT1, 3a, and 3b gene expression (81). Hsu *et al.,* showed that the sulforaphane induced decrease in DNMT levels are associated with a global decrease in DNA methylation (81). A more targeted analysis of the cyclin D2 promoter, an epigenetically silenced gene in prostate cancer cells (82), showed a local decrease in DNA methylation associated with increased cyclin D2 transcript levels. Similar findings have recently been reported in breast cancer cells looking at the human telomerase reverse transcriptase (hTERT) gene (83). However, in this study the authors found a decrease in DNMT expression associated with a decrease in DNA methylation and, surprisingly, a decrease in hTERT gene expression. Demethylation, in this instance, appears to allow transcriptional repressors to recognize and bind DNA elements previously unavailable. It is likely that similar phenomena occur in sulforaphane treated prostate cancer cells and that the relationship between DNA methylation and gene expression in transformed tissue is more complicated than a simple inverse association.

Sulforaphane induced changes in chromatin modifications and gene expression play a large role in mediating its cytotoxic effects, but do not account for all its activity. HDAC enzymes also localize outside the nucleus, where they target non-histone proteins and participate in cellular processes beyond chromatin regulation. HDAC6 is a class II HDAC localized primarily in the cytoplasm. It is a critical regulator of the cytoskeletal network and also plays a role in chaperoning ubiquitin tagged proteins to the perinuclear aggresome for turnover (84). HDAC6 appears to be an important sulforaphane target given that overexpressing HDAC6 in PC3 prostate cancer cells can abrogate a sulforaphane induced decrease in cell viability (80).

HDAC6 is directly inhibited by sulforaphane (76), leading to increased tubulin acetylation and filament stabilization. In addition to decreasing tubulin dynamics (85), sulforaphane treatment leads to an increase in insoluble tubulin (86). Although these findings were investigated in breast and lung cancer cells, and in a cell free system, increased tubulin acetylation has been noted in prostate cancer cells treated with sulforaphane (76). Similar changes in tubulin dynamics and solubility are therefore likely to be occurring in prostate cancer cells. One report noted that sulforaphane can directly bind tubulin, but does not lead to the collapse of the microtubule network (87); however, a direct binding effect may be unlikely *in vivo* due to extremely rapid glutathione conjugation. Microtubule stabilization caused by HDAC6 inhibition may be the mechanism behind the anti-metastatic and cell cycle stress properties associated with sulforaphane (57, 88).

HDAC6 is also involved in AR and other nuclear receptor signaling pathways through its regulation of heat shock protein 90 (HSP90) acetylation. Deacetylation of HSP90 by HDAC6 releases AR, allowing it to translocate into the nucleus and modulate gene expression (89). Androgen signaling is a strong driver of prostate cancer growth and is initially hormone-dependent. But as prostate cancer progresses, androgen signaling becomes hormone independent, and thus clinicians lose a valuable target to suppress prostate cancer growth. HDAC6 is required for hormone independent nuclear localization in advanced prostate cancer, and HDAC6 inhibition or knock-down decreases AR signaling (89). A separate report showed that sulforaphane-mediated inhibition of HDAC6 leads to AR degradation and decreased androgen signaling (76). HDAC6 inhibition may be a good target in advanced prostate cancer that is no longer sensitive to anti-androgen therapy.

1.4.3.2 Indole-3-Carbinol

DIM has recently been shown to significantly decrease cellular HDAC activity in prostate cancer cell lines (90). DIM does not directly inhibit HDAC activity, but leads to a decrease in HDAC2 protein level. These findings are consistent with an earlier report in colon cancer cells detailing class I HDAC degradation in response to DIM (91).

DIM also alters the expression of other epigenetic modulators, including the enzymes controlling histone methylation and microRNAs. In a small group of prostate cancer patient samples, Kong *et al.,* found a correlation between decreasing Let family microRNA expression and increasing expression of histone methyltransferase EZH2 (92), a marker associated with poor prognosis (93, 94). Forced expression of Let 7 family members in prostate cancer cell lines decreased EZH2 expression and inhibited colony growth, demonstrating a causative link between Let 7 and EZH2 expression, and prostate cancer growth. An *in vivo* assessment of these findings from a prostate cancer study population supplemented with BR-DIM confirmed *in vitro* findings. Study participants supplemented with BR-DIM for two to four weeks showed increased Let 7 expression and decreased EZH2 expression. In a related study, this same group showed decreased microRNA miR-34a associated with increased AR expression and signaling (95). BR-DIM supplementation again led to modest re-expression of the silenced miR-34a and decreased AR expression *in vivo*. These are exciting findings in that they demonstrate *in vivo* DIM effects that inhibit cancer growth and reverse changes associated with prostate cancer progression and poor clinical outcomes. They also confirm *in vitro* experimental data and provide a foundation for understanding how DIM intake is associated with prostate cancer inhibition in humans.

1.5 Future Directions

The biologically active phytochemicals sulforaphane and DIM have well established suppressive activity *in vitro* and growing evidence supports activity inhibiting prostate cancer progression *in vivo*. A number of clinical trials are currently investigating these phytochemicals in prostate cancer cases to determine tolerance and efficacy utilizing an array of sources, including administration of purified sulforaphane, broccoli sprout extract pills, I3C-rich food, and BR-DIM (see www.clinicaltrials.gov). Study endpoints for on-going sulforaphane and BR-DIM investigations include quantitation and characterization of treatment metabolites in prostate tissue, a critical piece of data that will shape study design moving forward.

Despite their very different chemical structures, sulforaphane and DIM share some common targets and treatment endpoints. One explanation for this overlap is that both chemicals target cancer epigenetically: histone modifications, DNA methylation, and microRNA expression are dysregulated in cancer, and may explain why cancer cells are hypersensitive to sulforaphane and DIM treatment relative to normal tissue. Importantly, sulforaphane and DIM do not directly induce DNA damage or disrupt chromatin structure. The multiple, overlapping molecular targets suggest very broad effects governing cell homeostasis and genome stability.

Both phytochemicals alter cellular HDAC activity, and while sulforaphane decreases DNA methyltransferase activity, DIM alters microRNA and histone methyltransferase EZH2 expression *in vivo*. This last finding is an excellent demonstration of the connectivity and interrelationship between the different systems that regulate the epigenetic characteristics of cancer cells. Furthermore, these findings are likely the tip of the iceberg – a growing body of research consistently finds that the phytochemicals discussed here target an array of cancers arising from disparate tissues (96, 97). This again supports sulforaphane and DIM as working through an epigenetic mechanism, targeting

cancer cells no matter the underlying mutations that feed unregulated cell growth and survival.

Although the Phase I / Phase II induction and blocking activity associated with sulforaphane and I3C are not typically thought of as being under epigenetic control, a recent report has demonstrated the importance of epigenetics in the nrf2 response in transformed prostate cancer cells (98). Nrf2 expression is dampened in prostate cancer cells, and treatment with trichostatin A (TSA), a pharmaceutical HDAC inhibitor, removes epigenetic marks associated with gene silencing. The effect is particularly strong when used in combination with the DNMT inhibitor 5-aza-2'-deoxycytidine. Although these effects were shown with pharmacological compounds, sulforaphane and I3C may have a similar effect; a decrease in HDAC activity in combination with decreased DNMT activity in response to sulforaphane, accompanied by the innate ability of sulforaphane and / or I3C to induce the Phase I / Phase II response, could help explain why these natural products are strong inducers of the detoxification response in transformed prostate cancer cells. Combination therapies that exploit the coordinated activity of classic genetic targets and epigenetic regulators will be an important area of research going forward.

Future investigations into the effects of inhibition of HDAC and histone methyltransferase activity should focus on connecting changes in post-translational acetylation / methylation of non-histone proteins to changes in protein activity. The recent publication of the human "acetylome" and the identification of proteins and protein complexes sensitive to HDAC inhibitors identified many transcription factors and chromatin binding complexes as being affected by acetylation (99, 100). Altered transcription factor acetylation or chromatin associated protein complex stability could explain the vast changes in gene expression and signaling networks induced by sulforaphane and DIM treatment. Aside from changes in gene expression, miRNA expression in response to sulforaphane and DIM is largely unmapped in prostate cancer.

Global analyses of changes in miRNA profile, and subsequent work identifying specific functional RNAs responsive to sulforaphane or DIM, will provide further insight into how changes in the activity of chromatin modifiers and transcriptional profile contribute to prostate cancer inhibition. Moving forward, it will be imperative that we characterize these changes and their downstream effects in order to understand how sulforaphane and DIM lead to tumor suppression and identify potential new molecular targets for prostate cancer therapy.

1.6 Conclusions

The natural products sulforaphane and I3C inhibit prostate cancer through both blocking of tumor initiation and suppression of transformed cell growth. They effect tumor suppression by inhibiting signaling networks known to have a role in prostate cancer growth and by triggering cell cycle arrest and apoptosis. More recent work has characterized activity as epigenetic modulators in prostate cancer cells *in vitro* and *in vivo*. Further investigation into the anti-cancer activity of sulforaphane and I3C will give us a better understanding of how these natural products are associated with decreased prostate cancer risk and uncover new targets for therapeutic intervention.

1.7 Acknowledgements

Our work is funded by NIH grants CA90890, CA65525, CA122906, CA122959, and CA80176 and by National Institute of Environmental Health Sciences (NIEHS) Center grant P30 ES00210.

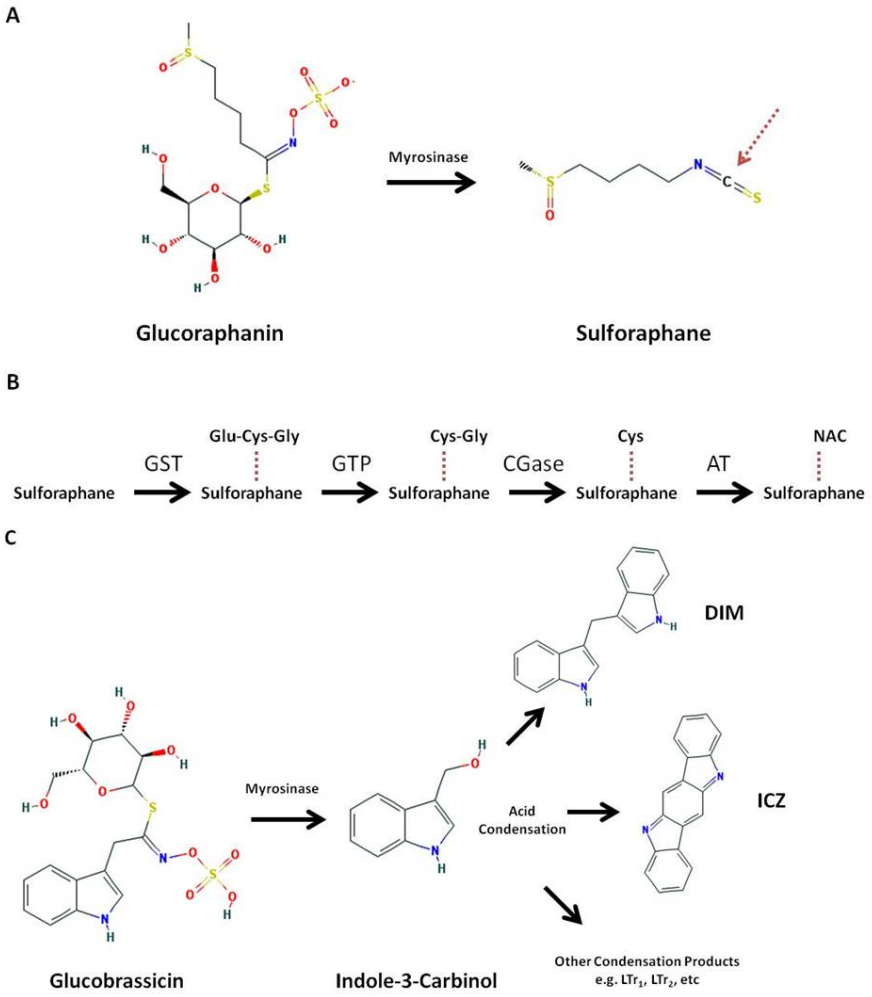

Figure 1.1. Metabolism of glucoraphanin and glucobrassicin to biologically active metabolites. (A) Sulforaphane is released from glucoraphanin by the plant enzyme myrosinase. Red dashed arrow marks the reactive carbon atom subject to glutathione conjugation. (B) Sulforaphane is metabolized via the mercapturic acid pathway into active metabolites. Glutathione-S-transferase (GST) first conjugates a GSH molecule (Glu-Cys-Gly) to the reactive carbon on sulforaphane. Glutamate is then removed by γ-glutamyltranspeptidase (GTP), followed by removal of the glycine residue by cysteinylglycinase (CGase). Cysteine is then acetylated by an acetyltransferase (AT) to sulforaphane-N-acetylcysteine, which is excreted in the urine. (C) Indole-3-carbinol is released from the glucosinolate glucobrassicin by myrosinase and undergoes spontaneous condensation in the acidic environment of the gut. Diindolylmethane (DIM) is the most abundant post-absorption acid condensation product. Acid condensation products can be modified further post-absorption. LTr_1: Linear trimer 1. LTr_2: Linear trimer 2. Structures from PubChem at National Center for Biotechnology Information (NCBI).

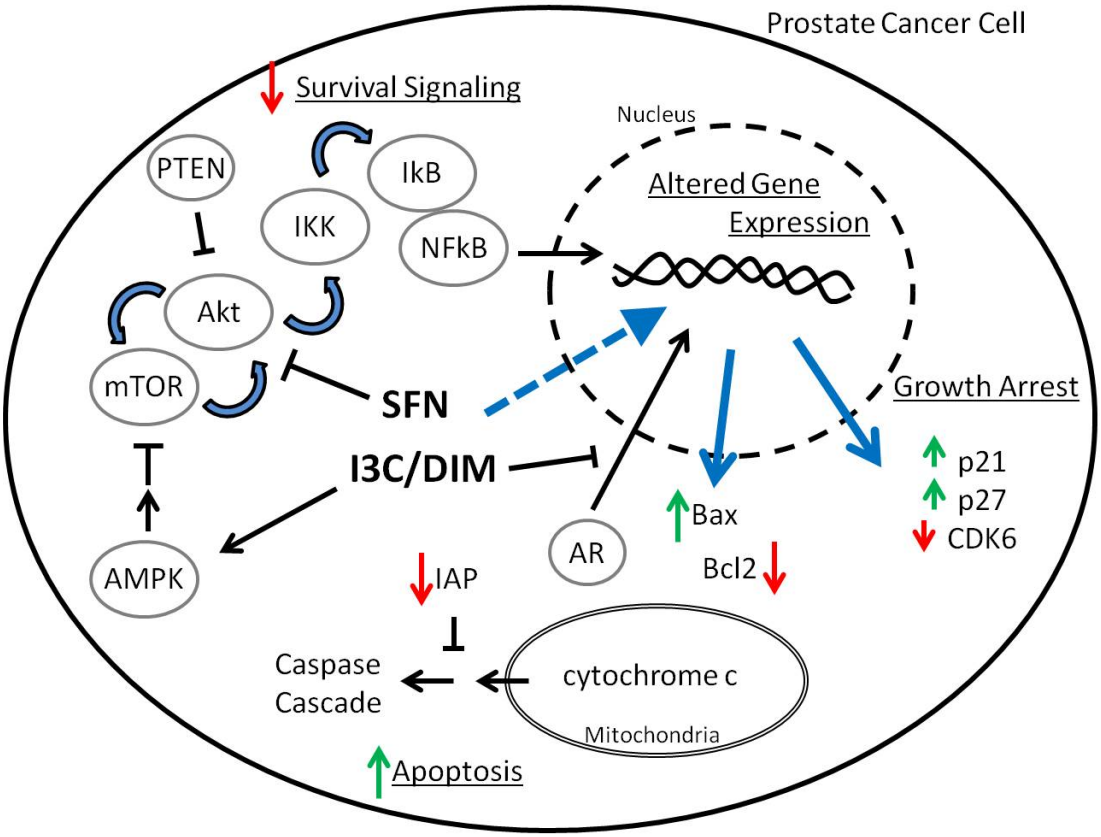

Figure 1.2. Selected non-epigenetic effects of sulforaphane and I3C/DIM on prostate cancer cells. Sulforaphane (SFN) and I3C/DIM inhibit the Akt signaling axis, a signaling pathway often hyperactive in prostate cancer. Inhibition of this pathway decreases pro-survival signaling by mTOR, Akt, and NFkB. Sulforaphane and I3C/DIM treatment also lead to changes in gene expression (blue arrow) that trigger growth arrest and apoptosis. The expression of proteins controlling the cell cycle (e.g. p21, p27, CDK6) are altered to effect growth arrest, and apoptosis is finally induced through the mitochondrial pathway. Abbreviations: AR – Androgen Receptor, CDK6 – cyclin dependant kinase 6, IAP – inhibitors of apoptosis.

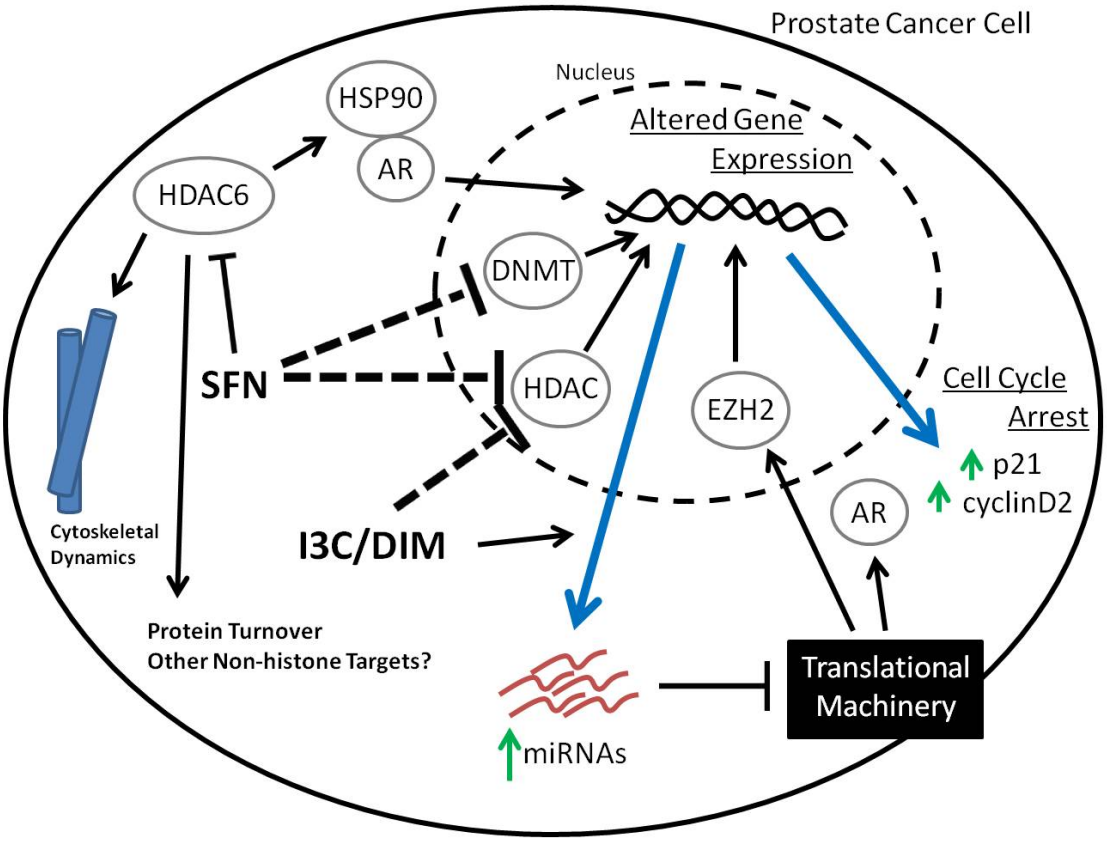

Figure 1.3. Sulforaphane and I3C/DIM suppress prostate cancer through epigenetic modulation. Sulforaphane (SFN) decreases cellular DNA methyltransferase (DNMT) and histone deacetylase (HDAC) activity, leading to altered chromatin structure and gene expression (blue arrow). Sulforaphane also directly inhibits cytoplasmic HDAC6, which controls the acetylation of many non-histone proteins, leading to a decrease in AR signaling, altered cytoskeletal dynamics, disrupted protein turnover, and, ultimately, increased cell stress. I3C/DIM also decreases cellular HDAC activity, leading to changes in gene expression (blue arrow). The expression levels of microRNAs (miRNAs) are also disrupted, and lead to changes in protein levels of chromatin associated protein EZH2 and nuclear receptor AR through post-transcriptional regulation.

Chapter 2

SUV39H1/H3K9me3 attenuates sulforaphane-induced apoptotic signaling in PC3 prostate cancer cells

Gregory Watson, Samanthi Wickramasekara, Zoraya Palomera-Sanchez, Chelsea Black, Claudia Maier, David Williams, Roderick Dashwood, Emily Ho

Published in Oncogenesis

Nature Publishing Group

75 Varick Street

9th Floor

New York, NY 10013-1917

USA

Volume 3 December 2014

Watson, G. W., et al. "SUV39H1/H3K9me3 attenuates sulforaphane-induced apoptotic signaling in PC3 prostate cancer cells." *Oncogenesis* 3.12 (2014): e131.

2.1 Abstract

The isothiocyanate sulforaphane is a promising molecule for development as a therapeutic agent for patients with metastatic prostate cancer. Sulforaphane induces apoptosis in advanced prostate cancer cells, slows disease progression *in vivo*, and is well tolerated at pharmacological doses. However, the underlying mechanism(s) responsible for cancer suppression remain to be fully elucidated. In this investigation we demonstrate that sulforaphane induces posttranslational modification of histone methyltransferase SUV39H1 in metastatic, androgen receptor-negative PC3 prostate cancer cells. Sulforaphane stimulates ubiquitination and acetylation of SUV39H1 within a C-terminal nuclear localization signal peptide motif and coincides with its dissociation from chromatin and a decrease in global H3K9me3 levels. Exogenous SUV39H1 expression leads to an increase in H3K9me3 and decreases sulforaphane-induced apoptotic signaling. SUV39H1 is thus identified as a novel mediator of sulforaphane cytotoxicity in PC3 cells. Our results also suggest SUV39H1 dynamics as a new therapeutic target in advanced prostate cancers.

2.2 Introduction

Prostate cancer is one of the most commonly diagnosed cancers in the United States, the incidence of which is expected to increase as the population ages. Several treatment strategies have been developed for prostate cancer therapy, including surgical removal of the prostate, radiation therapy, hormone or androgen deprivation therapy and chemotherapy. A majority of cases initially respond to front-line treatments; however, despite best efforts, resistant clones arise to resume growth and seed distal sites with metastatic tumors (1). Once this occurs, survival rates decrease dramatically and treatment options are limited.

Sulforaphane (1-isothiocyanato-4-methylsulfinylbutane) is an isothiocyanate derived from cruciferous vegetables that is known to possess

cancer-suppressive activity (2). The compound is well tolerated and is cytotoxic specifically toward transformed cells, inducing cell cycle arrest and apoptosis. Although differences in sensitivity between cell lines do exist, the tissue of origin or genetic profile does not appear to be determinant: sulforaphane is cytotoxic to many human cancer cell lines *in vitro*, including prostate (3), breast (4), ovarian (5,6), colon (7), and pancreatic cancers (8), and can suppress cancer progression in genetic models of colon (9) and prostate (10) carcinoma. Sulforaphane has been shown to (i) induce cell death in metastatic prostate cancer cell lines while sparing primary prostate epithelial cells (3), (ii) decrease metastases in a genetically engineered mouse model of prostate cancer (10), (iii) and is not associated with adverse effects when administered at pharmacological doses in rodents (11). These observations make sulforaphane a compound of interest for development as a prostate cancer therapeutic agent.

Several investigations have characterized broad alterations in the epigenome in prostate cancer patients and suggested that epigenetic profile and expression levels of chromatin modifying enzymes (CME) have some prognostic value (12-15). Progressive dysregulation of the epigenome as cells adopt a malignant phenotype is now recognized as an active contributor to transformation that works in tandem with genetic alterations to allow cancer progression. Because epigenetic state is reversible, targeting the epigenome is an attractive therapeutic strategy. Indeed, a number of small molecule inhibitors targeting CMEs are approved or are in clinical and preclinical trials as chemotherapeutic agents (16). Recent investigations characterizing sulforaphane-induced changes in the level and activity of CMEs has led to the hypothesis that modulation of these enzymes contributes to cell cycle arrest and apoptosis in prostate cancer cells. Sulforaphane leads to a decrease in global histone deacetylase (HDAC) activity in prostate cancer cells through depletion of specific HDAC isoforms (3). Sulforaphane has also been shown to decrease DNA-methyltransferase (DNMT) levels in prostate cancer cells (17). Little is known concerning the effects of

sulforaphane on histone methylation – only one investigation has characterized an influence on histone H3 lysine 27 trimethylation (H3K27me3)(ref. 18) – despite the fact that DNMT, HDAC, and histone methyltransferases (HMT) and demethylases (HDM) physically interact and work cooperatively in larger protein complexes to maintain or alter chromatin structure (19-21). Furthermore, any postulated heterochromatin-dependent contribution of HDAC or DNMT depletion is likely secondary to changes in histone methylation since DNMT functions downstream of HMTs, and HDAC enzymes lack protein domains that can independently recognize chromatin (22-24). This led us to investigate whether changes in global histone methylation accompany changes in CME protein level and activity in sulforaphane-treated prostate cancer cells. Because HDAC and DNMT enzymes facilitate heterochromatin formation and stabilization, and sulforaphane depletes these proteins in prostate cancer cells, we hypothesized a decrease in histone methyl-marks associated with heterochromatin in sulforaphane-treated prostate cancer cells.

Histone methylation is more complex than the chromatin marks controlled by HDAC (acetylation) and DNMT (DNA methylation) enzymes: As opposed to existing in one of two states, each with a characteristic association with chromatin structure, the outcome of histone methylation is residue and mark-specific (see Martin and Zhang and references therein for summary (25)). We focused our investigation on the archetypal heterochromatin mark trimethyl-histone H3 lysine 9 (H3K9me3), and conducted our mechanistic investigation in PC3 cells, a culture model of metastatic, aggressive, androgen receptor-negative prostate cancer. PC3 cells are an advantageous prostate cancer cell line to test our hypothesis because sulforaphane depletes HDAC (3) and DNMT (17) enzymes in these cells and the H3K9me3 mark is controlled by one HMT, SUV39H1, with no functional redundancy (26). Here we present evidence supporting a model where a decrease in H3K9me3 mediated by posttranslational regulation of SUV39H1 enhances apoptotic signaling in PC3 cells in response to

sulforaphane, suggesting indirect inhibition or destabilization of SUV39H1 as a potential treatment strategy.

2.3 Results

2.3.1 Sulforaphane decreases global trimethyl-H3K9 levels

Sulforaphane treatment leads to a global decrease in H3K9me3 in PC3 cells (Figure 2.1). The decrease was detectable as early as six hours post-treatment and remained at a depressed level through twelve hours. At twenty-four hours, H3K9me3 returned to control levels (not shown). An assessment of H3K9me3 level in sulforaphane-treated LNCaP and DU145 metastatic prostate cancer cell lines showed no global response (not shown).

Sulforaphane has previously been shown to induce G2/M arrest in PC3 cells (27), and H3K9me3 levels have recently been found to fluctuate with the cell cycle, increasing at the centromere through metaphase before reaching a peak and declining through anaphase (28). The global decrease in H3K9me3 we observed following sulforaphane treatment suggests that large blocks of chromatin, possibly megabases in length, are undergoing H3K9me3 depletion, which would be consistent with alterations in centromeric H3K9me3 levels. This raises the possibility that a global decrease in H3K9me3 in sulforaphane-treated cells is an artifact of cell-cycle arrest and not depletion of heterochromatic CMEs *per se*. Cyclin B1 protein level was therefore analyzed to assess the possibility of a cell-cycle effect. An analysis of cyclin B1 protein level (Figure 2.2), known to accumulate in metaphase arrested PC3 cells (29), showed no difference between treatment groups within our treatment period of interest, suggesting the decrease in H3K9me3 is independent of cell cycle and not a consequence of arrest. Visualization of DAPI stained sulforaphane-treated nuclei also indicated arrest prior to metaphase (not shown).

2.3.2 Sulforaphane does not affect the protein level of H3K9 methyl-modifiers

H3K9 methylation is controlled by multiple HMTs and HDMs, with several enzymes capable of catalyzing specific modifications. A decrease in global H3K9me3 levels could be caused by a decrease in HMT activity, an increase in HDM activity, or some combination of the two. SUV39H methyltransferase proteins (specifically isoform 1) control H3K9me3 at pericentromeric and centromeric chromatin domains (30), suggesting depletion or inactivation of SUV39H1 could account for the global decrease in H3K9me3 we observed by western blot. Furthermore, targeted knock-down of SUV39H1 by siRNA in PC3 cells leads to a global decrease in H3K9me3 and has a minimal effect on global gene expression (26), suggesting SUV39H1 is solely responsible for H3K9 trimethylation with little or no functional redundancy, and that SUV39H1-specific effects are independent of gene promoter regulation. We observed a transient increase in SUV39H1 in sulforaphane-treated cells and no change in SUV39H2 protein level over the treatment period (Figure 2.1).

HDM enzymes are a relatively recent discovery and less is known about their role in genome maintenance; we nevertheless assessed the protein level of several HDMs known to have activity toward H3K9 (ref. 31). No significant increase in the level of HDM LSD1 (KDM1A), JMJD1A (KDM3A), or JMJD2C (KDM4C) was maintained over the twelve hour treatment period (Figure 2.3).

No sustained change in the protein level of the enzymes that control H3K9 methylation suggests regulation through a posttranslational mechanism. We focused our investigation on SUV39H1 since it can influence global H3K9me3 and is known to physically interact with HDAC and DNMT enzymes (32, 33). We hypothesized an increase in posttranslational modifications associated with decreased SUV39H1 activity or stability in response to sulforaphane.

2.3.3 Sulforaphane leads to SUV39H1 posttranslational modification

SUV39H1 is known to be regulated posttranslationally: the protein is subject to phosphorylation (30), acetylation (34), ubiquitination (35) and methylation (36), all of which have been associated with changes in localization or decreased stability and activity. Discrete lysine residues on SUV39H1 have been characterized as subject to posttranslational modification. Acetylation of lysine 266 has been shown to inhibit catalytic activity (34), and ubiquitination of lysine 87 has been shown to facilitate degradation (35). We used liquid chromatography-coupled tandem mass spectrometry (LC-MS/MS) to assess sulforaphane-induced posttranslational modifications of endogenous SUV39H1 protein in PC3 cells (Figure 2.4, Figure 2.5). We identified ubiquitinated (ub-K393-SUV39H1) and acetylated SUV39H1 (ac-K394-SUV39H1) only in sulforaphane treated cells on an overlapping C-terminal peptide (379-MDSNFGLAGLPGSPKKRVR-397). Ubiquitinated SUV39H1 (ub-SUV39H1) was confirmed by immunoprecipitation (Figure 2.6). Increased ub-SUV39H1 occurred despite a global decrease in ubiquitinated proteins.

Sirtuin 1 (SirT1) is reported to control SUV39H1 ubiquitination and acetylation (34, 35), suggesting SUV39H1 modification may be the result of sulforaphane-induced changes in the protein level or activity of SirT1. Sulforaphane has been found to influence the protein level of some Sirtuins in colon cancer cells (37). We did not observe a hypothesized decrease in SirT1 protein level that would explain SUV39H1 destabilization or inhibition in sulforaphane-treated PC3 cells (Figure 2.7). A test of direct inhibition of SirT1 catalytic activity by the intracellular metabolites of sulforaphane at relevant intracellular concentration (3, 38, 39) also revealed no activity as a direct inhibitor (Figure 2.7). These data suggest SirT1-independent posttranslational control of SUV39H1 protein.

2.3.4 Sulforaphane leads to a decrease in chromatin-associated SUV39H1

The effects of lysine 393 or 394 modification are not known, but these residues fall within a predicted nuclear localization signal (NLS) peptide motif (391-SPKKRVRIE-399) (predicted by three independent motif recognition tools (40-42)) (Figure 2.8). This led us to hypothesize that modification of these residues would be associated with a change in SUV39H1 localization. Visualization by immunofluorescence revealed discrete nuclear foci characteristic of chromatin-associated SUV39H1. A separate pool of mobile SUV39H1 was also identified in the perinuclear cytoplasmic region and spread diffusely within the nucleus (Figure 2.9). Quantification by western blot showed an increase in cytoplasmic (or mobile) SUV39H1, and a decrease in nuclear (or immobile, histone associated) SUV39H1 in sulforaphane-treated cells (Figure 2.9).

2.3.5 Exogenous expression of SUV39H1 decreases sulforaphane-induced apoptotic signaling

SUV39H1 modification, altered localization, and decreased global H3K9me3 levels in sulforaphane-treated PC3 cells suggests that SUV39H1 and/or H3K9me3 depletion may have a role in sulforaphane-induced cytotoxicity (3, 43). To test whether SUV39H1 or global H3K9me3 contribute to sulforaphane-triggered apoptosis in PC3 cells, we overexpressed SUV39H1 by transient transfection to increase H3K9me3, then treated with sulforaphane and monitored cleaved poly-ADP ribose polymerase (cPARP) – a terminal cleavage event in apoptotic signaling – to assess changes in cytotoxicity (Figure 2.10, Figure 2.11). Exogenous SUV39H1 expression (SUV) increased global H3K9me3 levels relative to control (GFP), and sulforaphane did stimulate apoptotic signaling as measured by cPARP. We noted a decrease in cPARP in SUV39H1-overexpressing cells in response to sulforaphane relative to GFP-control, suggesting SUV39H1/H3K9me3 is protective against sulforaphane-

induced cytotoxicity and that a global decrease in H3K9me3 contributes to cell death in PC3 cells.

2.4 Discussion

In this investigation we characterized a novel response to the natural compound sulforaphane in PC3 prostate cancer cells involving the histone modifier SUV39H1. We present evidence supporting a model where sulforaphane-induced posttranslational modification of SUV39H1 decreases the chromatin-associated cellular fraction, leading to a decrease in H3K9me3 (Figure 2.1, 2 4, 2.6, 2.9). We go on to show that SUV39H1/H3K9me3 decreases apoptotic signaling in PC3 cells (Figure 2.10), suggesting the changes in SUV39H1 dynamics in sulforaphane-treated PC3 cells contributes to cytotoxicity. Taken together, these results suggest that posttranslational modification of SUV39H1 may be a promising therapeutic strategy in the treatment of advanced prostate cancer.

Perturbations in SUV39H1 protein level in normal cells is known to increase cancer risk: engineered mice that are SUV39H-null show an increased susceptibility to cancer (44), and mice that overexpress SUV39H1 show defects in cell differentiation and proliferation that can result in chronic myeloid leukemia (45). SUV39H1 can also influence metastatic potential in transformed cells: a potentially chromatin-independent role for SUV39H1 in facilitating cell motility and invasion has recently been characterized in hepatocellular carcinoma cells (46). SUV39H1 knock-down specifically in PC3 cells also supports a gene expression-independent role in cell proliferation (26). Chemotherapeutic strategies pursuing direct SUV39H1 inhibition are being investigated, though the *in vivo* activity of the leading candidate, chaetocin, is debatable (47-50). Our data suggests an alternative strategy for targeting SUV39H1 involving indirect destabilization or modulation of the posttranslational-modifiers that regulate SUV39H1, several of which have been characterized (34, 35). Small molecule

modulators are currently being tested that target such proteins (e.g. MDM2 inhibitors (51)), yet the contribution, if any, of SUV39H1-modification to the activity of these molecules is not known. Assessing this possible contribution will be important to gain a complete understanding of how and why such molecules are effective agents.

Although sulforaphane is known to induce cellular stress and general protein turnover through the ubiquitin-proteasome pathway (52) and induction of the autophagic pathway (53), the data presented here suggests that sulforaphane leads to directed SUV39H1 modification in PC3 cells. We observed an increase in ubiquitinated SUV39H1 despite a global decrease in ubiquitinated proteins in sulforaphane treated cells (Figure 2.6), suggesting controlled regulation as opposed to general turnover. We also noted no significant increase in SUV39H1 protein level in SUV39H1-overexpressing PC3 cells despite a global increase in H3K9me3 (Figure 2.10). The finding that global H3K9me3 levels are not affected in sulforaphane-treated LNCaP and DU145 cells also suggests directed regulation in response to sulforaphane in PC3 cells. Further work will be needed to identify the factors accounting for the differential response between cell lines and will be important in developing a genetic signature of the subset of advanced prostate cancers that would be susceptible to exploiting modulation of SUV39H1 dynamics to enhance apoptotic signaling.

An increase in global H3K9me3 levels in SUV39H1-transfected cells with no corresponding increase in SUV39H1 protein level (Figure 2.10) suggests SUV39H1 protein level is tightly regulated in PC3 cells through posttranslational control and that SUV39H1 dynamics are what determine global H3K9me3. Taken together with the shift in SUV39H1 pools from chromatin-associated to mobile in sulforaphane-treated cells (Figure 2.9), these data suggest a model where SUV39H1 rate-of-renewal at heterochromatic sites is the parameter affected by sulforaphane-induced modification. The increase in cytoplasmic (or mobile) SUV39H1 should therefore be interpreted as a delayed renewal time at

chromatin, which we propose to be a consequence of modification of a conserved NLS. An alternative hypothesis could propose decreased enzymatic activity through interference with conserved putative zinc-coordinating cysteines in the adjacent post-SET domain (Figure 2.8). Mutagenesis studies have shown these cysteines to be required for enzymatic activity in other post-SET domain-containing H3K9 methyltransferases (54). However, given the rather modest decrease in global H3K9me3 in sulforaphane-treated cells compared to catalytically-impaired SUV39H1 mutants (35, 55, 56), inhibition of SUV39H1 activity is less likely. This interpretation is also in agreement with a recent report by Park *et al* (57) where they characterized CDK2-dependent phosphorylation of SUV39H1 at lysine 391, a mark we identified in sulforaphane-treated PC3 lysate by mass spectrometry (Figure 2.4). Mutagenesis at lysine 391 to mimic phosphorylation did not alter enzymatic activity, but did influence occupancy at heterochromatin and led to a decrease in H3K9me3 at specific repeat elements. This supports our model proposing that modification of this region leads to decreased H3K9me3 through a shift from chromatin-associated to mobile SUV39H1 and not through impaired enzymatic activity.

This is the first investigation to characterize changes in SUV39H1/H3K9me3 in the response to sulforaphane in any cell type. Although SUV39H1 turnover rate and recovery time have been shown to have a significant impact on global H3K9me3 and genome stability (35), the impact in the context of sulforaphane treatment is not known. We found that increased H3K9me3 in SUV39H1-transfected cells associated with decreased apoptotic signaling (Figure 2.10), indicating that H3K9me3 is protective in sulforaphane-treated PC3 cells and suggesting that modulation of this methyl-mark and modifier actively contributes to sulforaphane cytotoxicity.

An important aspect of our investigation is the characterization of SUV39H1 modification within twelve hours of sulforaphane treatment. Sulforaphane is rapidly metabolized and excreted from the body (58, 59). Even

when administered intravenously at a pharmacological dose to achieve ~15 μM plasma concentration in a rat model, the majority of sulforaphane and its metabolites are cleared in less than twelve hours (11). Our treatment periods exist within the pharmacokinetic parameters of sulforaphane metabolism *in vivo*, suggesting our results may be achievable in a clinical setting.

Here, we implicated a new chromatin mark and CME in the cellular response to sulforaphane in PC3 prostate cancer cells. We propose a model where sulforaphane causes a decrease in H3K9me3 through posttranslational modification of H3K9 methyltransferase SUV39H1, and that this actively contributes to sulforaphane-induced apoptotic signaling. These findings suggest that targeting SUV39H1 dynamics to enhance cell death signaling may be a strategy worth exploring in treating advanced metastatic cancers.

2.5 Materials and Methods

2.5.1 Cells and Reagents

Prostate cancer cells (PC3 and LNCaP) were purchased from American Type Culture Collection (Manassas, VA, USA) or received as a gift (DU145 line from Dr. Philippe T. Georgel, Marshall University). Cells were maintained in RPMI-1640 media with L-glutamine supplemented with FBS (50 ml FBS / 500 ml media) at 37°C 5% CO_2. PC3 and LNCaP cell lines were validated by Idexx Radil (Columbia, MO, USA) on December 24, 2012. Sulforaphane was purchased from LKT Laboratories (St. Paul, MN, USA). Sulforaphane-glutathione and sulforaphane-cysteine were purchased from Toronto Research Chemicals (Toronto, ON, Canada). MG132 was purchased from Santa Cruz Biotechnology (Dallas, TX, USA). Primary antibodies against ubiquitin (Santa Cruz), SUV39H2 (Santa Cruz), SUV39H1 (Santa Cruz, Millipore [Billerica, MA, USA]), SirT1 (eBioscience, San Diego, CA, USA), β-actin (Sigma, Saint Louis, MO, USA), trimethyl histone H3 lysine 9 (Millipore), cleaved PARP (Cell Signaling, Danvers, MA, USA), cyclin B1 (Cell Signaling), fibrillarin (Cell Signaling), LSD1 (Abcam,

Cambridge, MA, USA), JMJD1A (Abcam), JMJD2C (Abcam), α-tubulin (Sigma) and histone H3 (Bethyl, Montgomery, TX, USA), and HRP-conjugated secondary antibodies (Santa Cruz) were used in accordance with the manufacturer's protocol. SirT1 Activity Assay was conducted in accordance with the manufacturer's protocol (Sigma). Sulforaphane-cysteine and sulforaphane-glutathione conjugates were produced in house. LC-MS grade solvents were purchased from Millipore. Subconfluent cells were treated with control [dimethyl sulfoxide (DMSO)], sulforaphane (15 μM), and/or MG132 (at the indicated dose) and incubated at 37°C 5% CO_2 until harvest.

2.5.2 Protein Analysis

Protein lysates were prepared in RIPA protein lysis buffer (150 mM NaCl, 1% Triton X-100, 0.5% NaDOC, 0.1% SDS, 20 mM Tris pH 8.0) supplemented with protease inhibitor cocktail (Thermo, Waltham, MA, USA) followed by sonication in an ice-cold waterbath. Lysates were cleared by centrifugation at 4°C and quantitated by DCA Protein Assay (BioRad, Hercules, CA, USA). For SUV39H1 localization, cells were incubated in 0.5% Triton X-100 PBS with protease inhibitor cocktail for 15 minutes on ice. Cells were then vortexed and nuclei spun out. Nuclei were washed in PBS and resuspended in RIPA lysis buffer and incubated on ice 10 minutes. Lysates were then subjected to sonication in an ice-cold waterbath.

Proteins were separated by SDS-PAGE and blotted to a PVDF membrane (BioRad) using NuPAGE Reagents and equipment in accordance with the manufacturer's protocols (Invitrogen, Carlsbad, CA, USA). Membranes were blocked and probed for proteins of interest following manufacturer's protocols. Membranes were incubated in SuperSignal West Femto Reagent (Thermo) and developed on the AlphaInnotech FluorChem 8900 system. Membranes were stripped using ReBlot Plus Strong Solution as needed in accordance with the manufacturer's protocol (Millipore). Densitometric analyses were performed on

the native membrane image using AlphaInnotech FluorChem 8900 software. For each membrane, the relative densitometric value of each replicate for a given probe was normalized to the corresponding relative level of the normalizing protein. For graphing, treatments are expressed relative to Control (set to the value 1). Proteins are normalized to β-actin unless otherwise indicated.

2.5.3 Immunoprecipitation

Lysates were prepared by one freeze-thaw in non-denaturing lysis buffer (137 mM NaCl, 1% Triton X-100, 2 mM EDTA, 20 mM Tris pH 8.0), cleared by centrifugation, and quantitated by DCA Protein Assay (BioRad). Equal protein lysate (2-3 mg) was incubated with primary antibody (anti-ubiquitin or anti-SUV39H1) overnight at 4°C, then with Protein A agarose (Sigma) or Protein A/G PLUS agarose (Santa Cruz) for 2-4 hours at 4°C. Immunoprecipitations were washed 3-5 times in non-denaturing lysis buffer and eluted in 2% SDS TBS at room temperature for 15 minutes.

2.5.4 Immunofluorescence

Immunofluorescence was carried out following standard protocols. Briefly, PC3 cells were grown and treated on glass coverslips. Cells were fixed in 100% methanol then in 4% paraformaldehyde. Fixed cells were permeabilized in 0.4% Triton X-100 PBS and blocked in 5% BSA 0.1% NP-40 PBS. Cells were probed with SUV39H1 antibody (Santa Cruz), followed by incubation in anti-rabbit Alexa Fluor-555 (Invitrogen), and finally with DAPI (Millipore). Coverslips were mounted on glass slides using ProLong Gold Antifade Reagent (Invitrogen) and images captured on a Nikon Eclipse E400 microscope using Nikon NIS-Elements software.

2.5.5 Mass Spectrometry

PC3 cells were washed twice in 50 mM sodium bicarbonate and subjected to one freeze-thaw at -80°C in 50 mM sodium bicarbonate. Liberated proteins were separated from cellular debris by centrifugation at 13,000 rpm for 10 minutes at 4°C. Proteins were reduced, alkylated and digested using Trypsin Gold in presence of ProteaseMax surfactant according to the manufacturer's protocols (Promega, Madison, WI, USA).

LC-MS/MS analysis was carried out using a nanoAcquity UPLC system (Waters Corporation, Milford, MA, USA) coupled to a LTQ-FT MS instrument (Thermo Fisher Scientific, San Jose, CA, USA). A binary solvent system consisting of solvent A (water with 0.1% formic acid) and solvent B (acetonitrile with 0.1 % formic acid) was used for the analyses. Tryptic peptides (2 µL) were loaded onto a peptide trapping column (Michrom Cap Trap, Bruker Daltonics Inc, Billerica, MA, USA) and separated using a C18 analytical column (Agilent Zorbax 300SB-C18, 250 x 0.3 mm, 5 µm). Peptides were trapped and washed with 3% solvent B for 3 min at a flow rate of 5 µL/min. Peptide separation was achieved using a linear gradient from 10% to 30% B at a flow rate of 4 µL/min over 102 min. The LTQ-FT mass spectrometer was controlled by Xcaliber 2.0 (Thermo Fisher Scientific, San Jose, CA, USA) and operated in data-dependent MS/MS acquisition (DDA) with MS precursor ion scan, performed in the ICR cell, from 350-2000 m/z. Instrument resolving power was set to 100,000 at m/z 400, and MS/MS scans were performed by the linear ion trap on the five most abundant doubly or triply charged precursor ions detected in the MS scan.

Thermo RAW data files were processed with Mascot database analysis software (v2.3) (Matrix Science, Boston, MA, USA) within Proteome Discoverer v1.4.0. Data files were searched against the Human protein RefSeq database downloaded from NCBI (http://www.ncbi.nlm.nih.gov/protein) and to an in-house database containing SUV39H1 protein sequence (NP_003164.1) and decoy protein sequences including common contaminants.

The following parameters were used to search the database: the digestion enzyme was set to Trypsin and three missed cleavage sites were allowed. The precursor ion mass tolerance was set to 20 ppm, and the fragment ion tolerance was set to 1.0 Dalton. Dynamic modifications that were considered included carbamidomethyl-cysteine (+57.02 Da), oxidated methionine (+15.99 Da), deamidated asparagine or glutamine (+0.98 Da), phospho-serine, -threonine, or -tyrosine (+97.98 Da), ubiquitinated lysine (+114.04 Da), methyl-lysine (+14.02), and acetyl-lysine (+42.01 Da). Automatic target decoy search with 1% false discovery rate (FDR) was included into the Mascot search. Scaffold_3.3.1 (Proteome Software, Portland, OR, USA) was used for search data compilation and data evaluation with an embedded X!Tandem database searching algorithm. Protein identifications were accepted if they could be established at greater than 90.0% probability and contained at least 2 identified peptides per protein with a FDR < 5%. Assigned spectra were inspected manually for quality. Spectra assigned to both databases (Human RefSeq and in-house DB) were manually assigned using custom python scripts and the best match selected.

2.5.6 Quantitative Real-Time PCR

Total RNA was harvested by TRIzol reagent in accordance with the manufacturer's protocol (Invitrogen). cDNA was prepared from 1 µg RNA using the SuperScript III kit from Invitrogen. Approximately 50 ng cDNA was amplified by Fast SYBR Green Reagent in accordance with the manufacturer's protocol (Invitrogen) on a 7900HT Real Time PCR Machine (Applied Biosciences).

Primers: GAPDH (sense 5'-CGAGATCCCTCCAAAATCAA-3', antisense 5'-TTCACACCCATGACGAACAT-3'); HO1 (sense 5'-CTTCTTCACCTTCCCCAAC-3', antisense 5'-GCTCTGGTCCTTGGTGTCATA-3'); SUV39H1 (sense 5'-GCTAGGCCCGAATGTCGTTA-3', antisense 5'-GCCTTCTGCACCAGGTAGTT-3')

2.5.7 SUV39H1 Cloning

SUV39H1 coding sequence was amplified from PC3 cDNA using primers to append a 5' EcoRI and 3' NotI restriction site (sense 5'-CTGCCGCCGAATTCCCCGAATGTCGTTAGCCGTGGGGAAAG-3', antisense 5'-ATCTGAGAGCGGCCGCCACGGCCACAGCCCTGAACG-3'). SUV39H1 coding sequence was digested and ligated into pCMV6-AC-GFP destination vector (Origene, Rockville, MD, USA). The ligation mixture was transformed into One Shot TOP10 Chemically Competent *E. coli* following the manufacturer's protocol (Invitrogen). Plasmid was isolated using the QIAprep Spin Miniprep Kit (Qiagen). Candidates were screened for insert using SUV39H1 primers (sense 5'-GCTAGGCCCGAATGTCGTTA-3', antisense 5'-GCCTTCTGCACCAGGTAGTT-3') and restriction digest fingerprinting. The final construct selected for PC3 transfection was validated by sequencing at the Center for Genome Research and Bioinformatics (CGRB) at Oregon State University (sense 5'-GCTAGGCCCGAATGTCGTTA-3', antisense 5'-GCCTTCTGCACCAGGTAGTT-3', antisense 5'-ATCTGAGAGCGGCCGCCACGGCCACAGCCCTGAACG-3'). The final construct was found to contain the SUV39H1 RefSeq coding sequence (NM_003173.3).

2.5.8 Transient Transfection of PC3 Cells

PC3 cells were grown to 70-80% confluence in 6-well plates and transfected with pCMV6-AC-GFP or pCMV6-SUV39H1 plasmid using Lipofectamine 2000 according to the manufacturer's recommendations (Invitrogen). Briefly, growth media was replaced with unsupplemented DMEM prior to transfection. Cells were transfected with 5 ug plasmid per well and allowed to rest 12 hours. Media was then replaced with growth media and cells allowed to recover for 24 hours before beginning treatments.

2.6 Acknowledgements

This work was supported by the National Institutes of Health (P01CA090890). Oregon State University mass spectrometry facility is supported in part by a grant from the National Institute of Environmental Health Science (P30ES000210).

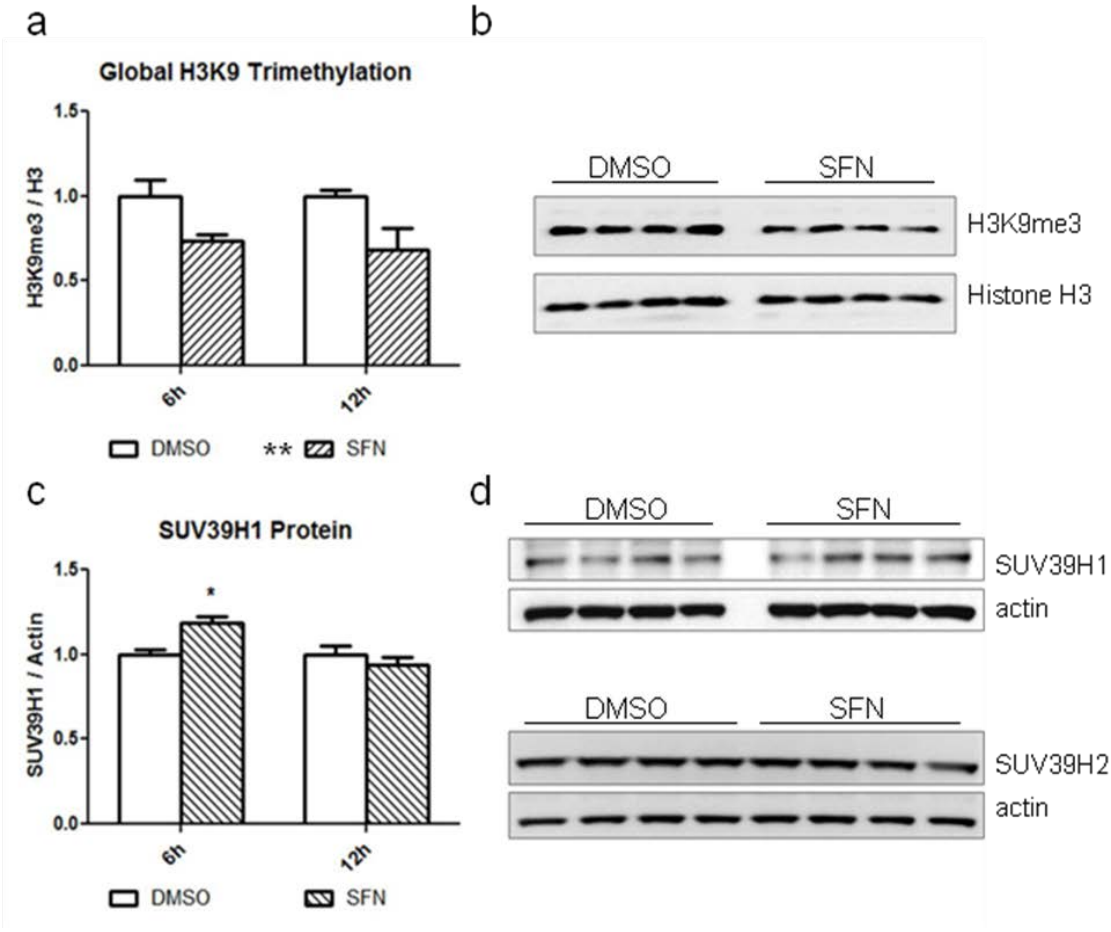

Figure 2.1. (a) Sulforaphane causes a global decrease in H3K9-trimethylation in PC3 cells. H3K9me3 was decreased relative to global histone H3 at 6 and 12 hours post-treatment ($p < 0.01$ by two-way ANOVA with Bonferroni post-test, mean + SEM for three independent experiments). (b) Representative blot from one of three independent experiments at 12 hours post-treatment. (c) SUV39H1 is increased at 6 hours post-treatment ($p < 0.05$ by two-way ANOVA with Bonferroni post-test, mean + SEM for three independent experiments). The early increase in SUV39H1 was not maintained, with the protein returning to control level by 12 hours. (d) Representative blots from one of three independent experiments at 12 hours post-treatment. β-actin was probed as a loading control. (SFN: sulforaphane).

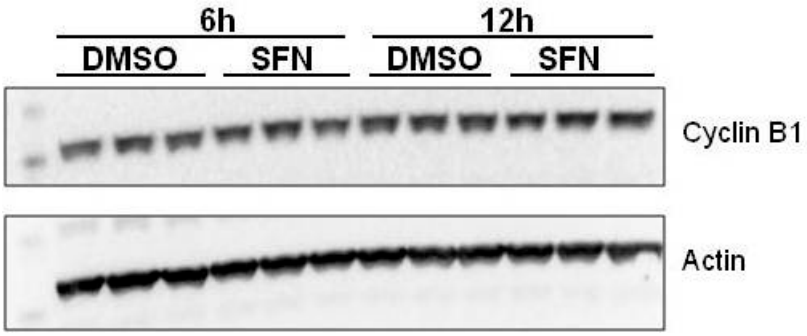

Figure 2.2. Cyclin B1 is not increased in sulforaphane treated cells relative to control at 6 or 12 hours post-treatment. β-actin was probed as a loading control.

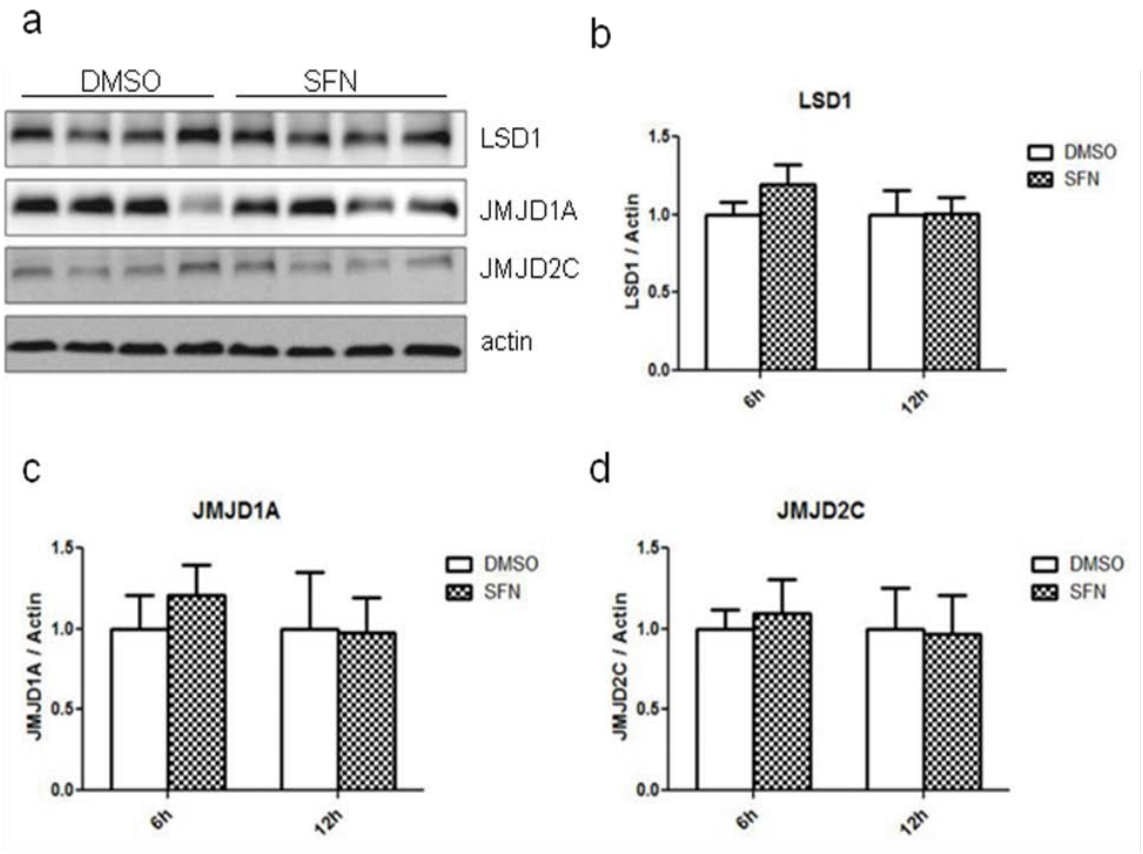

Figure 2.3. (a) Sulforaphane does not significantly alter the global level of selected H3K9 demethylases, though the expression in highly variable in PC3 cells (12h blot pictured). No change in (b) LSD1 (KDM1A), (c) JMJD1A (KDM3A) or (d) JMJD2C (KDM4C) was noted in sulforaphane-treated cells (two-way ANOVA with Bonferroni post-test, mean + SD). (SFN: sulforaphane).

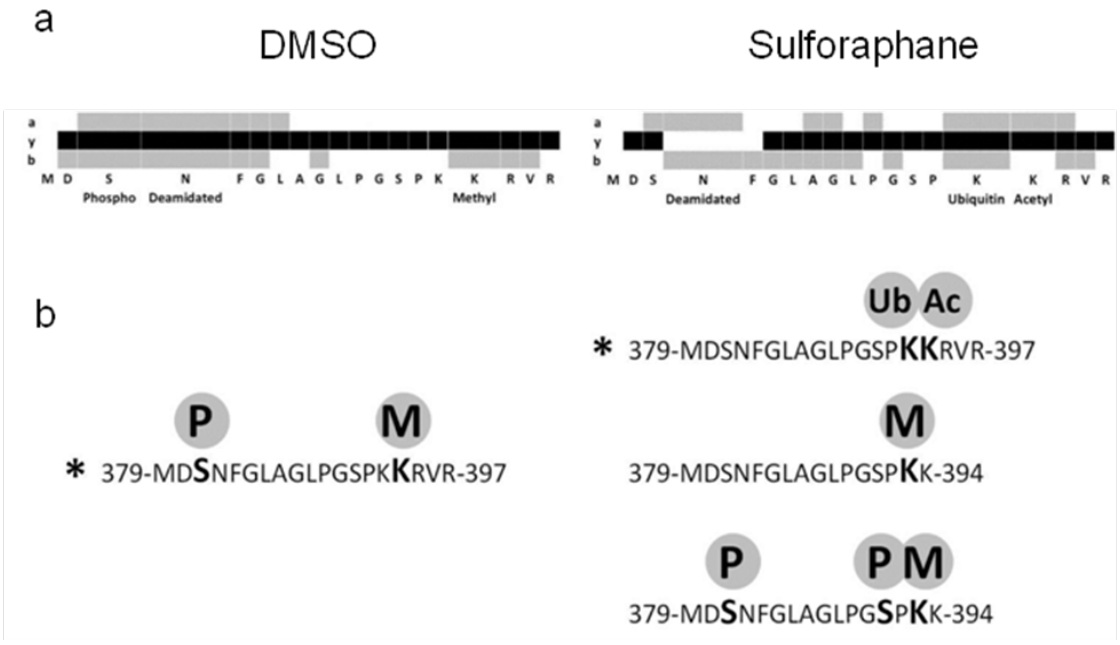

Figure 2.4. Identification of ubiquitinated and acetylated lysine residues on SUV39H1 in sulforaphane-treated PC3 cells. (a) a, y, and b ion peptide coverage by LC-MS/MS of the C-terminal peptide 379-MDSNFGLAGLPGSPKKRVR-397 in control-treated (DMSO) (left) and sulforaphane-treated (right) cell lysate. Coverage corresponds to asterisked peptides in (b). (b) peptides and modifications of the C-terminal region. The C-terminal region of interest is phosphorylated (P) and methylated (M) in both DMSO control and sulforaphane-treated lysates. Ubiquitinated (Ub) and acetylated (Ac) lysines were only identified in sulforaphane-treated cells. Spectra for the asterisked peptides in (b) can be found in Figure 2.5.

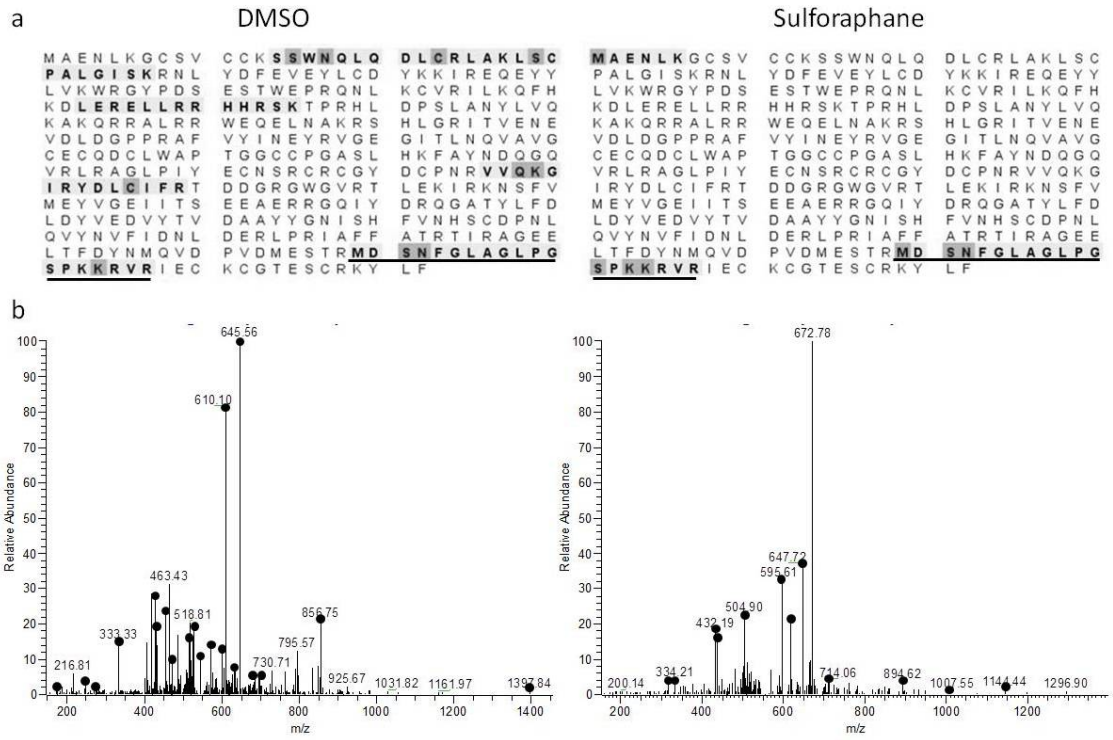

Figure 2.5. Peptides assigned to SUV39H1 by LC-MS/MS. (a) peptides assigned to SUV39H1 in DMSO-treated (left) and sulforaphane-treated (right) PC3 cell lysates shaded in grey. SUV39H1 protein sequence (NP_003164.1) is shown wrapped (N-terminus to C-terminus). The ubiquitinated and acetylated C-terminal peptide shown in Figure 2.4 is under lined. (B) Tandem mass spectra of the ubiquitinated and acetylated peptide; assigned fragment ions are marked with a black dot.

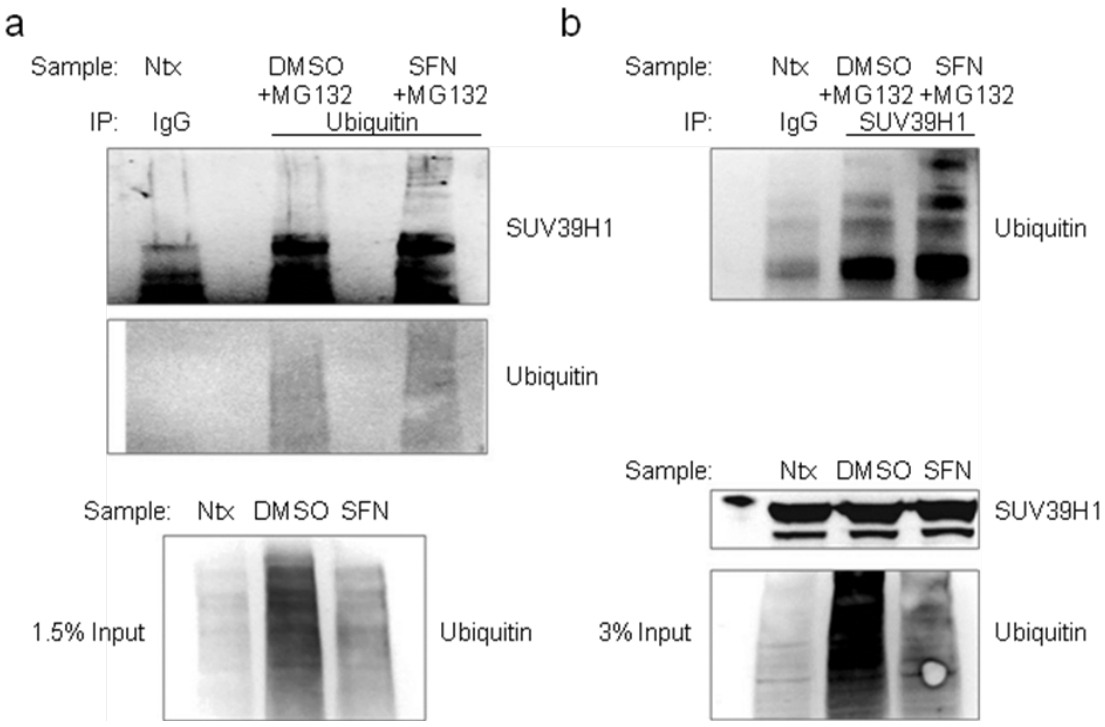

Figure 2.6. (a) PC3 cells were co-treated with MG132 (10 μM) and DMSO or sulforaphane for 9 hours. Ubiquitinated proteins were immunoprecipitated from lysates and subsequently analyzed for SUV39H1 protein. An increase in ubiquitinated SUV39H1 was noted in sulforaphane-treated cells. The increase in high-molecular weight SUV39H1 occurred despite a global decrease in ubiquitinated protein levels. Untreated PC3 lysate (Ntx) was immunoprecipitated with normal IgG and analyzed in parallel as a control. (b) The reverse immunoprecipitation (SUV39H1 immunoprecipitation → ubiquitin analysis) under the same experimental conditions as (a) confirmed increased ubiquitinated SUV39H1 in sulforaphane treated cells. (SFN: sulforaphane).

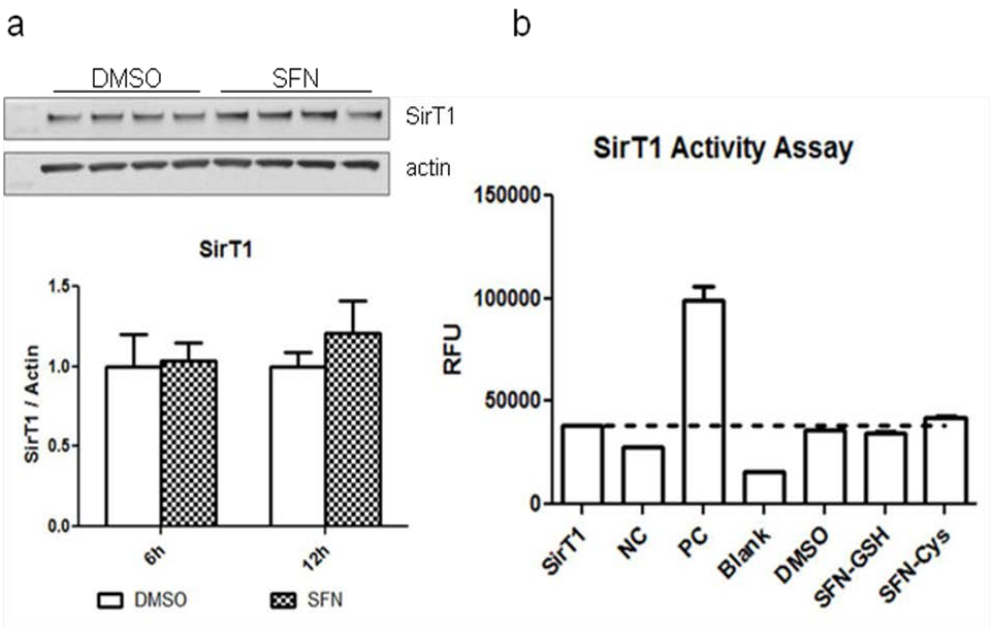

Figure 2.7. (a) Sulforaphane does not affect SirT1 protein level at 6 or 12 hours post-treatment. Sample blot from 12 hour time-point pictured (two-way ANOVA with Bonferroni post-test, mean + SD). (b) intracellular sulforaphane metabolites do not directly inhibit or activate SirT1 catalytic activity (student's T-test, mean + SD). RFU: relative fluorescence units, Sirt1: basal enzyme activity, NC: negative control (nicotinamide solution), PC: positive control (resveratrol), Blank: no enzyme, SFN-GSH: sulforaphane-glutathione (1 mM), SFN-Cys: sulforaphane-cysteine (150 µM).

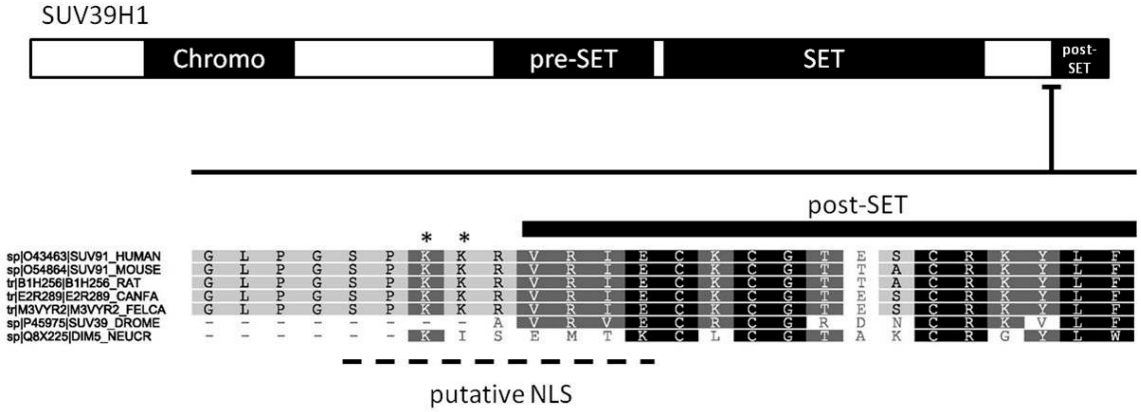

Figure 2.8. Domain architecture of SUV39H1 (upper) and expanded region of interest [lower (residue 387-412)] containing putative nuclear localization signal (NLS). Modified lysines identified by LC-MS/MS marked by asterisk. The putative NLS was predicted by three independent motif searching tools. Alignment of selected orthologous SUV39H1 protein sequences revealed the putative NLS is conserved in vertebrates [from top to bottom: *Homo sapiens* (human), *Mus musculus* (mouse), *Rattus norvegicus* (rat), *Canis familiaris* (dog), *Felis catus* (cat), *Drosphila melanogaster* (fruit fly), *Neurospora crassa* (fungi)].

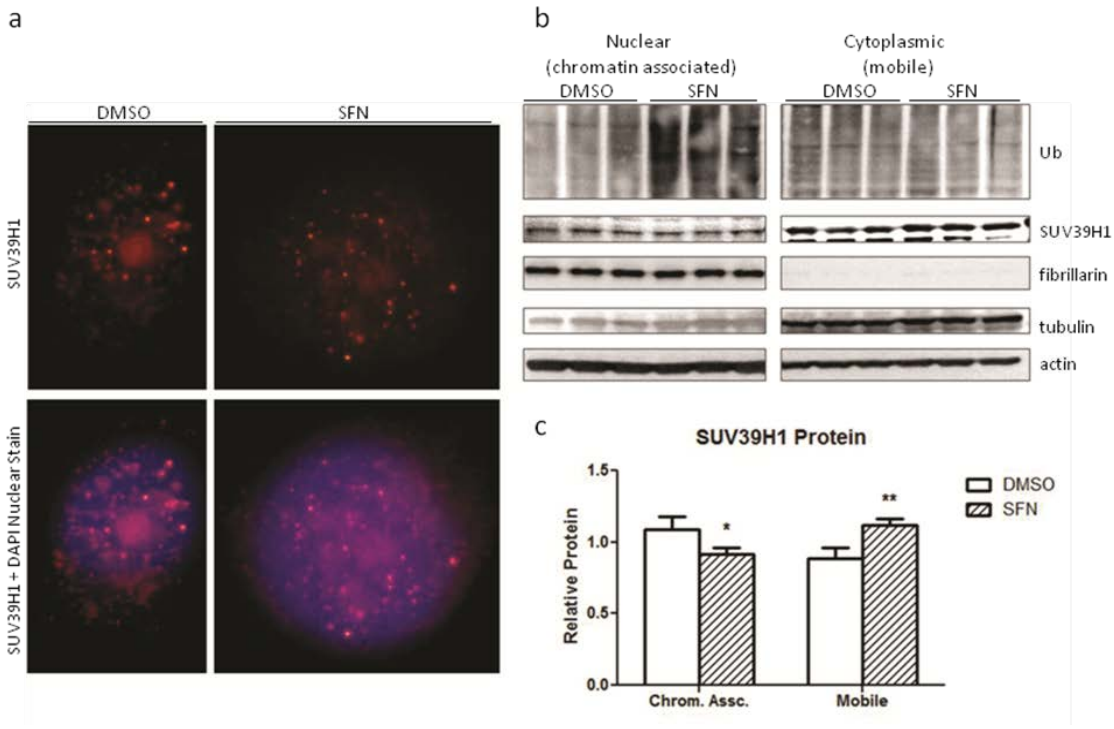

Figure 2.9. (a) representative image of control (DMSO) and sulforaphane-treated (12 hour) PC3 cells with nuclear (DAPI) and SUV39H1 labeling for immunofluorescent imaging. The chromatin-associated SUV39H1 foci and dispersed nuclear and perinuclear mobile fractions are readily visible. (b) Sulforaphane leads to a decrease in chromatin-associated SUV39H1. PC3 cells were treated for 8 hours with sulforaphane. MG132 was spiked into the culture dishes at a final concentration of 50 μM for the last 2 hours of the treatment. The high dose, short duration treatment was to halt a sulforaphane-stimulated increase in proteasome activity and decrease the impact of any MG132 toxicity. The experimental conditions did inhibit protein degradation (increase in ubiquitinated proteins in sulforaphane-treated PC3 cells). (c) densitometry showed a decrease in histone-associated SUV39H1 and an increase in mobile SUV39H1 (* $p < 0.05$, ** $p < 0.01$ by two-way ANOVA with Bonferroni post-test, mean + SD). Histone-associated (nuclear, immobile) SUV39H1 normalized to nuclear marker fibrillarin. Mobile (cytoplasmic) SUV39H1 normalized to β-actin. (SFN: sulforaphane).

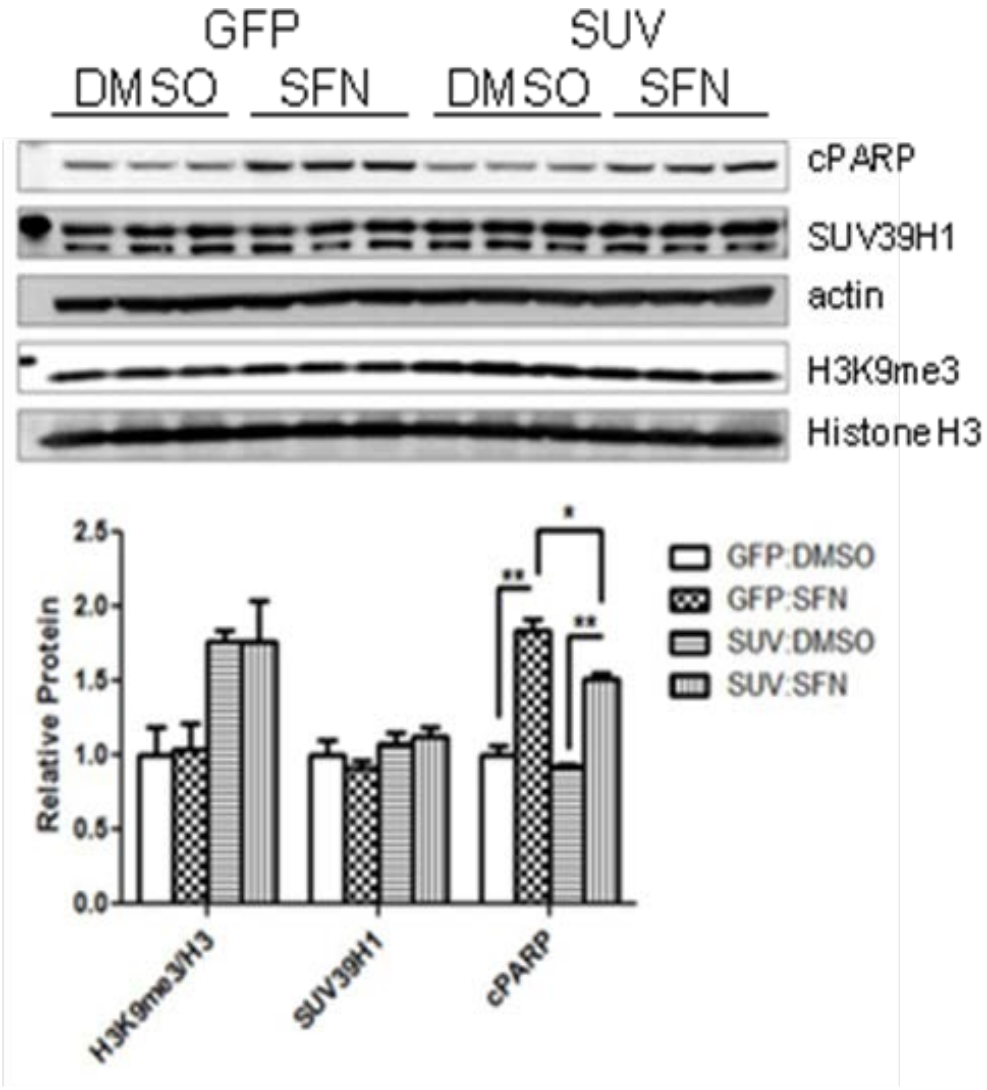

Figure 2.10. SUV39H1 decreases cleaved PARP in sulforaphane-treated PC3 cells. PC3 cells were transfected with GFP (control) or SUV39H1 (SUV) expression vector and allowed to recover for 36 hours. Cells were incubated with sulforaphane for 24 hours prior to harvesting whole cell lysates. H3K9me3 is increased in SUV39H1-transfected PC3 cells (SUV:DMSO, SUV:SFN) relative to GFP control (GFP:DMSO, GFP:SFN) (normalized to histone H3), though no increase in total SUV39H1 protein was noted (normalized to β-actin). Sulforaphane treatment significantly increased apoptotic signaling as assessed by cleaved PARP (cPARP) in GFP and SUV39H1 transfected cells. SUV39H1 overexpression significantly decreased cPARP protein levels, indicating decreased apoptotic signaling (* p <0.05, ** p < 0.01 by one-way ANOVA with Bonferroni post-test for each protein, mean + SEM for two independent experiments; blot from representative experiment pictured).

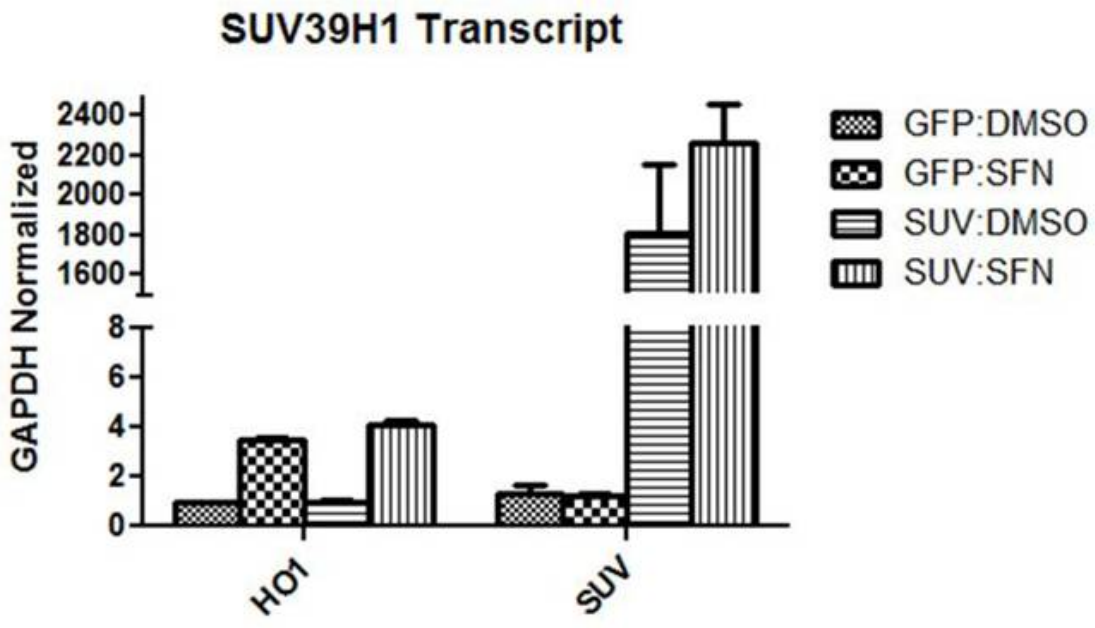

Figure 2.11. SUV39H1 (SUV) expression is increased approximately 2 000 fold in transfected PC3 cells. RNA was isolated 12 hours post-treatment to assess SUV39H1 expression. Heme-oxygenase 1 (HO1) expression was analyzed as a positive control for sulforaphane exposure [3] and to confirm that the transfection procedure did not dramatically alter the response to sulforaphane.

Chapter 3.

Analysis of autophagic flux in response to sulforaphane in metastatic prostate cancer cells

Gregory Watson, Samanthi Wickramasekara, Yufeng Fang, Zoraya Palomera-Sanchez, Claudia S Maier, David E Williams, Roderick H Dashwood, Viviana I Perez, Emily Ho

Molecular Nutrition and Food Research

WILEY-VCH Verlag GmbH & Co. KGaA

P. O. Box 10 11 61

D-69451 Weinheim

Germany

Submitted April 10, 2015

3.1 Abstract

Scope: The phytochemical sulforaphane has been shown to decrease prostate cancer metastases in a genetic mouse model of prostate carcinogenesis, though the mechanism of action is not fully known. Sulforaphane has been reported to stimulate autophagy, and modulation of autophagy has been proposed to influence sulforaphane cytotoxicity; however, no conclusions about autophagy can be drawn without assessing autophagic flux, which has not been characterized in prostate cancer cells following sulforaphane treatment.

Methods and Results: We conducted an investigation to assess the impact of sulforaphane on autophagic flux in two metastatic prostate cancer cell lines at a dose shown to decrease metastasis *in vivo*. Autophagic flux was assessed by multiple autophagy related proteins and substrates. We found that sulforaphane can stimulate autophagic flux and cell death only at high concentrations, above what has been observed *in vivo*.

Conclusion: These results suggest that sulforaphane does not directly stimulate autophagy or cell death in metastatic prostate cancer cells under physiologically relevant conditions, but instead supports the involvement of other *in vivo* factors as important effectors of sulforaphane- mediated prostate cancer suppression.

3.2 Introduction

Sulforaphane (1-isothiocyanato-4-methylsulfinylbutane) is a plant-derived isothiocyanate that has been the subject of scientific investigation for several decades. The compound is bioactive and induces an array of cellular responses that are associated with health benefits [1]. In the cancer field, sulforaphane has long been known as an effective “blocking agent” [2]. Sulforaphane is a well-characterized inducer of cytoprotective enzymes, particularly the Phase I and Phase II detoxifying enzymes controlled by nuclear factor erythroid-derived 2 factor 2 (nrf2) transcription factor [3]. This effect has been shown to have an important role in genome protection by increasing a cell’s ability to neutralize and

remove electrophiles and reactive intermediates and effectively limit cancer initiating events.

More recent work has suggested that sulforaphane may also possess cancer-suppressive properties in addition to its blocking activity. A number of investigations have demonstrated a cytotoxic response in transformed cells relative to normal cells at equi-dose pharmacological concentrations, though the sensitivity to sulforaphane between cell lines is highly variable [4, 5]. High-dose sulforaphane (i.e. pharmacological doses exceeding a typical dietary exposure) has been reported to stimulate stress-response pathways in addition to the antioxidant response mediated by nrf2, including increased heat shock protein and chaperone expression [6], increased proteasomal degradation capacity [6], cell-cycle arrest [1] and induction of autophagy (specifically macroautophagy) [7, 8]. Modulation of autophagy is a particularly interesting finding because autophagy is known to be dysregulated in cancer cells and has been proposed as a direct therapeutic target or as a chemo-sensitizer to enhance the efficacy of other agents [9]. Over 40 clinical trials are currently registered with the National Institutes of Health investigating modulation of autophagy as a therapeutic strategy (clinicaltrials.gov).

Autophagy is the process by which cellular substrates are engulfed by a double membrane vacuole and delivered to the lysosome for degradation [10]. The double membrane is marked by lipidated LC3 (LC3-II, LC3-PE) and sequesters substrates either non-specifically or specifically through autophagy adaptor proteins (e.g. p62 / SQSTM1). Autophagic activity (i.e. autophagic flux) can thus be assessed by monitoring the levels of these proteins [11, 12]. Although autophagy has been implicated in the cellular response to sulforaphane both *in vitro* in prostate cancer cell lines [7] and *in vivo* in a mouse model of prostate cancer [13], no study has characterized the effect on flux in prostate cancer cells. Because autophagy is a dynamic process, movement of substrates through the degradation pathway must be addressed to assess whether

sulforaphane enhances or impairs autophagy [11]. We also now know that autophagy and apoptosis often co-occur and share a subset of molecular components [14], suggesting induction of autophagy may be a concurrent but inconsequential result of apoptotic stimulation in response to sulforaphane. In addition, nearly all previous *in vitro* studies characterizing autophagy and cell death in prostate cancer cells utilize sulforaphane at concentrations above what is relevant *in vivo* or for treatment periods that do not match *in vivo* sulforaphane pharmacokinetics [4, 7, 15-28]. We therefore undertook an investigation to clarify the relationship between autophagy, apoptosis and sulforaphane in metastatic prostate cancer cells under more physiologically relevant conditions.

3.3 Materials and methods

3.3.1 Chemicals and Reagents

R,S-Sulforaphane was purchased from LKT Laboratories (St. Paul, MN, USA) and resuspended in dimethyl sulfoxide (DMSO) (EMD Millipore, Darmstadt, Germany). Chaetocin was purchased from Sigma-Aldrich (St. Louis, MO, USA) and resuspended in DMSO. Ammonium chloride (NH_4Cl) (Sigma-Aldrich) was prepared in sterile water. Mitochondrial dye MitoTracker Deep Red FM was purchased from Invitrogen (Carlsbad, CA, USA) and resuspended in DMSO. Primary antibodies for p62 (Santa Cruz Biotechnology), LC3A/B (Cell Signaling Technology, Danvers, MA, USA), cleaved poly-ADP ribose polymerase (cPARP) (Cell Signaling Technology), cytochrome c (CYCS) (Santa Cruz Biotechnology) and β-actin (Sigma-Aldrich) were used in accordance with the manufacturer's protocol. HRP-conjugated secondary antibodies (Santa Cruz Biotechnology) for Western Blotting detection and AlexaFluor-conjugated secondary antibodies for immunofluorescence/confocal imaging (Invitrogen) were used in accordance with the manufacturer's protocol.

3.3.2 Cell Lines and Culture Conditions

PC3 [androgen receptor (AR) negative] and LNCaP (AR positive) metastatic prostate cancer cell lines were purchased from American Type Culture Collection (ATCC, Manassas, VA, USA). Cells were maintained in RPMI-1640 media with L-glutamine supplemented with fetal bovine serum (FBS, 50 ml FBS / 500 ml media) at 37°C 5% CO_2. Cell lines were validated by Idexx Radil (Columbia, MO, USA) on December 24, 2012. Subconfluent cells were treated under the indicated conditions prior to harvest. Treatment reagents were used at the following concentrations: sulforaphane as indicated, 30 mM NH_4Cl, 500 nM chaetocin (CHAE). DMSO, or other appropriate carrier control, was used as needed for control treatments. For serum deprivation/starvation (SS), cells were rinsed thoroughly in PBS three times then cultured in RPMI-1640 with L-glutamine for the treatment period.

3.3.3 Protein Preparation and Western Blot Analysis

Protein lysates were prepared in RIPA cell lysis buffer (150 mM NaCl, 1% Triton X-100, 0.5% sodium deoxycholate, 0.1% SDS, 20 mM TRIS pH 8.0) supplemented with protease inhibitor cocktail (Thermo, Waltham, MA, USA). Cell lysate was cleared of insoluble material by centrifugation at 4°C (10 minutes, 13,000 RPM) and quantitated by the DCA Protein Assay (BioRad, Hercules, CA, USA). Equal amounts of protein were separated by SDS-PAGE and blotted to a PVDF membrane (BioRad) using NuPAGE Reagents and equipment in accordance with the manufacturer's protocol (Invitrogen). Membranes were blocked and probed for the indicated proteins following standard protocols. For protein detection membranes were incubated in SuperSignal West Femto Reagent (Thermo) and developed on the AlphaInnotech FluorChem 8900 system (ProteinSimple, San Jose, CA, USA). Densitometric analyses were performed on the native membrane image using AlphaInnotech FluorChem 8900 software (ProteinSimple). For each membrane, the relative densitometric value of each

replicate for a given probe was normalized to the corresponding relative level of the normalizing protein (β-actin). For graphing, treatments are expressed relative to Control (set to the value 1).

3.3.4 Mitochondrial Staining and Confocal Imaging

Cells were grown and treated on glass coverslips. Mitochondria were stained using MitoTracker Deep Red FM probe following the manufacturer's protocol. The MitoTracker probe was added at 200 nM during the final 30 minutes of cell treatment and then cells were prepared for immunostaining following standard protocols. Briefly, cells were rinsed in PBS and fixed/permeabilized in ice-cold 100% methanol for 10 minutes at -20°C. Cells were blocked in 1X PBS, 5% BSA, 0.3% Triton X-100. Cells were probed with primary antibodies in 1X PBS, 1% BSA, 0.3% Triton X-100 overnight at 4°C. After incubation with secondary antibodies cells were rinsed three times in PBS, with the final rinse containing DAPI nuclear stain. Coverslips were mounted on glass slides using ProLong Gold Antifade Reagent (Invitrogen) and allowed to set. Slides were visualized on a Zeiss LSM 510 Meta Confocal Microscope (Oberkochen, Germany) at the Center for Genome Research and Biocomputing (CGRB) at Oregon State University.

3.3.5 Quantitative Real-Time PCR

Total RNA was harvested by TRIzol reagent in accordance with the manufacturer's protocol (Invitrogen). cDNA was prepared from 1 µg RNA using the SuperScript III kit from Invitrogen. cDNA was amplified by Fast SYBR Green Reagent in accordance with the manufacturer's protocol (Invitrogen) on a 7900HT Real Time PCR Machine (Applied Biosciences).

Primers: GAPDH (sense 5'-CGAGATCCCTCCAAAATCAA-3', antisense 5'-TTCACACCCATGACGAACAT-3'); HMOX-1 (sense 5'-CTTCTTCACCTTCCCCAAC-3', antisense 5'-GCTCTGGTCCTTGGTGTCATA-

3'); p62 (sense 5'-CATCGGAGGATCCGAGTGTG-3', antisense 5'-TTCTTTTCCCTCCGTGCTCC-3').

3.3.6 Statistical Analysis

Graphing and statistical analyses were performed using GraphPad Prism Software (La Jolla, CA, USA). Figures depict one representative experiment. Graphs depict mean + SEM for at least two independent experiments. Statistical significance was determined by Student's *t*-Test or one-way analysis of variance (ANOVA) with Tukey's post-test where appropriate. Significance is indicated by asterisk, with * = $p < 0.05$, ** = $p < 0.01$, *** = $p < 0.001$.

3.4 Results

3.4.1 Sulforaphane does not directly influence autophagic activity in metastatic prostate cancer cells

To test whether sulforaphane has any direct influence on autophagic activity in metastatic prostate cancer cells, PC3 and LNCaP cells were treated with sulforaphane under conditions relevant to an *in vivo* therapeutic exposure (15 μM for 4 hours) [29]. Cells were co-treated in the presence of the lysosomotropic degradation inhibitor ammonium chloride (AC; NH_4Cl) to assess delivery of substrates to the lysosome [11, 12]. Protein levels of the autophagy adaptor p62 (SQSTM1) and LC3 [microtubule associated protein 1 light chain 3 (MAP1LC3)] were monitored to determine autophagic activity. Culturing in AC for 4 hours indicated both cells types are undergoing constant autophagic flux as assessed by an accumulation of LC3-II (Figure 3.1, Lane 1 and 2). In PC3 cells, serum starvation (SS) (positive control for flux) stimulated autophagic activity as indicated by a significant increase in p62 protein level and accumulation of LC3-II (Figure 3.1A, Lane 2 and 4). No significant change in p62 protein or LC3-II was noted in sulforaphane treated cells (Figure 3.1A, Lane 2 and 3), indicating no

influence on autophagic flux. Analyses in LNCaP cells also showed that sulforaphane did not influence autophagic activity (Figure 3.1B).

3.4.2 Sulforaphane does not influence autophagic flux following prolonged exposure

Sulforaphane leads to a dose-dependent increase in reactive oxygen species (ROS) and activation of cytoprotective programs [1, 16, 30], suggesting prolonged exposure to sulforaphane may indirectly influence autophagic flux. To address this issue, PC3 cell were treated with sulforaphane and/or various flux-modifiers for 24 hours to determine whether sulforaphane inhibits or stimulates autophagic flux (Figure 3.2).

We did not find sulforaphane to influence autophagic flux following an extended 24 hour treatment period. Sulforaphane did not decrease flux: we observed no increase in p62 or LC3-II in sulforaphane-treated cells as is seen in AC-treated cells (Figure 3.2A Lane 1, 2 and 3); we also noted no increase in p62 or LC3-II under conditions of high flux (Figure 3.2A Lane 5 and 6).

Sulforaphane also did not increase flux under these conditions: we observed no increase in p62 in sulforaphane-treated cells as is seen in SS-treated cells (positive control for flux) in the presence of AC (Figure 3.2A Lane 3, 4 and 7). In agreement with no increase in p62 protein in sulforaphane-treated cells (Figure 3.2A Lane 2 and 1, Lane 4 and 3, Lane 6 and 5, Lane 8 and 7), sulforaphane did not significantly increase p62 gene expression at this dose (Figure 3.3).

In addition to p62 and LC3 as indicators of autophagic flux, we also assessed potential mitochondrial involvement since mitochondria are reportedly required for sulforaphane-stimulated cell death [19] and damaged mitochondria are both a ROS source and an autophagy substrate [31]. Flux analysis indicated that mitochondria are not significantly turned over through the lysosome during

our treatment period (Figure 3.2A Lane 1 and 3) and that sulforaphane does not stimulate mitochondrial turnover (Figure 3.2A Lane 3 and 4) as assessed by cytochrome c (CYCS) levels. We also observed no colocalization of mitochondria and LC3 puncta in sulforaphane-treated cells (Figure 3.2B), confirming that mitochondria are not directed toward sites of autophagy following sulforaphane treatment. Analysis of neutral lipid as an autophagy indicator by counting neutral lipid-positive cells also suggested sulforaphane does not influence autophagic flux (data not shown) [32-34].

Visualization of LC3 puncta also did not suggest an increase in flux (Figure 3.2B). We noted LC3 puncta in both control and sulforaphane-treated cells, which is in agreement with constitutive flux we observed in the flux assay (Figure 3.1, Figure 3.2A). Although sulforaphane did lead to an increase in LC3-II at 24 hours, we also observed an increase in LC3-I (Figure 3.2A Lane 1 and 2, Figure 3.3B). This resulted in no observed increase in LC3-II/LC3-I ratio, indicating no increase in autophagic flux (Figure 3.3B). This may be a result of increased LC3 gene expression in response to sulforaphane, which has been observed in breast cancer cells [35].

Previous work has suggested that altering autophagic activity can influence apoptotic signaling in response to cytotoxic agents in cancer cells [9] and sulforaphane has been reported to induce apoptosis in prostate cancer cells [4, 7, 13]. We therefore tested whether inhibiting lysosomal degradation (AC treatment) or enhancing autophagy through SS sensitizes prostate cancer cells to 15 μM sulforaphane using cleaved poly-ADP ribose polymerase (cPARP) levels as a readout for apoptotic signaling (Figure 3.2A). Blocking lysosomal degradation (Figure 3.2A, Lane 3) or enhancing flux (Figure 3.2A, Lane 5) did not induce apoptosis in PC3 cells. Blocking degradation or enhancing flux also did not sensitize cells to sulforaphane (Figure 3.2A, Lane 4 and 6, respectively). Sulforaphane alone was unable to directly stimulate apoptosis under these treatment conditions (Figure 3.2A, Lane 2). Simultaneously driving autophagic

flux while inhibiting lysosomal degradation did not trigger apoptosis (Figure 3.2B, Lane 7) or sensitize cells to sulforaphane (Figure 3.2A, Lane 8). In contrast, exposing cells to chaetocin (CHAE), a potent ROS-inducer [36], strongly triggered cell death.

3.4.3 High-dose sulforaphane stimulates autophagic flux and cell death

To test whether sulforaphane influences autophagic flux at higher doses we conducted a dose escalation experiment in LNCaP cells (Figure 3.4). Cells were transiently exposed to sulforaphane for 4 hours to mimic an *in vivo* exposure [29]. Cells were treated with chaetocin (CHAE) in parallel as a positive control. Sulforaphane did stimulate autophagic flux at high concentrations (Figure 3.4A and 3.4B). At 150 and 300 µM we observed a decrease in p62 protein and an increase in LC3-II (Figure 3.4A). Sulforaphane treatment in the presence of ammonium chloride (AC) partially rescued the decrease in p62 protein and showed an increase in LC3-II protein (Figure 3.4B), confirming protein degradation through the lysosomal pathway. Sulforaphane treatment at 150 and 300 µM also lead to a phenotypic response (Figure 3.5) but was not sufficient to directly stimulate cell death in LNCaP cells within 4 hours, whereas chaetocin potently stimulated cell death as evidenced by the appearance of cleaved PARP (cPARP) (Figure 3.4A).

Although we did not observe induction of apoptosis at 4 hours, high-dose sulforaphane could lead to cell death at a later time point if the cells sustain an irrecoverable amount stress. To test this, LNCaP cells were treated for 4 hours as in Figure 3.4A and then the media was replaced with normal growth media for 40 hours and the cells monitored for recovery as evidenced by continued growth. As seen in Figure 3.4C, control (DMSO) and 15 µM sulforaphane-treated cells continued to grow to confluence, as was expected given no indication of cell stress (Figure 3.1A, Figure 3.3, Figure 3.4A). All chaetocin-treated cells were dead 40 hours after media removal, consistent with the apoptotic signaling we

observed at 4 hours (Figure 3.4A). Cells transiently exposed to sulforaphane at 150 μM did recover from the treatment, suggesting that this dose is not sufficient to overcome cytoprotective responses stimulated by sulforaphane. Sulforaphane at 300 μM was sufficient to cause an irrecoverable amount of stress as evidenced by cellular debris and minimal outgrowth of LNCaP cells 40 hours after media removal (Figure 3.4C, Figure 3.6).

3.5 Discussion

Previous investigations have suggested the involvement of autophagy in sulforaphane-mediated cytotoxicity in prostate cancer cells based on the presence of autophagosomes and LC3-II production [7, 13]; however, the presence of these markers cannot differentiate between induction or inhibition of autophagic flux. These same markers would be expected to accumulate under conditions where autophagosome-lysosome fusion is impaired. To clarify the relationship between sulforaphane, autophagy and cell death we tested whether sulforaphane has any influence specifically on autophagic flux in metastatic prostate cancer cells at a dose shown to decrease metastasis *in vivo* (15 μM) [29]. Our results show that sulforaphane cannot directly stimulate autophagic flux and cell death in metastatic prostate cancer cells at this dose *in vitro*, but can directly stimulate flux and lead to cell death at higher concentrations (Figure 3.1, Figure 3.2, Figure 3.3B, Figure 3.4). This is consistent with previous investigations showing that high levels of sulforaphane and/or extended treatment periods are required to trigger cell death in metastatic prostate cancer cells *in vitro* [4, 7, 15-22].

In our analysis of sulforaphane as a flux-modifier under conditions where flux is already impaired or up-regulated (AC and SS, respectively) (Figure 3.2), we found that sulforaphane does not further influence flux, suggesting no context specificity for a sulforaphane effect on flux. We also noted that modulation of flux did not sensitize cells to sulforaphane at the *in vivo* therapeutic dose of 15 μM

even at an extended 24 hour treatment period (Figure 3.2). Recent work in pancreatic carcinoma cells using different autophagy modifiers (chloroquine and rapamycin) has also demonstrated that these agents do not alter sulforaphane cytotoxicity [37]. Autophagy therefore may, under some conditions, influence sulforaphane cytotoxicity [35, 38], but the effect is cell-type and dose dependent.

In this investigation we chose a 4 hour sulforaphane exposure because *in vivo* data characterizing decreased prostate cancer metastasis following sulforaphane treatment showed that sulforaphane quickly reaches a plasma concentration peak of ~16 µM and is then rapidly eliminated from circulation in 4 hours (Figure 3.1, Figure 3.5) [29]. The *in vivo* pharmacokinetics observed in this model of prostate cancer are in agreement with other *in vivo* analysis in mice and rats showing a spike in plasma concentration shortly after exposure followed by rapid elimination from the plasma and tissues [23-28]. Under these shorter transient treatment periods intended to simulate an *in vivo* exposure, we found that only very high doses of sulforaphane are able to directly lead to cell death in LNCaP cells (Figure 3.4). Even a 150 µM dose (~10 fold higher than *in vivo* circulating concentration) was not sufficient to lead to cell death following a transient exposure (Figure 3.4C). Recovery and continued growth after transient sulforaphane exposure has also been noted in two colon cancer cell lines [39, 40], and although the outcome of repeated 15 µM exposures that mimic *in vivo* sulforaphane pharmacokinetics have not been tested in prostate cancer cells *in vitro*, repeated low-dose exposures in astrocytes has been shown to be protective against oxidative stress [41], likely through stimulating the same cytoprotective programs associated with genome protection in normal cells [13, 26-29, 42].

The inability of sulforaphane to induce autophagy and apoptosis *in vitro* when used at concentrations and treatment periods that mimic *in vivo* exposure (Figure 3.2, Figure 3.4) may suggest the existence of important *in vivo* factors that contribute to prostate cancer suppression that are difficult to address *in vitro*.

A few reports have suggested a role for enhanced immune cell activation toward cancer cells following sulforaphane treatment [29, 43], and any potential influence of sulforaphane on other tumor associated cells – such as tumor associated fibroblasts – is largely unexplored. This will be an interesting area of future research and will be important in understanding how sulforaphane leads to prostate cancer suppression *in vivo*.

3.6 Acknowledgements

The authors would like acknowledge Dr. Donald Jump for providing reagents, equipment and technical assistance, and Dr. Carmen Wong for providing feedback during manuscript drafting. This work was supported by the National Cancer Institute (CA090890), National Institute of Environmental Health Sciences (P30 ES000210), National Institutes of Health (1S10RR107903-01) and Oregon Agricultural Experimental Station. The authors wish to acknowledge the Confocal Microscopy Facility of the Center for Genome Research and Biocomputing and the Environmental and Health Sciences Center at Oregon State University.

3.7 Conflict of interest

The authors declare no conflicts of interest.

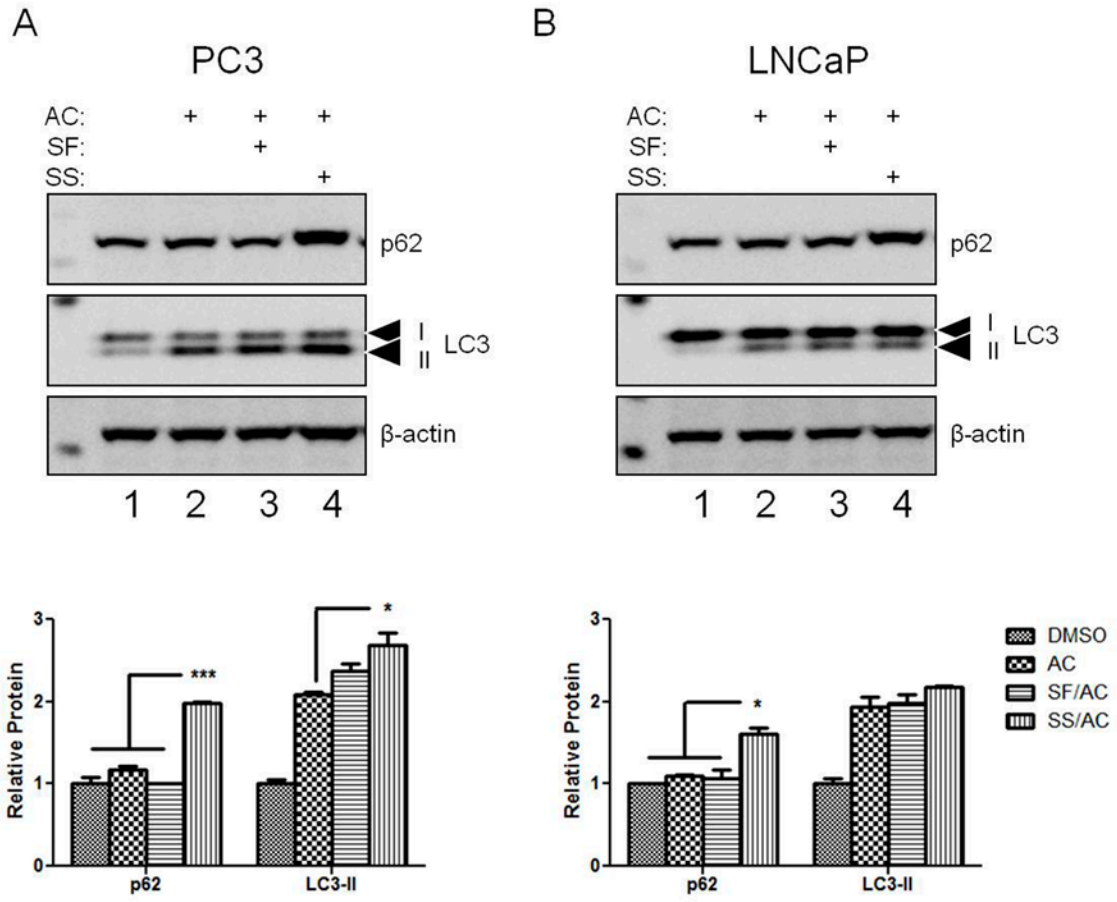

Figure 3.1. Sulforaphane does not directly stimulate autophagic flux in metastatic prostate cancer cells. (A) PC3 or (B) LNCaP cells were grown for 4 hours under the appropriate conditions to assess autophagic flux. Lane 1: no treatment (DMSO control). Lane 2: lysosomal degradation inhibitor ammonium chloride (AC). Lane 3: sulforaphane (SF) 15 μM and AC. Lane 4: serum starvation (SS) and AC. One representative experiment of multiple independent experiments pictured (upper). Relative levels of p62 and LC3-II from two independent experiments were graphed and analyzed (lower). Proteins are expressed relative to β-actin.

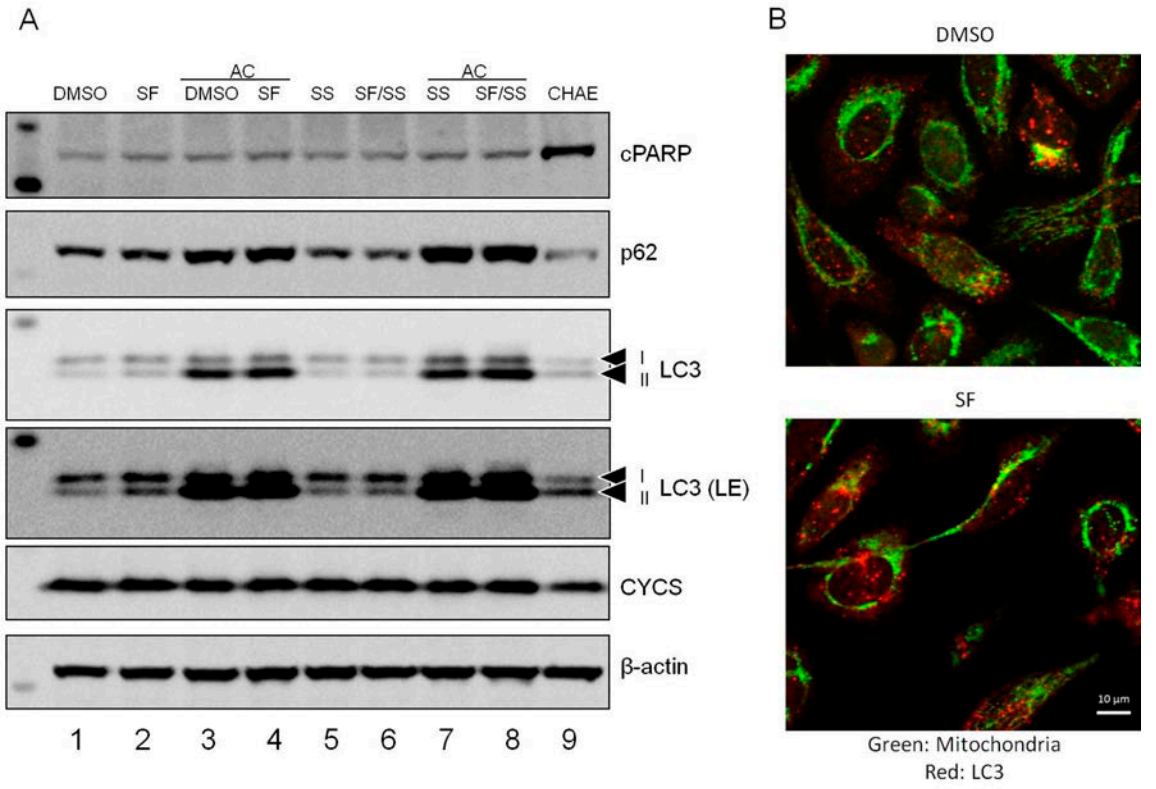

Figure 3.2. Sulforaphane does not influence autophagic flux following prolonged exposure. (A) PC3 cells were treated for 24 hours under varying conditions to assess flux. Lane 1: DMSO (control). Lane 2: sulforaphane (SF) 15 µM. Lane 3: ammonium chloride (AC). Lane 4: SF and AC. Lane 5: serum starvation (SS). Lane 6: SF and SS. Lane 7: AC and SS. Lane 8: SF, AC and SS. Lane 9: chaetocin (CHAE). Cleaved poly-ADP ribose polymerase (cPARP) was assayed to assess apoptotic signaling. The autophagy adaptor/substrate p62, autophagosome marker/substrate LC3, and mitochondrial marker cytochrome c (CYCS) were assayed to assess autophagic flux. β-actin was probed as a loading control. LC3 (LE) indicates a Longer Exposure during membrane visualization. (B) PC3 cells treated with DMSO (control) (upper) or SF (lower) for 24 hours then processed for visualization of mitochondria (Green) and LC3 (Red). Scale bar is 10 µm.

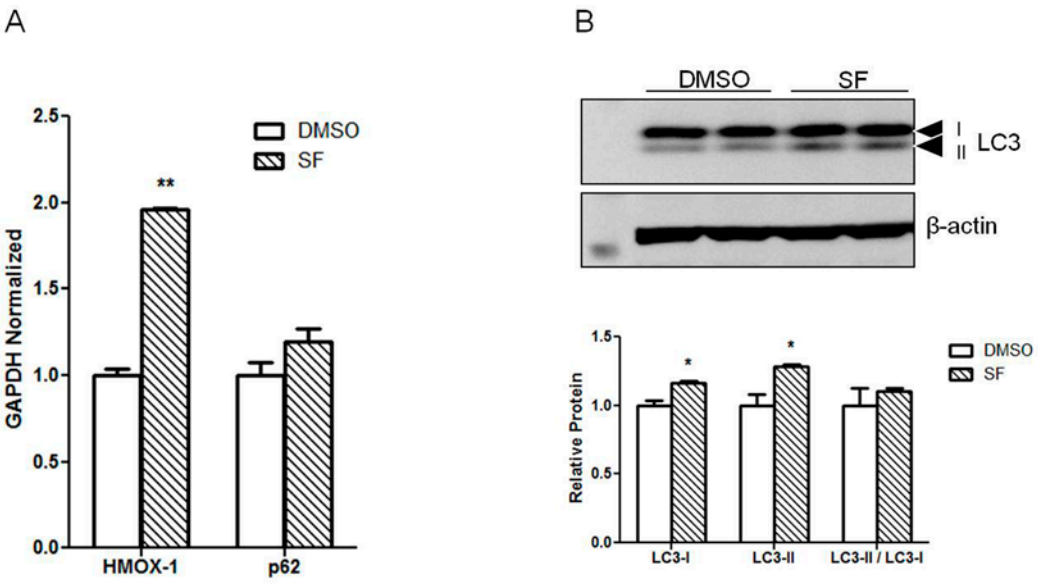

Figure 3.3. (A) Gene expression analysis in PC3 cells treated for 24 hours with DMSO (control) or sulforaphane (SF). Data are from two independent experiments. Heme-oxygenase 1 (HMOX-1) is a positive control for SF treatment. (B) PC3 cells treated 24 with DMSO or SF. Blot depicts two independent experiments (upper). Quantification of LC3-I and LC3-II (lower). β-actin was probed as a loading control.

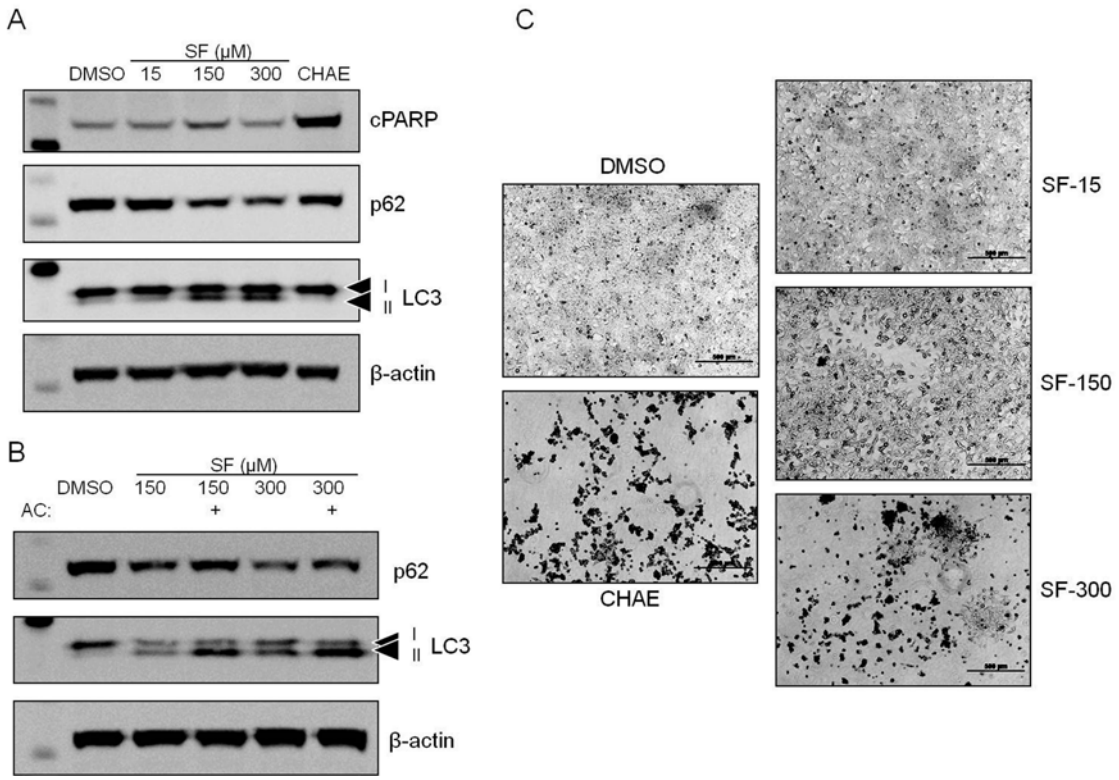

Figure 3.4. High-dose sulforaphane stimulates autophagic flux and cell death. (A) LNCaP cells were treated with increasing amounts of sulforaphane (SF) for 4 hours. Cells were also treated with chaetocin (CHAE) as a positive control for cytotoxicity. Cleaved poly-ADP ribose polymerase (cPARP) was assayed to assess apoptotic signaling. The autophagy adaptor/substrate p62 and autophagosome marker/substrate LC3 were assayed to assess autophagic flux. β-actin was probed as a loading control. Representative blot from two independent experiments shown. (B) LNCaP cells were treated for 4 hours with high-dose sulforaphane in the absence or presence of ammonium chloride (AC) to impair lysosomal degradation. p62 and LC3 were assayed to assess autophagic flux. β-actin was probed as a loading control. (C) LNCaP cells were treated with SF at the indicated dose or with CHAE for 4 hours. Media was then replaced with normal growth media and the cells allowed to recover for 40 hours. Representative bright-field image shown at 4X magnification. Scale bar is 500 μm. Higher magnification can be seen in Fig. S3.

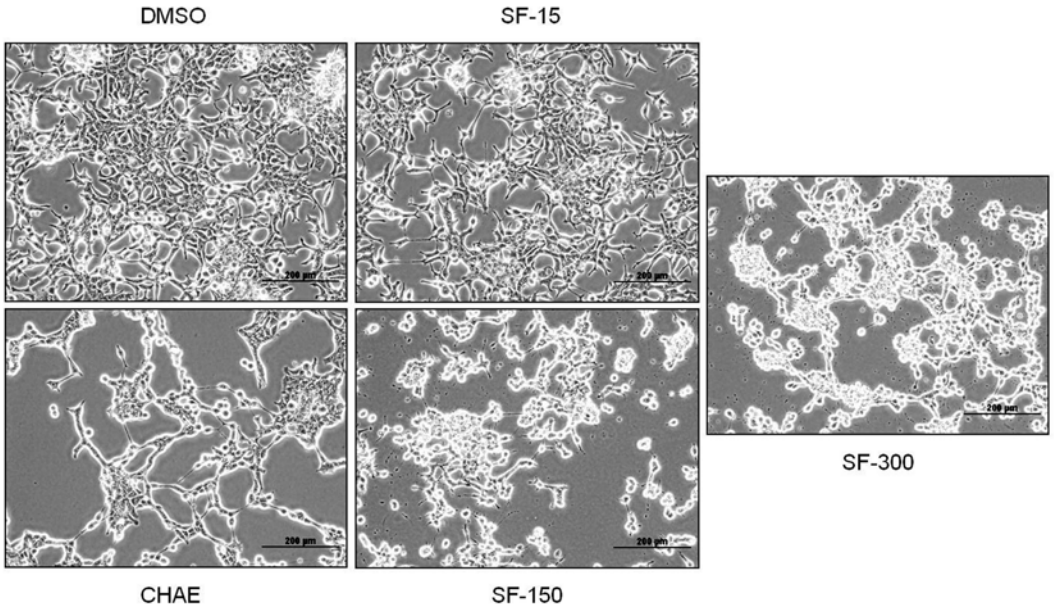

Figure 3.5. Representative bright-field images of LNCaP cells treated for 4 hours with DMSO (control) or the indicated concentration of sulforaphane (SF) or chaetocin (CHAE). Images at 10X magnification. Scale bar is 200 µm.

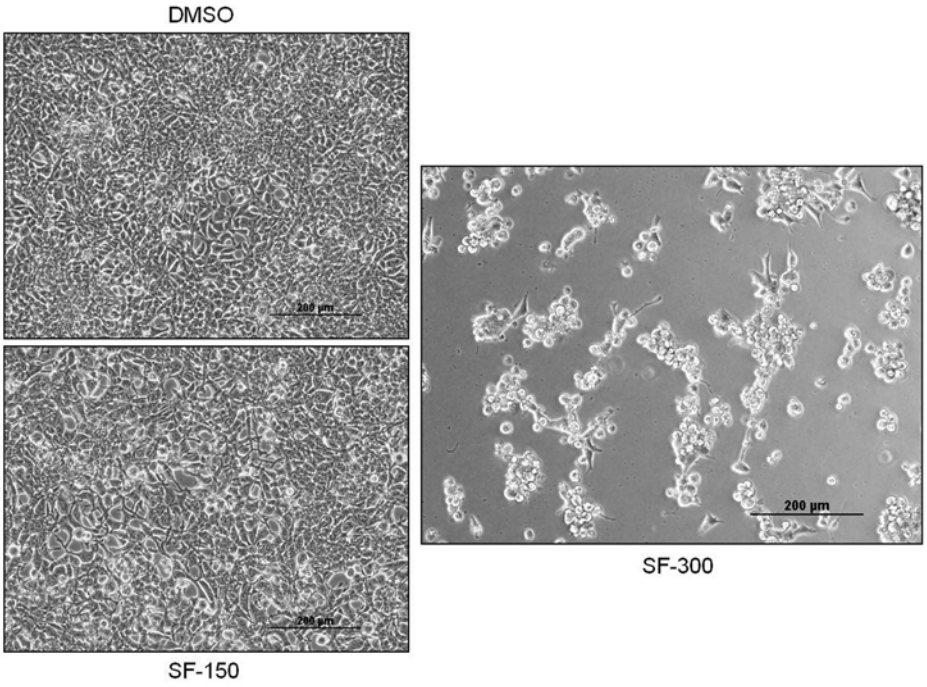

Figure 3.6. Representative bright-field images of LNCaP cells 40 hours after treatment removal. Images at 10X magnification. Scale bar is 200 µm.

Chapter 4.

Analysis of autophagic flux following tubacin treatment in metastatic prostate cancer cells

Gregory W Watson, Samanthi Wickramasekara, Yufeng Fang, Claudia S Maier, David E Williams, Roderick H Dashwood, Viviana I Perez, Emily Ho

Clinical Epigenetics

236 Gray's Inn Road

London WC1X 8HB

United Kingdom

Submitted May, 2015

4.1 Abstract

Histone deacetylase 6 (HDAC6) is a multifunctional lysine deacetylase that is recently emerging as a central facilitator of response to stress and may play an important role in cancer cell proliferation. The HDAC6 inhibitor tubacin has been shown to slow the growth of metastatic prostate cancer cells and sensitize cancer cells to chemotherapeutic agents. However, the proteins HDAC6 interacts with, and thus its role in cancer cells, remains unknown. To address this gap we characterized the HDAC6-interacting proteins in LNCaP metastatic prostate cancer cells and found that HDAC6 interacts with proteins involved in several cellular processes, including autophagy. HDAC6 deacetylase activity has recently been shown to be required for efficient basal autophagic flux. Autophagy is often dysregulated in cancer cells and may confer stress resistance and allow for cell maintenance and a high proliferation rate. Based on our interaction screen, we assessed the impact of tubacin on autophagic flux in two metastatic prostate cancer cell lines and found that tubacin does not influence autophagic flux. HDAC6 therefore controls cell proliferation through an autophagy-independent mechanism in metastatic prostate cancer cells.

Keywords: autophagy, metastatic prostate cancer, HDAC6, tubacin

Abbreviations:
HDAC6: histone deacetylase 6
HDAC6i: HDAC6-inhibition
AC: ammonium chloride

4.2. Introduction

Histone deacetylase 6 (HDAC6) is a cytoplasmic lysine deacetylase that has a role in maintaining homeostasis in response to cellular stressors (1). HDAC6 facilitates aggregation and turnover of misfolded proteins and is

protective during misfolded-protein stress (2, 3); its ubiquitin-binding domain is required for heat shock factor 1 (HSF1) activation and downstream induction of cytoprotective chaperone proteins (4); and its deacetylase activity is required for efficient fusion of autophagosomes and lysosomes for autophagic flux (5). Despite this critical role in homeostasis, how HDAC6 is regulated, the proteins it interacts with, its substrates and cell-type specific functions are only recently coming to light (6-8).

The cytoprotective functions of autophagy suggest this process would be important in maintaining cell viability under conditions of heightened stress, such as during rapid proliferation or nutrient limitation. This is particularly relevant to cancer because the tumor microenvironment is an inherently stressful niche characterized by low nutrient concentrations, hypoxia, and damaging reactive oxygen species (ROS). Furthermore, metastatic cancers are likely evolved to require autophagy in response to selective pressures exerted throughout the process of dissemination (9-11). Consequently, autophagy is under investigation as a therapeutic target in cancer cells with the goal of inhibiting its cytoprotective function to slow growth or sensitize cancer cells to established therapeutic agents (12, 13). HDAC6 is proposed to regulate autophagic flux though posttranslational control of cortactin at the interface of autophagosomes and lysosomes (5). HDAC6 catalytically-impaired mutant fibroblasts display an accumulation of autophagosomes, indicating deacetylase activity is required for basal flux.

Consistent with its in role in cell maintenance and stress response, HDAC6 inhibition (HDAC6i) or depletion has been shown to slow cancer cell growth and migration and sensitize cancer cells to chemotherapeutic agents (14-16). A cytoprotective role in cancer cells is also supported by associative clinical data showing a tendency toward increased expression of HDAC6 in patient tumors (17) (The Cancer Genome Atlas datasets (18, 19)). The HDAC6 inhibitor

tubacin (20) has been shown to slow growth and sensitize LNCaP metastatic prostate cancer cells to chemotherapeutic agents (14).

We hypothesized that growth retardation and a synergistic decrease in cell viability in combination with other therapeutic agents may be a result of decreased autophagic flux in response to HDAC6i. To test this hypothesis, we first characterized the proteins that interact with HDAC6 in LNCaP cells to gain insight into the protein's role in metastatic prostate cancer cells. We found HDAC6 to interact with proteins associated with autophagy and subsequently tested whether HDAC6i influences autophagic flux (21) in two metastatic prostate cancer cell lines.

4.3. Materials and Methods

4.3.1 Chemicals and Reagents

Tubacin (N_1-[4-[(2*R*,4*R*,6*S*)-4-[[(4,5-diphenyl-2-oxazolyl)thio]methyl]-6-[4-(hydroxymethyl)phenyl]-1,3-dioxan-2-yl]phenyl]-N_8-hydroxyoctanediamide) was purchased from Santa Cruz Biotechnology (Dallas, TX, USA) and resuspended in dimethyl sulfoxide (DMSO) (EMD Millipore, Darmstadt, Germany). Ammonium chloride (NH_4Cl) (Sigma-Aldrich) was prepared in sterile water. Mitochondrial dye MitoTracker Deep Red FM was purchased from Life Technologies (Carlsbad, CA, USA) and resuspended in DMSO. Primary antibodies for p62 (Santa Cruz Biotechnology), LC3A/B (Cell Signaling Technology, Danvers, MA, USA), glyceraldehyde-3-phosphate dehydrogenase (GAPDH) (Santa Cruz Biotechnology), cytochrome c (CYCS) (Santa Cruz Biotechnology), ubiquitin (Ub) (Santa Cruz Biotechnology), acetylated-α-tubulin (Sigma, St. Louis, MO, USA), α-tubulin (Sigma) and β-actin (Sigma) were used in accordance with the manufacturer's protocol. HRP-conjugated secondary antibodies (Santa Cruz Biotechnology) for Western Blotting detection and AlexaFluor-conjugated secondary antibodies for immunofluorescence/confocal imaging (Life Technologies) were used in accordance with the manufacturer's protocol.

4.3.2 Cell Lines and Culture Conditions

PC3 and LNCaP prostate cancer cell lines were purchased from American Type Culture Collection (ATCC, Manassas, VA, USA). Cells were maintained in RPMI-1640 media with L-glutamine supplemented with fetal bovine serum (FBS, 50 ml FBS / 500 ml media) at 37°C 5% CO_2. Cell lines were validated by Idexx Radil (Columbia, MO, USA) on December 24, 2012. Cells were treated under the indicated conditions prior to harvest. Treatment reagents were used at the following concentrations: 8 µM tubacin, 30 mM NH_4Cl. DMSO or other appropriate carrier was used as needed for control treatments.

4.3.3 Protein Preparation and Western Blot Analysis

Protein lysates were prepared in radioimmunoprecipitation assay (RIPA) protein lysis buffer (150 mM NaCl, 1% Triton X-100, 0.5% sodium deoxycholate, 0.1% SDS, 20 mM TRIS pH 8.0) supplemented with protease inhibitor cocktail (Thermo Scientific, Waltham, MA, USA). Lysates were cleared of insoluble material by centrifugation (10 minutes, 13000 rpm) at 4°C and quantitated by the DCA Protein Assay (BioRad, Hercules, CA, USA). Equal amounts of protein were separated by SDS-PAGE and blotted to a PVDF membrane (BioRad) using NuPAGE reagents and equipment in accordance with the manufacturer's protocol (Life Technologies). Membranes were blocked and probed for the indicated proteins following standard protocols. Membranes were stripped and reprobed as needed. Membranes were incubated in SuperSignal West Femto Reagent (Thermo Scientific) and developed on the AlphaInnotech FluorChem 8900 system for visualization (San Jose, CA, USA). Densitometric analyses were performed on the native membrane image using AlphaInnotech FluorChem 8900 software. For each membrane, the relative densitometric value of each replicate for a given probe was normalized to the corresponding relative level of the normalizing protein (β-actin). DMSO (control) was set to 1.

4.3.4 Immunofluorescent Staining

Cells were grown and treated on glass coverslips. Mitochondria were stained using MitoTracker Deep Red FM probe following the manufacturer's protocol. The MitoTracker probe was added at 200 nM during the final 30 minutes of cell treatment and then cells were prepared for immunostaining. Briefly, cells were rinsed in PBS and fixed/permeabilized in ice-cold 100% methanol for 10 minutes at -20°C. Cells were placed in blocking buffer (1X PBS, 5% BSA, 0.3% Triton X-100). Cells were probed with primary antibodies in antibody dilution buffer (1X PBS, 1% BSA, 0.3% Triton X-100) overnight at 4°C. After incubation with secondary antibodies cells were rinsed three times in PBS, with the final rinse containing DAPI nuclear stain. Coverslips were mounted on glass slides using ProLong Gold Antifade Reagent (Life Technologies) and allowed to set. Slides were visualized on a Zeiss LSM Meta Confocal Microscope (Oberkochen, Germany) at the Center for Genome Research and Biocomputing (CGRB) at Oregon State University. Colocalization quantification was done using Coloc 2 (Fiji distribution for ImageJ2) (22).

4.3.5 Quantitative Real-Time PCR

Total RNA was harvested by TRIzol reagent in accordance with the manufacturer's protocol (Life Technologies). cDNA was prepared from 1 µg RNA using the SuperScript III kit from Life Technologies. Approximately 50 ng cDNA was amplified by Fast SYBR Green Reagent in accordance with the manufacturer's protocol (Life Technologies) on a 7900HT Real Time PCR Machine (Applied Biosciences, Life Technologies).

Primers: GAPDH (sense 5'-CGAGATCCCTCCAAAATCAA-3', antisense 5'-TTCACACCCATGACGAACAT-3'); p62 (sense 5'-CATCGGAGGATCCGAGTGTG-3', antisense 5'-TTCTTTTCCCTCCGTGCTCC-3'); HDAC6 (sense 5'-CAGCACAGTCTTATGGATGG-3', antisense 5'-

CGGTGGATGGAGAAATAGAG-3'). Relative expression was determined by the Comparative Ct Method ([delta][delta]Ct = [delta]Ct,sample - [delta]Ct,reference). Graphing was done using GraphPad Prism Software (La Jolla, CA, USA). Graphs depicts mean + SEM for two independent experiments.

4.3.6 HDAC6 Immunoprecipitation and Liquid Chromatography Tandem Mass Spectrometry (LC-MS/MS)

LNCaP cell lysate (3 mg) was immunoprecipitated with HDAC6 antibody in 1% Triton X-100, 137 mM NaCl, 2 mM EDTA, 20 mM Tris-HCl pH 8.0 overnight at 4°C. The following day, Protein G agarose (Life Technologies) was added and incubated for an additional 2 hours. Immunocomplexes were isolated by low-speed centrifugation and washed twice in 50 mM ammonium bicarbonate. The last wash was removed and immunocomplexes were resuspended in 50 µl 0.5 M urea, 5 mM DTT, 50 mM Tris pH 8.0. Samples were then sonicated in a water bath (2X 1 minute), vortexed and spun down. Each sample was digested with 500 ng Trypsin Gold (Promega, Madison, WI, USA) at 37°C.

LC-MS/MS was carried out as described previously (23). High-confidence protein identifications were made under the following conditions: Protein Threshold 99.0%, Minimum # of Peptides = 2, Peptide Threshold 5% FDR.

4.4. Results

4.4.1 Identification of HDAC6-interacting proteins in LNCaP cells

HDAC6 has been shown to have a significant role in many cellular processes in various cell types (17, 24, 25). However, the proteins that interact with HDAC6 in metastatic prostate cancer cells have not been fully characterized. To address this issue we immunoprecipitated HDAC6 and subjected co-immunoprecipitated proteins to LC-MS/MS analysis. We identified 52 high-confidence proteins as the major HDAC6-interacting proteins in LNCaP

cells (Table I). As expected, we identified many well-characterized HDAC6 interacting proteins, including components of the cytoskeletal network (26, 27) and heat shock proteins (27, 28). We also identified more recently reported HDAC6-interacting proteins such as myosin-9 (7) (Table I).

Several of the most abundant HDAC6-associated proteins were found to be involved in autophagy. We identified proteins that are characterized macroautophagy substrates and mediators, including mitochondria-associated proteins, ribosomes, actin and tubulin (Table I) (3, 29-32). HDAC6 interaction with tubulin was confirmed by co-immunoprecipitation and mitochondrial association was assessed by confocal microscopy (Figure 4.1).

We also identified proteins associated with chaperone-mediated autophagy. Chaperone-mediated autophagy (CMA) delivers a subset of cytosolic proteins to the lysosome via heat shock cognate 71 kDa protein (hsc70) and the lysosomal receptor LAMP2A (33). Hsc70 has recently been reported as an HDAC6 substrate (7). Our LC-MS/MS screen for HDAC6 interacting proteins also identified hsc70 as a prominent HDAC6-interactor in LNCaP cells (Table I). In addition to hsc70, we also identified multiple recently characterized CMA substrates involved in regulation of cellular energy production, including α-enolase (ENO1), pyruvate kinase (PKM) and glyceraldehyde-3-phosphate dehydrogenase (GAPDH) (34, 35) (Table I).

4.4.2 Tubacin does not inhibit autophagy in metastatic prostate cancer cells

The interaction of HDAC6 with proteins and substrates involved in autophagy in LNCaP cells suggests that tubacin may slow LNCaP growth by interfering with autophagic flux. To test this hypothesis we treated LNCaP and PC3 metastatic prostate cancer cells with tubacin and monitored autophagic flux (Figure 4.2). Ammonium chloride (AC) was used to assess delivery of substrates to the lysosome. The selective autophagy adaptor protein p62 (sequestosome 1,

SQSTM1) was monitored in addition to LC3-II turnover to assess macroautophagy (21, 36).

Tubacin did not influence overall HDAC6 protein level in either cell-type and AC treatment indicated that HDAC6 is not turned over through the lysosomal pathway (Figure 4.2 Lane 2 and 3). Tubacin did lead to an increase in p62 protein (Figure 4.2 Lane 2), suggesting impaired p62-selective flux. We did not observe an increase in p62 comparing AC treatment to the tubacin/AC combination treatment (Figure 4.2 Lane 4), indicating that the increase in p62 observed during tubacin treatment is not the result of an increase in gene expression. However, the p62 response in PC3 cells was not consistent (Figure 4.3). We observed on several occasions that tubacin enhanced p62 degradation (decrease in p62 protein with no associated decrease in gene expression). When assessing macroautophagy based on LC3-II levels, tubacin did not significantly impair or enhance flux under any treatment conditions (Figure 4.2 Lane 2 and Figure 4.3).

Tubacin did not influence CMA in either cell type as determined by GAPDH levels (Figure 4.2 Lane 2). However, we did not observe accumulation of GAPDH in AC-treated cells (Figure 4.2 Lane 3), suggesting no significant turnover of GAPDH under these experimental conditions.

The observed influence of tubacin on p62 levels suggests that although macroautophagy is occurring unimpeded, p62 substrate degradation may be specifically altered. To test this hypothesis we assayed turnover of global poly-ubiquitinated protein levels and mitochondria (Figure 4.4). Tubacin did not alter global poly-ubiquitinated proteins or mitochondria levels (as assessed by cytochrome c (CYCS)) despite increased p62 levels (Figure 4.4). No change in mitochondrial levels was also observed in circumstances where tubacin increased p62 degradation (Figure 4.3).

4.4.3 Tubacin leads to the appearance of HDAC6 puncta in PC3 cells

Accumulation or degradation of p62 in response to tubacin suggests direct regulation of p62 stability independent of autophagy. p62 is also a known HDAC6-interacting protein (37). We observed colocalization of p62 and HDAC6 under basal conditions in PC3 cells (Figure 4.5). Tubacin treatment led to an increase in p62 and HDAC6 puncta (Figure 4.5). Tubacin also led to an increase in association between p62 and HDAC6 foci: HDAC6-only foci were not observed in tubacin-treated cells, and colocalization analysis noted an increase in association as assessed by Pearson's R and Spearman's rank correlation (Figure 4.6). Analysis of LC3 by immunofluorescence showed an increase in LC3 puncta, indicating an increase in autophagosome formation in response to tubacin (Figure 4.7). LC3 puncta were also found to colocalize with p62 foci in tubacin-treated cells.

4.5 Discussion

In this investigation we characterized the proteins that HDAC6 interacts with in LNCaP metastatic prostate cancer to gain insight into how HDAC6i slows cancer cell proliferation. We found HDAC6 to interact with many proteins associated with autophagy (Table I) and subsequently tested the hypothesis that HDAC6i slows proliferation by impairing basal autophagic flux. Our results show that tubacin does not impair macroautophagy in metastatic prostate cancer cells, suggesting flux-inhibition is not responsible for slowed cancer growth associated with tubacin treatment.

Autophagic flux independent of HDAC6 tubulin deacetylase activity was not expected given its known role in mediating efficient autophagosome-lysosome fusion (5). However, in the context of metastatic prostate cancer, this finding may not be surprising. Cells undergo vast changes in metabolism and intracellular signaling pathways during transformation to enable rapid proliferation and enhanced survival (38). Metastatic prostate cancer cells are particularly

prone to constitutive activation of the PI3K/AKT/mTOR signaling axis (39, 40), a key regulator of autophagy (41). Curiously, activation of this signaling pathway does not inhibit autophagy (Figure 4.2): both LNCaP and PC3 cells contain mutations that disrupt PTEN, a negative regulator of the PI3K signaling axis (42, 43). This suggests that these cell lines, and perhaps metastatic prostate cancers in general, evolve to allow autophagic flux independent of well-established regulators. We confirmed HDAC6 interaction with proteins and substrates known to be involved in, or degraded by, autophagy (Table I, Figure 4.1 and Figure 4.5). The presence of HDAC6 at the site of autophagosomes can also be inferred from complete overlap of both LC3 and HDAC6 puncta with p62 foci in tubacin-treated cells (Figure 4.5 and Figure 4.7). Despite association with autophagy related proteins, HDAC6 activity appears to be dispensable for autophagic flux in these cells.

In addition to monitoring LC3-II levels, the autophagy adaptor and substrate p62 was assessed to evaluate flux. We unexpectedly found that tubacin influences p62 stability independent of autophagic flux (Figure 4.2 and Figure 4.3). HDAC6 and p62 physically interact in mouse embryonic fibroblasts (MEFs) and p62 has been proposed to influence HDAC6 activity (37). We also found a close association between these two proteins in metastatic prostate cancer cells (Figure 4.5); however, we found p62 stability to be dependent of HDAC6 activity (Figure 4.2 and Figure 4.3), suggesting a co-regulatory relationship. The observation that the outcome of HDAC6i on p62 protein level is variable also suggests the involvement of other factors - HDAC6 and p62 are both multifunctional proteins known to interact with an array of other proteins (7, 24, 44-46). Variable p62 stability or degradation may also be a result of overlapping function with other autophagy adaptors and shared substrates (e.g. neighbor of BRCA1 gene 1 (NBR1) or optineurin (OPTN) (47, 48)). Further work will be needed to understand how HDAC6 may regulate p62 stability.

Localization analyses suggested that tubacin stimulates autophagy as assessed by an increase in LC3 puncta that co-localized with p62 (Figure 4.7). This observation is difficult to reconcile with no accumulation of LC3-II protein in the flux assay (Figure 4.2 Lane 3 and 4). Autophagosomes and autophagy are closely associated with the ubiquitin proteasome system (UPS) (49, 50). Only recently has evidence emerged suggesting p62 is a proteasomal substrate in addition to being an autophagy adaptor (51), whereas a role for HDAC6 in proteasomal degradation of ubiquitinated proteins is well known. Autophagy-independent p62 activity may explain why p62 degradation was observed to be independent of LC3-II level (Figure 4.2 and Figure 4.3) and why we did not observe global changes in two p62 substrates (Figure 4.4). The characterized association between autophagosomes and UPS may also explain why we observed LC3 puncta and p62 colocalization; p62 may associate with the proteasome (and HDAC6), which in turn associates with autophagosomes.

Alternatively, HDAC6 foci may reflect more efficient trafficking across the cytoskeletal network as a result of increased microtubule acetylation (8, 52-54). Enhanced trafficking may lead to the accumulation of HDAC6 and p62 at degradation sites, leading to the appearance of discrete foci without significantly affecting overall autophagic vesicle fusion or proteasome activity. This would support a model where tubacin does not actively cause HDAC6 re-localization, but instead passively leads to deposition of HDAC6 at sites of protein degradation. This would be consistent with its function in trafficking substrates and not as an autophagy adaptor protein (HDAC6 is not an autophagy substrate (Figure 4.2 Lane 3)). This suggests that p62/HDAC6 foci represent either protein bodies that are de-ubiquitinated and degraded (50), or are sites of ubiquitin-independent basal protein turnover (55). It is unlikely that HDAC6 foci represent stress granules or P bodies as HDAC6 activity is required for their formation (6). We also did not observe obvious signs of cell stress and although tubacin slows

LNCaP cell growth, it is not associated with decreased cell viability (14). Further work will be needed to evaluate these various interpretations.

Our unbiased LC-MS/MS screen for HDAC6-interacting proteins suggested a role for HDAC6 in CMA (Table I). A test of whether tubacin influenced CMA in metastatic prostate cancer cells using GAPDH as a reporter indicated no major role (Figure 4.2). However, inhibition of lysosomal degradation by AC also revealed no increase in GAPDH, indicating no significant turnover under our experimental conditions (lysosomal turnover of GAPDH has been detected within 2 hours of inhibition of degradation in liver (35)). This may reflect cell-type specific metabolism and suggests HDAC6 may influence cellular energetics not through altering degradation of metabolic enzymes, but instead through direct regulation. This will be an interesting area of future research in understanding how HDAC6i may slow cancer growth.

In this investigation we showed that tubacin does not impede basal autophagic flux; however, this does not necessarily mean HDAC6 deacetylase activity is dispensable for flux in other circumstances. HDAC6 is known to have a context-dependent role in autophagic flux (5), suggesting HDAC6 may be required in a stimulus-dependent manner (56). This will be particularly relevant in exploring whether HDAC6 has a role in flux following exposure to chemotherapeutic agents (14). Additionally, other HDAC6 inhibitors may be evaluated to assess the potential for differential modes of action and effects on basal autophagic flux.

Tubacin thus slows proliferation in LNCaP cells through an autophagy-independent mechanism. Based on our analysis of HDAC6-interacting proteins, we proposed a potential role for HDAC6 in cellular energetics in LNCaP cells that could influence cell proliferation, but alternative processes could also be proposed (e.g. protein synthesis). Future characterization of how HDAC6i influences cell proliferation will be important in developing HDAC6 as a therapeutic target for metastatic prostate cancer.

4.6 Acknowledgements

The authors would like acknowledge Dr. Carmen Wong for providing feedback during manuscript drafting. This work was supported by the National Cancer Institute (CA090890), National Institutes of Health (1S10RR107903-01), National Institute of Environmental Health Sciences (P30 ES000210) and Oregon Agricultural Experimental Station. The authors wish to acknowledge the Confocal Microscopy Facility of the Center for Genome Research and Biocomputing and the Environmental and Health Sciences Center at Oregon State University.

Table I

HDAC6-Interacting Proteins in LNCaP Cells	Accession	EUSC	Assignment
40S ribosomal protein S15	4506687	2	AS (31)
40S ribosomal protein S15a	14165469	2	AS (31)
40S ribosomal protein S17-like	312284072	3	AS (31)
40S ribosomal protein S18	11968182	2	AS (31)
40S ribosomal protein S3 isoform 1	15718687	2	AS (31)
40S ribosomal protein S5	13904870	2	AS (31)
40S ribosomal protein S7	4506741	5	AS (31)
40S ribosomal protein SA	59859885	2	AS (31)
60 kDa heat shock protein, mitochondrial	31542947	9	MP (32)
60S acidic ribosomal protein P2	4506671	3	AS (31)
60S ribosomal protein L21	18104948	2	AS (31)
60S ribosomal protein L3 isoform a	4506649	2	AS (31)
actin, cytoplasmic 2	316659409	7	AM (5)
alpha-enolase isoform 1	4503571	6	AS (35)
ATP synthase subunit alpha, mitochondrial isoform c	382546190	3	MP (32)
ATP synthase subunit beta, mitochondrial precursor	32189394	6	MP (32)
ATP-dependent RNA helicase DDX3X isoform 2	301171467	4	
D-3-phosphoglycerate dehydrogenase	23308577	4	
E3 ubiquitin-protein ligase TRIM21	15208660	4	
elongation factor 1-alpha 1	4503471	2	
elongation factor 2	4503483	3	
eukaryotic initiation factor 4A-I isoform 1	4503529	3	
fatty acid synthase	41872631	10	AS (35)
FK506-binding protein 15	150010552	8	
glyceraldehyde-3-phosphate dehydrogenase isoform 2	378404908	3	AS (35)
heat shock 70 kDa protein 1A/1B	167466173	2	MP (32)
heat shock cognate 71 kDa protein isoform 2	24234686	4	H6S (7),AM (33)
heat shock protein HSP 90-beta isoform a	20149594	5	H6S (28)
heterogeneous nuclear ribonucleoprotein K isoform b	14165435	3	
heterogeneous nuclear ribonucleoprotein R isoform 1	156151394	16	
heterogeneous nuclear ribonucleoprotein U isoform b	14141161	4	
histone deacetylase 6	13128864	6	AM (5)
histone H2B type 1-B	10800140	2	
keratin, type I cytoskeletal 18	40354195	5	
lipoamide acyltransferase component of branched-chain alpha-keto acid dehydrogenase complex, mitochondrial precursor	392494079	2	MP (32)
myc box-dependent-interacting protein 1 isoform 1	21536400	27	
myosin light polypeptide 6 isoform 1	17986258	2	
myosin-10 isoform 1	365192532	2	AM (50)
myosin-9	12667788	5	H6S (7)
non-POU domain-containing octamer-binding protein isoform 1	224028244	2	
nucleolin	55956788	2	
nucleophosmin isoform 1	10835063	6	
PRKC apoptosis WT1 regulator protein	55769533	2	
protein-L-isoaspartate(D-aspartate) O-methyltransferase isoform 1	226530908	7	
pyruvate kinase isozymes M1/M2 isoform e	332164779	2	AS (34,35)
RNA-binding protein FUS isoform 3	283135173	3	
stress-70 protein, mitochondrial precursor	24234688	4	MP (32)
T-complex protein 1 subunit epsilon	24307939	5	
transformation/transcription domain-associated protein isoform 1	347360922	2	
tubulin alpha-1B chain	57013276	10	H6S (26), AM (3)
tubulin beta chain	29788785	20	H6S (26), AM (3)
tubulin beta-4B chain	5174735	5	H6S (26), AM (3)

EUSC: Exclusive Unique Spectrum Count

H6S = HDAC6 substrate; AS = autophagy substrate; MP = mitochondrial protein; AM = autophagy mediator

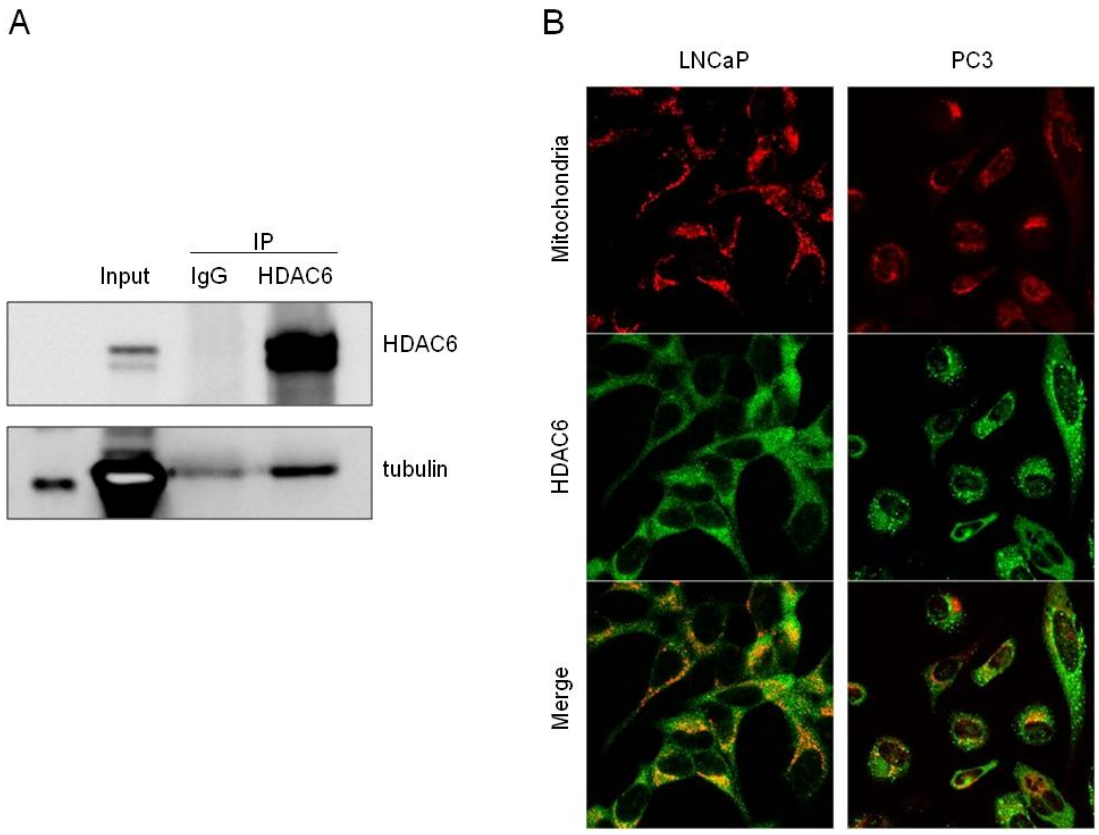

Figure 4.1. HDAC6 associates with autophagy related proteins and substrates. (A) HDAC6 interacts with tubulin in LNCaP cells. (B) HDAC6 associates with mitochondria in LNCaP and PC3 cells.

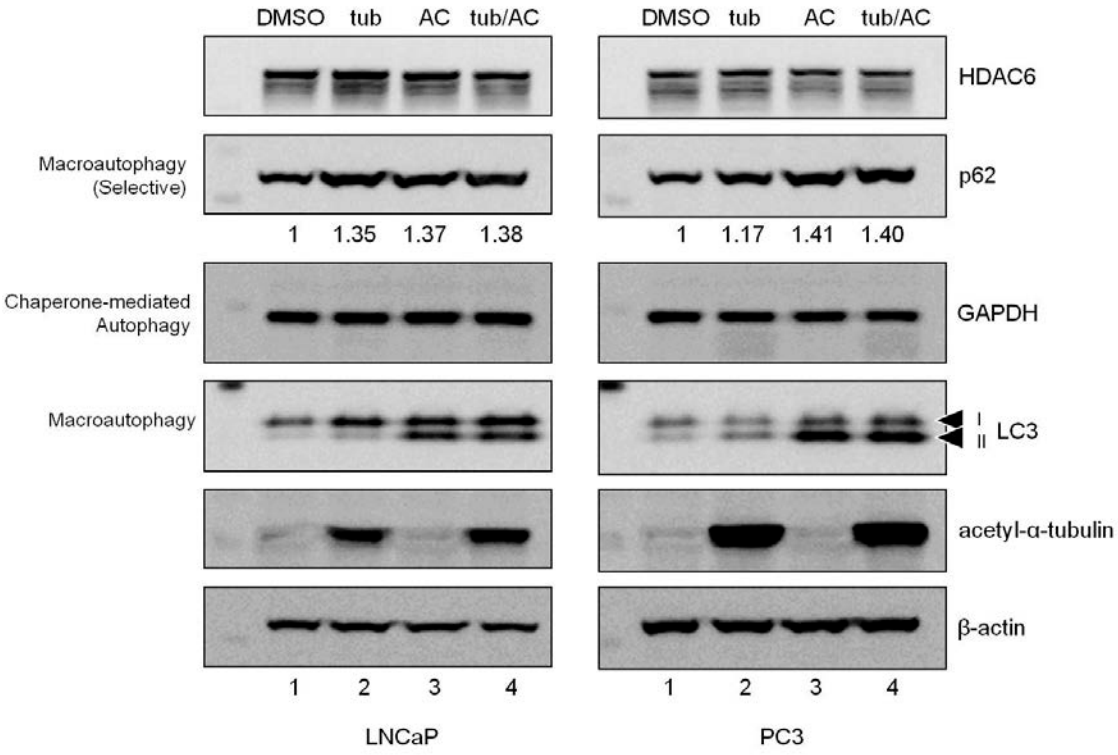

Figure 4.2. Tubacin does not influence autophagy in metastatic prostate cancer cells. LNCaP and PC3 cells were treated with control (DMSO, Lane 1), tubacin (tub, Lane 2), ammonium chloride (AC, Lane 3), or tubacin and AC (tub/AC, Lane 4) for 24 hours prior to harvesting for protein analysis. To assess autophagic flux, membranes were probed for the selective autophagy adaptor and substrate p62, the chaperone mediated autophagy substrate GAPDH, and autophagosome marker and autophagy substrate LC3. One representative experiment from at least three independent experiments is pictured. p62 levels (relative to DMSO control) are indicated. p62 was normalized to the loading control β-actin.

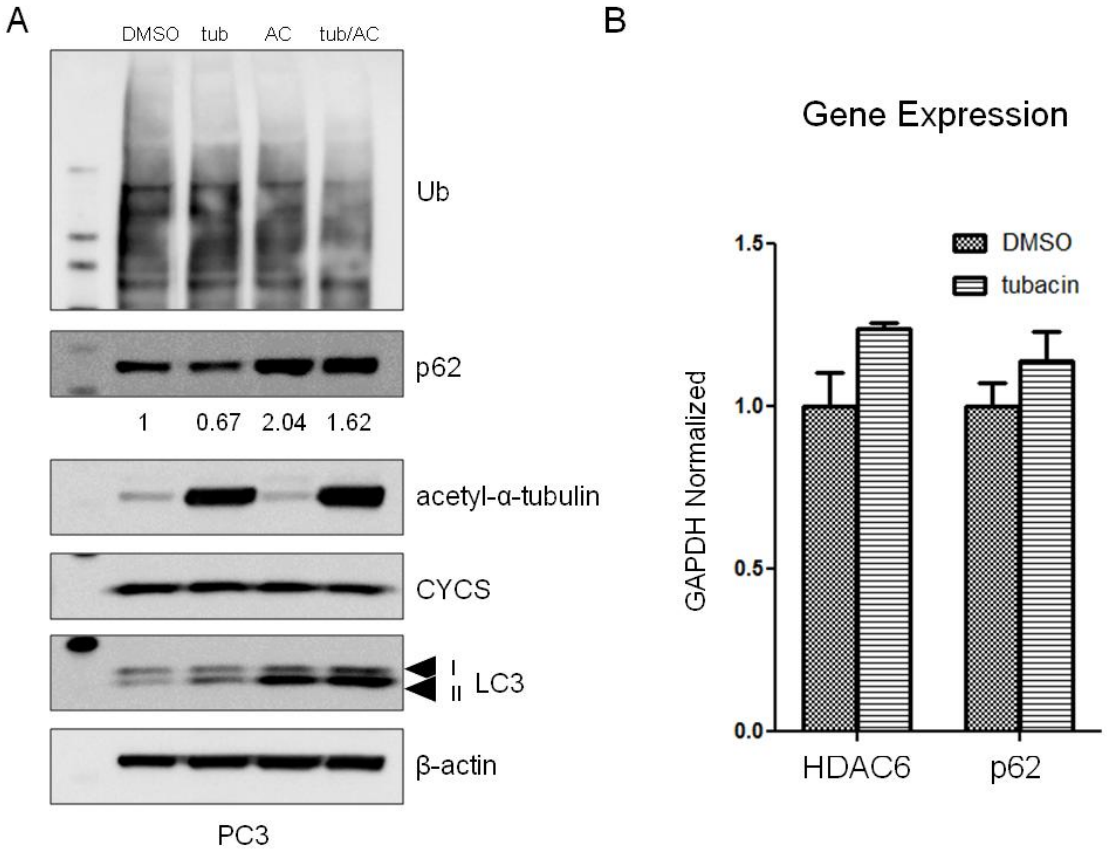

Figure 4.3. Tubacin was observed to increase autophagic flux in PC3 cells on several occasions. Cells were treated as described in Figure 4.2. (A) tubacin treatment decreased p62 protein level and led to an increase in LC3-II level in both the absence and presence of AC. (B) Tubacin does not lead to a decrease in HDAC6 or p62 gene expression.

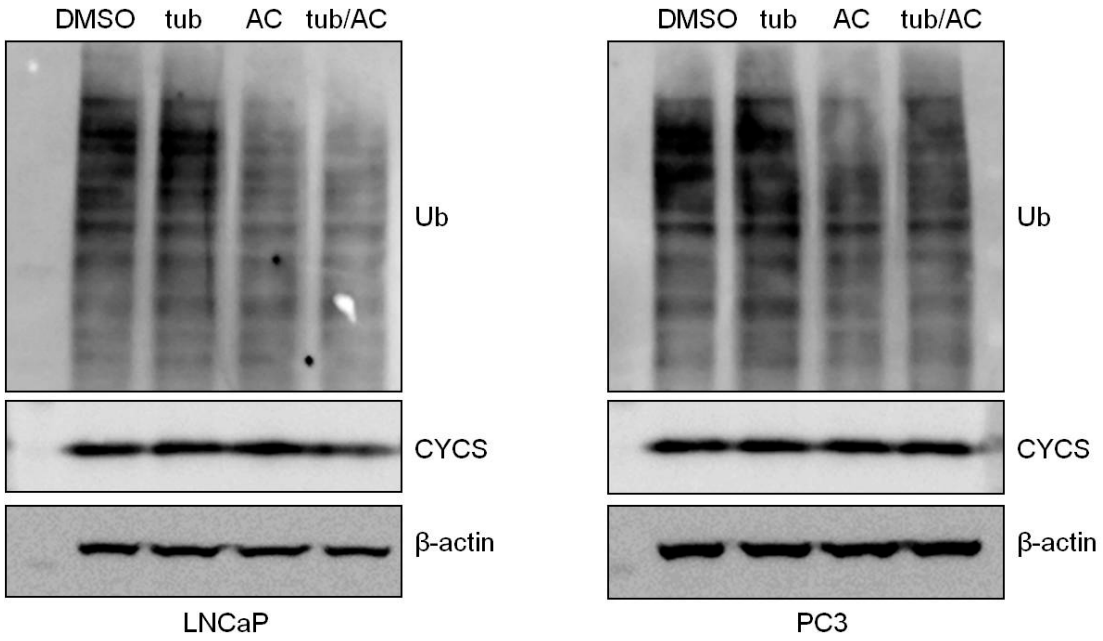

Figure 4.4. Tubacin does not influence global ubiquitinated protein levels or mitochondrial turnover. Known p62 and HDAC6 substrates were assessed to determine whether altered p62 levels influenced substrate degradation. PC3 and LNCaP cells were treated as in Fig. 1. Membranes were probed for poly-ubiquitin (Ub) and mitochondrial marker cytochrome c (CYCS). One representative blot from at least three independent experiments is shown (same samples depicted in Fig. 1).

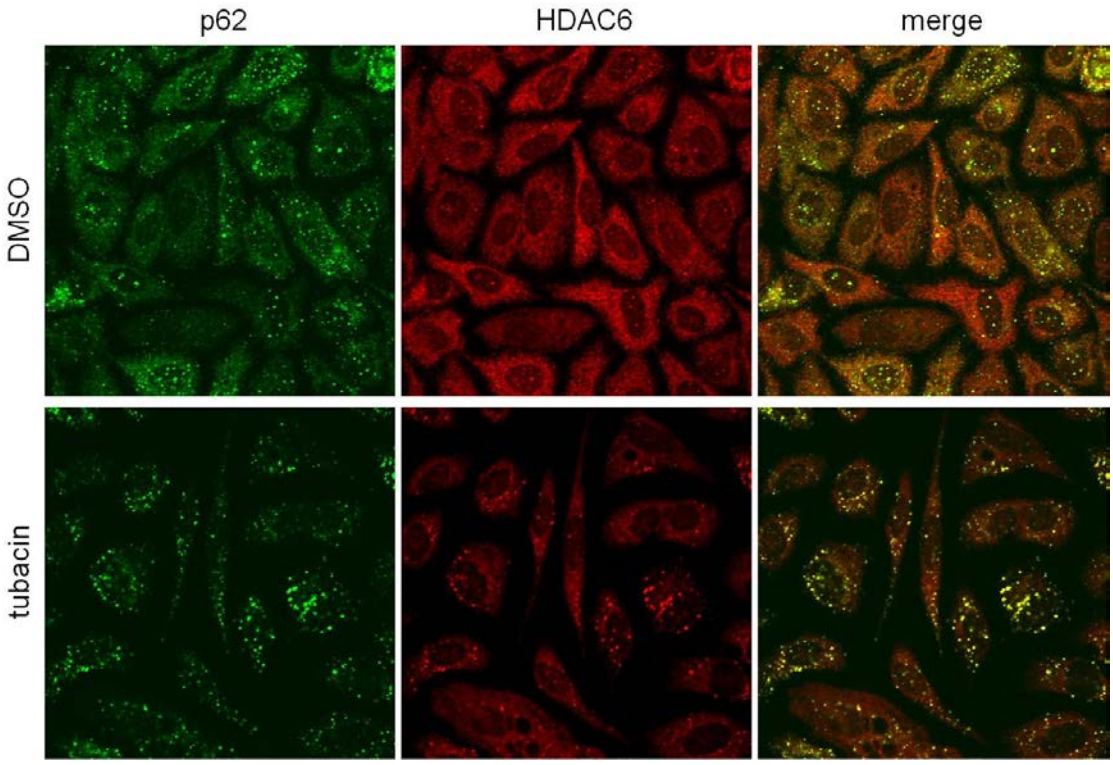

Figure 4.5. Tubacin leads to an increase in HDAC6 foci in PC3 cells. PC3 cells were treated with control (DMSO) or tubacin for 24 hours prior to processing for HDAC6 (red) and p62 (green) visualization by confocal microscopy. HDAC6 formed cytoplasmic foci in response to tubacin. HDAC6 foci strongly colocalized with p62 foci.

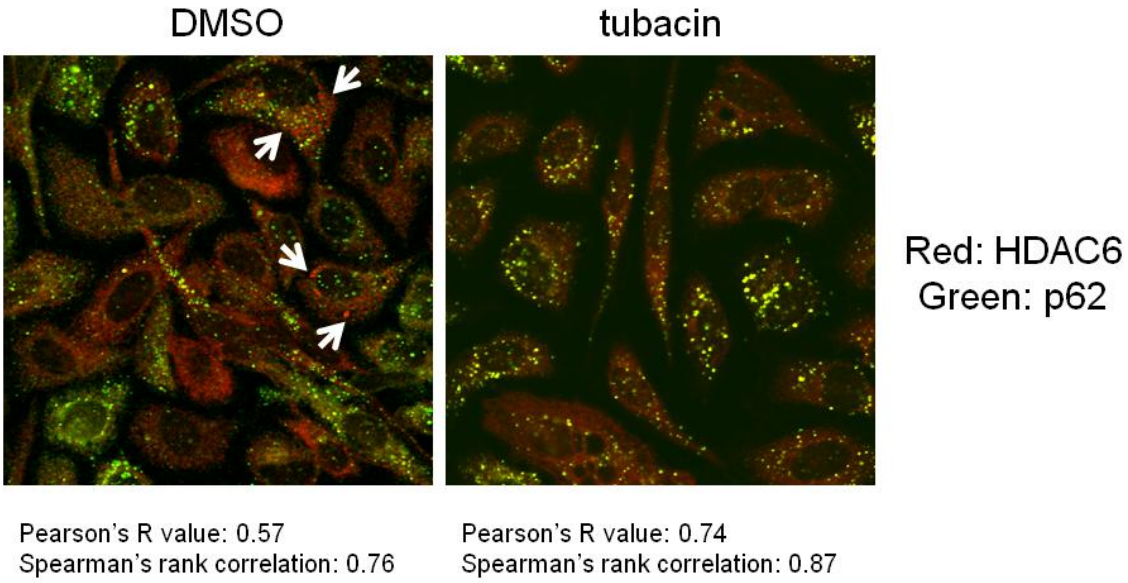

Figure 4.6. Tubacin stimulates increased HDAC6 and p62 association. PC3 cells were treated with control (DMSO) or tubacin for 24 hours and then processed for p62 (green) and HDAC6 (red) localization. HDAC6-only puncta are observed only in DMSO-treated cells (marked by white arrow). Analysis of colocalization by Pearson's R and Spearman's rank correlation indicated an increase in association following tubacin treatment.

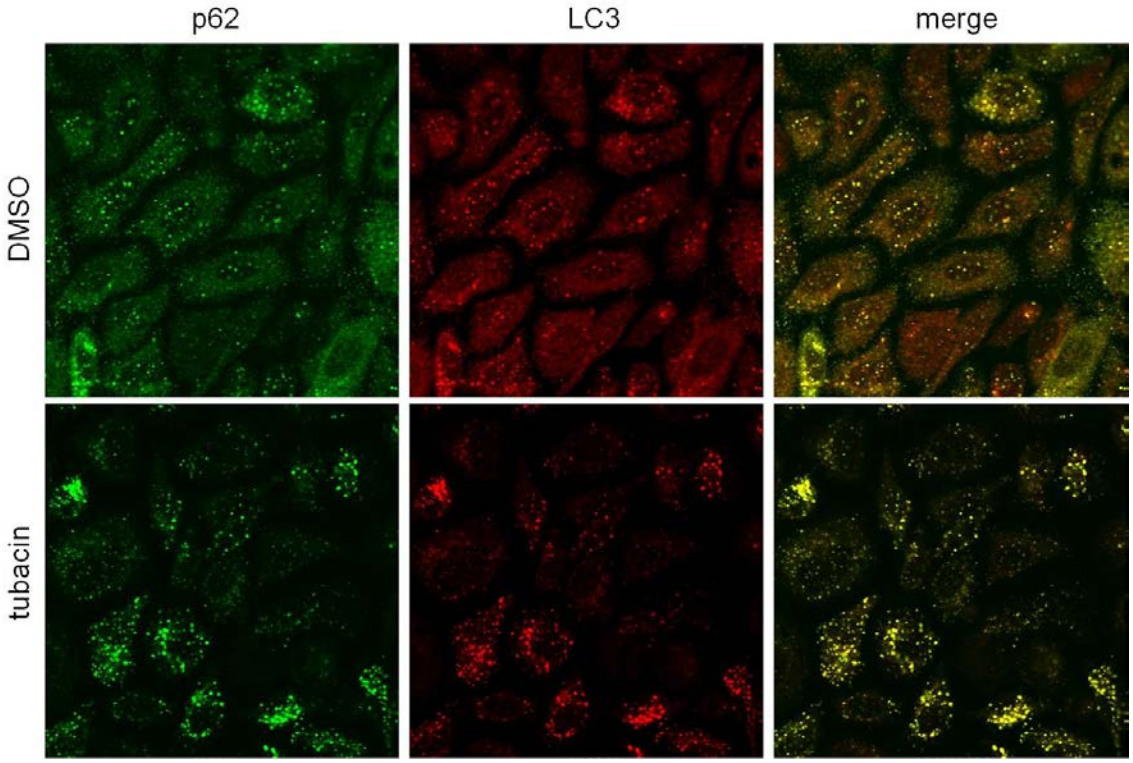

Figure 4.7. Tubacin leads to the appearance of LC3 puncta in PC3 cells. PC3 cells were treated with control (DMSO) or tubacin for 24 hours prior to processing for p62 (green) and LC3 (red) visualization by confocal microscopy. Tubacin led to an increase in LC3 puncta in PC3 cells. LC3 puncta colocalized with p62 foci.

Chapter 5.

Assessment of global proteome in LNCaP cells by 2D-RP/RP LC-MS/MS following sulforaphane exposure

Gregory W Watson, Samanthi Wickramasekara, Claudia S Maier, David E Williams, Roderick H Dashwood, Emily Ho

EuPA Open Proteomics

Elsevier Inc.

225 Wyman Street, Waltham, MA, USA

Submitted May 19, 2015

5.1 Abstract

The phytochemical sulforaphane can induce cell cycle arrest and apoptosis in metastatic prostate cancer cells, though the mechanism of action is not fully known. We conducted a global proteome analysis in LNCaP metastatic prostate cancer cells to characterize how global protein signature responds to sulforaphane. We conducted parallel analyses to evaluate semi-quantitative 1-dimensional versus 2-dimensional liquid chromatography tandem mass spectrometry (LC-MS/MS) and their utility in characterizing whole cell lysate. Our findings show that 2-dimensional LC-MS/MS can be a useful tool for characterizing global protein profiles and discovering proteins that have not previously been implicated in prostate cancer growth and maintenance.

Keywords: prostate cancer, sulforaphane, mass spectrometry

5.2 Introduction

Sulforaphane (1-isothiocyanato-4-methylsulfinylbutane) is a plant derived isothiocyanate that can stimulate cell death in metastatic prostate cancer cells while sparing normal prostate epithelial cells under similar conditions (1). Although this cytotoxic effect has been known for some time, the underlying proteins and signaling networks that control the response to sulforaphane are not fully characterized. Characterizing the response to sulforaphane in metastatic prostate cancer cells, and defining the biological significance of observed responses, may therefore identify proteins and/or pathways that confer cancer-selective cytotoxicity.

Sulforaphane stimulates a global change in gene transcription in prostate cells that is both dose- and time-dependent (2, 3). Analysis of such global expression data has been used to infer the outcome of sulforaphane treatment; however, there is reason to believe that this type of analysis fails to capture biologically relevant responses to sulforaphane that govern proliferation and cell

fate decisions. Gene transcription is known to correlate poorly with protein level in prostate cancer cells (4), which can be a consequence of many factors (e.g. protein stability, degradation rate, mutation, etc), suggesting that drawing conclusions regarding phenotypic outcome based on gene transcription alone may be misleading. Analysis of transcript levels also cannot provide a full picture of immediate responses that influence protein synthesis, stability or activity that is regulated through control of translation or post-translational modification (5). This is particularly relevant with respect to sulforaphane since previous research has noted a decrease in mammalian target of rapamycin (mTOR) activity, a master regulator of protein synthesis (6, 7), in response to sulforaphane that decreases global protein synthesis in prostate cancer cells (8). Furthermore, although some changes in gene transcription may lead to rapid protein production, others will take an extended time period to manifest at the protein level. These observations suggest that transcript analyses cannot provide a complete picture of the response to sulforaphane in prostate cancer cells and that alternative methods that directly assess protein levels will provide a clearer and more accurate characterization of the factors that control cell fate following sulforaphane exposure. We therefore applied proteomics to characterize the protein profile of LNCaP metastatic prostate cancer cells and how it responds to sulforaphane.

Proteomic approaches have previously been applied to identify sulforaphane-responsive proteins in several cell types (9-12), though none have utilized an analysis of whole cell lysate to assess the global proteome and how it responds to sulforaphane in prostate cancer cells. We therefore subjected control- and sulforaphane-treated LNCaP whole cell lysate to liquid-chromatography tandem mass spectrometry (LC-MS/MS) for unbiased assessment of potential alterations in global protein profile. We evaluated the standard protocol of peptide trapping and cleaning upstream of 1-dimensional (1D) separation in parallel with 2-dimensional (2D) reversed-phased (RP)/RP separation of lysate prior to MS/MS analysis. 2D-RP/RP-LC-MS/MS has been

shown to increase proteome coverage relative to standard methods (13-18) and could substantially increase our ability to detect changes in proteome in response to sulforaphane or identify proteins that have not yet been implicated in prostate cancer cell biology. Two-dimensional separation was found to be superior to standard 1D methods in terms of proteome coverage and protein coverage. Although we observed no global remodeling of the proteome in response to sulforaphane under our experimental conditions, increased proteome coverage by 2D separation methods did identify biologically relevant proteins that influenced cancer cell proliferation, suggesting 2D-RP/RP-LC-MS/MS may be a useful tool for the discovery of novel protein targets for therapeutic evaluation.

5.3 Materials and Methods

5.3.1 Chemicals and Reagents

Sulforaphane was purchased from LKT Laboratories (St. Paul, MN, USA) and resuspended in dimethyl sulfoxide (DMSO) (EMD Millipore, Darmstadt, Germany). Primary antibodies for TRIAP1 (Santa Cruz Biotechnology, Dallas, TX, USA), fibrillarin (Santa Cruz Biotechnology), p-S780-RB (Cell Signaling Technology, Danvers, MA, USA), cyclin B1 (Cell Signaling), cyclin D2 (Santa Cruz Biotechnology), p21 (Santa Cruz Biotechnology), NQO1 (Santa Cruz Biotechnology), cleaved poly-ADP ribose polymerase (cPARP) (Cell Signaling Technology), and GAPDH (Santa Cruz Biotechnology) were used in accordance with the manufacturer's protocol. HRP-conjugated secondary antibodies (Santa Cruz Biotechnology) for Western Blotting detection and AlexaFluor-conjugated secondary antibodies for immunofluorescence/confocal imaging (Life Technologies, Eugene, OR, USA) were used in accordance with the manufacturer's protocol. LC/MS grade solvents were purchased form EMD Millipore (Billerica, MA, USA).

5.3.2 Cells and Culture Conditions

LNCaP metastatic prostate cancer cells were purchased from American Type Culture Collection (ATCC, Manassas, VA, USA). Cells were maintained in RPMI-1640 media with L-glutamine supplemented with fetal bovine serum (FBS, 50 ml FBS / 500 ml media) at 37°C 5% CO_2. Cell lines were validated by Idexx Radil (Columbia, MO, USA) on December 24, 2012. Subconfluent cells were treated under the indicated conditions prior to harvest. Sulforaphane was used at 15 µM final concentration. DMSO was used for control treatments.

5.3.3 Sample preparation for LC/MS analysis

LNCaP cells were treated for 24 hours with DMSO (control) or sulforaphane prior to harvest. Treatments were performed as 2 independent experiments. Cells were rinsed in 50mM Tris-HCl pH 7.8 and harvested in 0.5M urea, 50mM Tris-HCl pH 7.8, 5mM DTT. Lysate was heated at 95°C for 20 minutes then cleared of insoluble material by centrifugation (10 minutes, 13000 rpm, 4°C). One milligram protein per sample was digested overnight with Trypsin-Gold in accordance with the manufacturer's instructions (Promega). Digestion was terminated with trifluoroacetic acid (TFA). Protein digests were analyzed at the Mass Spectrometry Core Facility at Oregon State University.

5.3.4 LC/MS analysis

Each sample was analyzed twice (two injections, technical replicates) for downstream determination of treatment response. Methods for 1D LC-MS/MS have been described previously (19). Waters 2D nano acquity UPLC system (Waters Corp., Milford, MA, USA) in "2D with dilution" configuration was used for the 2-dimentional analysis. System performance tests were conducted according to the manufacturer protocol prior to the experiments. Peptide sample solution (10 µl) was initially loaded onto XBridge300 (C18. 5um, 1.0x 50 mm) reverse phase column using 20 mM ammonium formate (pH10) with a flow rate of 2

ul/min for 20 mins. Peptide samples were then eluted from the high pH trapping column and loaded onto the analytical trapping column (Symmetry C18, 130Å, 5 µm, 300 µm X 50 mm) by using varying concentration of ACN fractions (11.1, 14.5, 17.4, 20.8, 45 and 65%). Eluted peptides were diluted with 0.1% formic acid at a flow rate of 20 ul/min for 5 min. After this period, the column valve was switched to allow the elution of peptides from the trapping column onto the analytical column. Separation of peptides was achieved by reverse-phase chromatography using a C18 column (Agilent Zorbax 300SB-C18, 250 x 0.3 mm, 5 µm) at flow rate of 5 ul/min. Water and ACN with 0.1% formic acid were used as solvent A and solvent B respectively. The linear gradient employed was 5–35% B in 45 min. Mass spectrometric analysis was carried out in the same manner as the 1D analysis.

For variation analysis, MASCOT and X!Tandem peptide identification and protein assignment were analyzed as groups based on technical replicates or treatment samples from the 2D dataset (Supplemental Data File). Spectra were summed across fractions for each protein to acquire total spectra count. Sample #4 was omitted from the technical variation analysis due to failure of Replicate #2. The mean spectra count between technical replicates or treatment samples was then calculated for each protein. Coefficient of variation (CV) for each protein was calculated based on standard deviation and the calculated mean spectra count. X!Tandem thresholds for this analysis: 5% false discovery rate (FDR) for protein identification, 5% FDR for peptide identification, 2 peptide minimum for positive protein identification. Data was plotted and analyzed using GraphPad Prism Software (La Jolla, CA, USA).

5.3.5 Protein Preparation and Western Blot Analysis

Protein lysates were prepared in RIPA protein lysis buffer (150 mM NaCl, 1% Triton X-100, 0.5% NaDOC, 0.1% SDS, 20 mM TRIS pH 8.0) supplemented with protease inhibitor cocktail (Thermo, Waltham, MA, USA). Lysates were

cleared by centrifugation at 4°C and quantitated by DCA Protein Assay (BioRad, Hercules, CA, USA). Equal amounts of protein were separated by SDS-PAGE and blotted to a PVDF membrane (BioRad) using NuPAGE Reagents and equipment in accordance with the manufacturer's protocol (Life Technologies). Membranes were blocked and probed for the indicated proteins following standard protocols. For protein detection, membranes were incubated in SuperSignal West Femto Reagent (Thermo) and developed on the AlphaInnotech FluorChem 8900 system (ProteinSimple, San Jose, CA, USA). Densitometric analyses were performed on the native membrane image using AlphaInnotech FluorChem 8900 software (ProteinSimple). For each membrane, the relative densitometric value of each replicate for a given probe was normalized to the corresponding relative level of the normalizing protein. For graphing, treatments are expressed relative to Control (set to the value 1).

5.3.6 TRIAP1 Cloning

TRIAP1 was amplified from LNCaP cDNA prepared as described previously (19) using the following primers: Sense 5' – TACTACTTAAGCTTATGAACAGTGTGGGGGAGGCATGCACGGACATGAA – 3', Antisense 5' – TCTGAGAGCGGCCGCTTAATTAATTATCAAGAAGAATTTTCAGGCTTTTCTTTGCCATG – 3'. The amplification product was cloned into pCR2.1 TOPO TA cloning vector in accordance with the manufacturer's protocol (Life Technologies). Plasmids were isolated using the PureLink Quick Plasmid Miniprep Kit from Life Technologies and checked for TRIAP1 insert by PCR amplification (Sense: 5' – CGACCTCTTCAAGCGCTACC – 3', Antisense: 5' – CCCATGAACTCCAGTCCTTCAA – 3'). TRIAP1 coding sequence was moved into pCMV6-AC-GFP expression vector by *EcoRI* digest and T4 DNA Ligase (Life Technologies) in accordance with the manufacturer's protocol (New England Biolabs, Ipswich, MA, USA). Ligation products were transformed and grown in

TOP10 competent cells following the manufacturer's instructions (Life Technologies). Plasmids were isolated as above and screened for insert and directionality by PCR (TRIAP1 primers listed above and VP1.5 primer). The correct construct was verified by assaying protein expression following transient transfection in LNCaP cells.

5.3.7 Analysis of Exogenous TRIAP1 in LNCaP Cells

LNCaP cells were grown in 6-well plates and transfected with pCMV6-AC-GFP or pCMV6-TRIAP1 with Lipofectamine 2000 in accordance with the manufacturer's protocol (Life Technologies). Cells were placed under G418 selection (500 µg/ml) 24 hours post-transfection. Cells were taken off selection for 24 hours after non-transfected cells were eliminated (4-6 days) prior to beginning treatments. After the indicated treatment period, cells were harvested for protein analysis as described above.

For growth analysis, transfected LNCaP cells were prepared as above. After elimination of non-transfected cells, G418 selection was lowered to 200 µg/ml and cells allowed to expand. Cells were seeded at 50,000 cells per well in 24-well plates for growth analysis. At 24 hours, media was replaced with selective media (200 µg/ml G418). Cells from triplicate wells were treated with trypsin, collected and counted at the indicated time-points on a hemocytometer. Media was refreshed every other day.

5.3.8 Statistical Analysis

Graphing and statistical analyses were performed using GraphPad Prism Software. Figures depict one representative experiment. Graphs depict mean + SEM for at least two independent experiments. Statistical significance was determined by Student's *t*-Test. Significance is indicated by asterisk, with * = $p < 0.05$, ** = $p < 0.01$, *** = $p < 0.001$.

5.4 Results

5.4.1 2-dimensional analysis improves protein identification and coverage in cell lysate

A significant drawback to analysis of complex mixtures such as whole cell lysate by LC-MS/MS using standard 1D separation techniques is co-elution of parent peptides (i.e. low resolution). One method to decrease the impact of this complication is to apply 2D separation techniques to complex peptide mixtures prior to MS/MS analyses. We therefore applied 2-dimensional separation reverse-phase (RP)/RP LC-MS/MS to tryptic digests of LNCaP metastatic prostate cancer cells to assess potential changes in protein profile and identify candidate biologically relevant proteins that may have a role in the cellular response to sulforaphane (Figure 5.1). Two-dimensional analyses significantly increased the number of high-confidence proteins identified in LNCaP whole cell lysate compared to 1D analysis (Figure 5.1A): 244 proteins versus 117 (DMSO) and 219 versus 121 (SF). Increasing separation also significantly increased the coverage of proteins identified (Figure 5.1B-D). Two-dimensional analyses increased percent coverage by an average of 44% in proteins identified in both 1D and 2D analyses.

5.4.2 Sulforaphane does not alter global protein profile in LNCaP cells

To test whether sulforaphane stimulates a rapid response in the cellular proteome in metastatic prostate cancer cells, LNCaP cells were exposed to DMSO (control) or 15 µM sulforaphane for 24 hours and then processed for proteomic analyses. Treatments were carried out as two biological replicates, and each replicate was analyzed as two technical replicates (two injections) for downstream analysis and signal determination. To assess whether sulforaphane stimulates a change in the relative level of proteins identified in both control- and sulforaphane-treated LNCaP cells, coefficient of variation (CV) was plotted

against mean spectra count for data analyzed as technical replicate samples (open circles) or as treatment samples (red triangles) (DMSO versus sulforaphane) (Figure 5.3). A large CV between treatment samples will indicate high variability in protein level and a potential sulforaphane effect. As seen in the log transformed plot in Figure 5.3A, log CV decreases as log mean spectra count increases. A residual plot of deviation from a line fit to each group for each data point in Figure 5.3A showed that variation between treatment samples is consistent with technical variation, suggesting no treatment effect (Figure 5.3B). A box plot of residuals for technical replicates and treatment samples also did not indicate specific proteins deviate from what is technical variation (Figure 5.3C).

The above analysis is appropriate for assessing relative change in protein level, but could miss rapid induction or degradation between treatments. An analysis for proteins unique to one technical replicate or one treatment group was therefore conducted (Figure 5.3D). The percent of unique proteins between treatment groups was lower than what was observed between technical replicates (31.1% versus 40.9%, respectively) (Figure 5.3D). A box plot of spectra count for unique proteins identified in technical replicates and treatment samples also suggested that sulforaphane does not lead to rapid protein induction/degradation at the global level (Figure 5.3E). Proteins with a spectra count under 4 in our analysis dominated the population of unique protein identifications, suggesting that identification of low-spectra count proteins may be largely stochastic.

5.4.3 Identification of TRIAP1 in LNCaP cells

Although sulforaphane did not lead to a rapid shift in protein profile at a global level, the phytochemical is known to stimulate induction, modification or degradation of discrete proteins (20). We therefore manually analyzed the proteins identified by 2D analysis for high-confidence proteins that may be involved in the cellular response to sulforaphane. Global analyses identified

proteins involved in a wide array of cellular processes (Supplemental Data File). We narrowed our focus to proteins involved in cell proliferation and/or apoptosis since we are interested in using increased proteome coverage to identify novel proteins that may respond to sulforaphane and have a role in these processes in metastatic prostate cancer cells. TP53-regulated inhibitor of apoptosis 1 (TRIAP1; p53CSV) was identified in sulforaphane-treated LNCaP lysate and has not previously been reported as a sulforaphane-responsive protein. TRIAP1 is regulated by p53, an key transcription factor in stress response, cell fate and apoptosis, and sulforaphane is known to stimulate a p53 response in LNCaP cells (21-24). We therefore focused our analyses on determining whether TRIAP1 responds to sulforaphane and whether TRIAP1 has a role in LNCaP cell-maintenance. Sulforaphane treatment led to a transient decrease in TRIAP1, though the effect did not reach statistical significance (Figure 5.4).

5.4.4 TRIAP1 influences growth rate in LNCaP cells

TRIAP1 has not previously been reported as a sulforaphane-responsive protein and the consequences of altered expression levels in metastatic prostate cancer cells are not known. To understand what role TRIAP1 may play in LNCaP cells and in the response to sulforaphane, we provided exogenous TRIAP1 and then treated cells with sulforaphane or DMSO (control).

Exogenous TRIAP1 decreased proliferation in LNCaP cells (Figure 5.5A). Despite slowing proliferation rate, increased TRIAP1 levels did not significantly alter the protein level of select cell-cycle regulators relative to GFP-control (Figure 5.5B). We observed no influence on the level of phospho-Retinoblastoma (p-S780-RB), cyclin B1, cyclin D2 or p21. TRIAP1 also did not significantly influence the cellular response to sulforaphane in LNCaP cells; sulforaphane led to decreased cyclin levels, increased p21 and increased NQO1 protein levels and was not dependent on TRIAP1 levels (Figure 5.5B). An assessment of cleaved-polyADP-ribose polymerase (cPARP) also suggested that TRIAP1 does

not impair mitochondrial integrity or sensitize LNCaP cells to sulforaphane (Figure 5.6).

5.5 Discussion

In this investigation we utilized an unbiased 2D LC-MS/MS approach to characterize potential changes in the cellular proteome in LNCaP metastatic prostate cancer cells following sulforaphane treatment. Characterizing the proteome and potential changes in response to sulforaphane can provide a broad view of the proteins and processes that may mediate the cancer-cytotoxic effects associated with sulforaphane as well as identify new proteins that influence LNCaP cell growth/survival and may be evaluated as potential novel therapeutic targets.

Sulforaphane is known to stimulate global changes in gene expression and has been shown to enhance protein degradation through the proteasome in some cell types, including metastatic prostate cancer cells (2, 3, 9, 19, 25-29). This suggests a remodeling of the cellular proteome following exposure. However, we did not identify any change in global protein signature following sulforaphane treatment in LNCaP cells (Figure 5.3). This suggests that although sulforaphane can modulate the expression of many genes, from a global view, the proteome is relatively stable. This is not to suggest that sulforaphane does not influence the level of discrete proteins. In our molecular analysis we did confirm well characterized changes in specific cell cycle regulators and cytoprotective enzymes (Figure 5.5). Our global view likely missed these proteins for several reasons. Although 2D analysis is superior to 1D analysis (Figure 5.1), it may still lack sufficient resolution to identify low-abundance proteins or proteins that have been transcriptionally activated but have not accumulated to a high enough level to be detected. Increasing the number of fractions per sample may provide further improvements in detecting lower-abundance proteins. In addition, other techniques such as data-independent acquisition and SWATH-MS (30)

may be better suited to identify lower-abundance proteins in complex whole cell lysate and could be worth exploring in future work. Despite these limitations, expanding proteome coverage by 2D LC-MS/MS did identify many proteins for assessment for biological relevance in LNCaP proliferation and/or survival (Fig. 1).

TRIAP1 was identified in our 2D LC-MS/MS analysis and has not previously been characterized in LNCaP cells. TRIAP1 expression is controlled by p53, and sulforaphane is known to induce a cell stress response that leads to p53 stabilization and activation in LNCaP cells (21-23). This suggests that TRIAP1 may be a downstream mediator of the p53 response in LNCaP cells. TRIAP1 has been reported as having a role in cell cycle regulation in several cancer cell lines, though its role is cell-line-dependent. The protein is reported to directly influence p21 protein levels and therefore influence cell cycle arrest and apoptosis (31). TRIAP1 has also been reported to have a more direct role in apoptosis through maintaining mitochondrial integrity (32). We found that sulforaphane led to a transient decrease of TRIAP1 in LNCaP cells (Figure 5.4), suggesting a potential role in influencing cell growth and survival.

To assess any role for TRIAP1 in cell proliferation we provided exogenous TRIAP1 in LNCaP cells and then monitored cell cycle regulators and growth (Figure 5.5). TRIAP1 did not significantly influence p21 levels, indicating TRIAP1 does not directly regulate p21 in LNCaP cells. Exogenous TRIAP1 also did not influence other selected cell cycle regulators (Figure 5.5B) or basal apoptotic signaling as assessed by cPARP (Figure 5.6). Having discovered no direct influence on previously characterized TRIAP1 processes in LNCaP cells, we assessed a potential role for influencing the response to sulforaphane (Figure 5.5B and Figure 5.6). Sulforaphane led to similar decreases in p-S780-RB, cyclin B1 and cyclin D2, and similar induction in p21 and NQO1 regardless of TRIAP1 level. Increased TRIAP1 also did not influence apoptotic signaling in response to sulforaphane in LNCaP cells (Figure 5.6). Although TRIAP1 did not influence

select proteins involved in cell cycle regulation, exogenous expression did significantly decrease cell proliferation (Figure 5.5A) and is consistent with it being a downstream effector of p53. Further work will be needed to understand how TRIAP1 leads to decreased growth and will be an interesting area of future research.

5.6 Conclusion

2D-RP/RP-LC-MS/MS is a useful tool for analyzing global protein profile in an unbiased manner from whole cell lysate. This method provided greater coverage of the global proteome and also increased the coverage of discrete proteins relative to standard methods. Enhanced proteome coverage by 2D methods can be used to identify previously unreported proteins that influence cell behavior in metastatic prostate cancer cells and thus identify new potential targets for therapeutic development.

5.7 Acknowledgements

The authors would like acknowledge Dr. Carmen Wong for providing feedback during manuscript drafting. This work was supported by the National Institutes of Health (CA090890), National Institute of Environmental Health Sciences (P30 ES000210), and Oregon Agricultural Experimental Station.

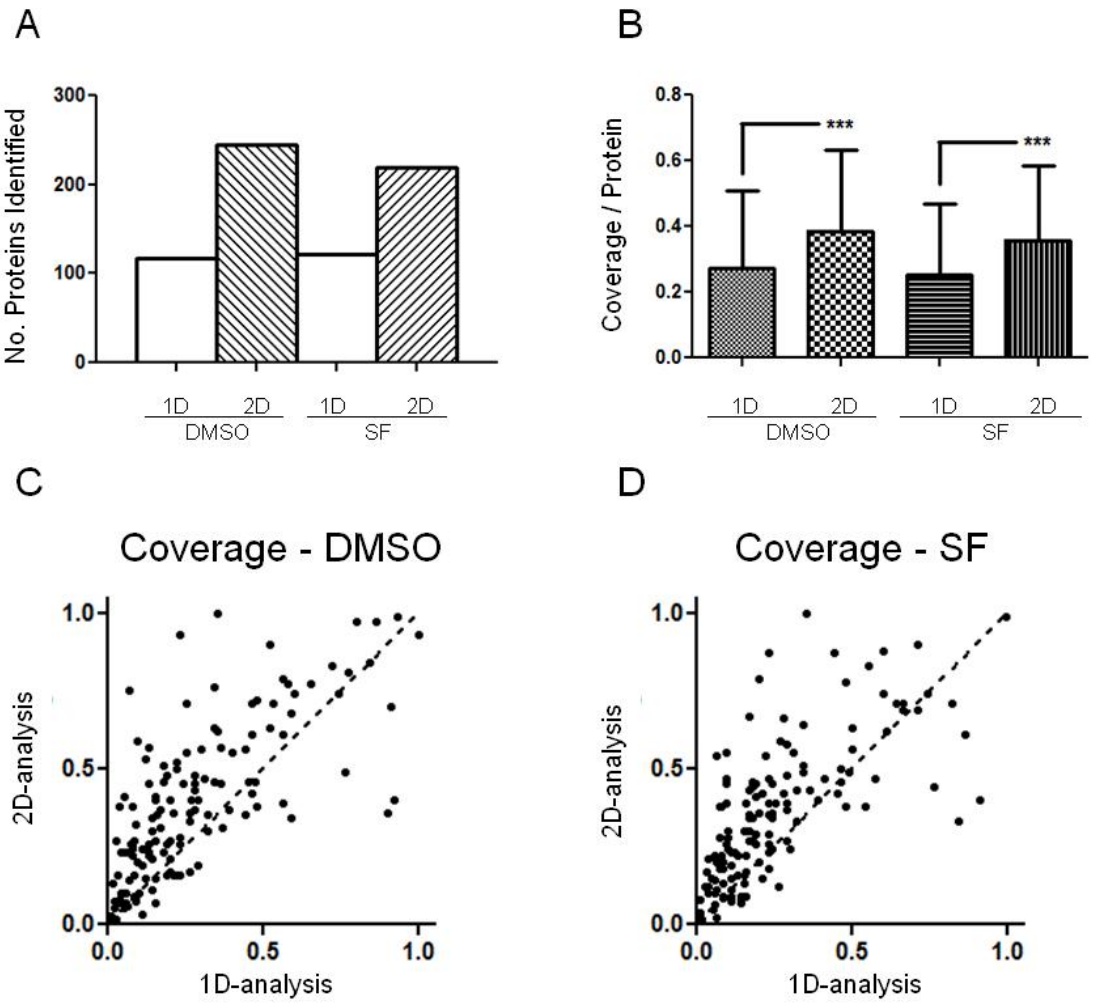

Figure 5.1. Two-dimensional separation of whole cell lysate increases protein identification and coverage. LNCaP cells were treated with DMSO or sulforaphane for 24 hours prior to harvest. Lysate was subjected to 1D and 2D LC-MS/MS analysis for assessment of cellular proteins. (A) The number of proteins identified by 1D and 2D analysis by treatment group in LNCaP whole cell lysate. (B) Average coverage per protein identified in the analyses. 2D methods significantly increased coverage per protein. (C and D) Scatter plots by treatment group of 2D coverage versus 1D coverage. Each point represents a unique protein identified by both 1D and 2D method.

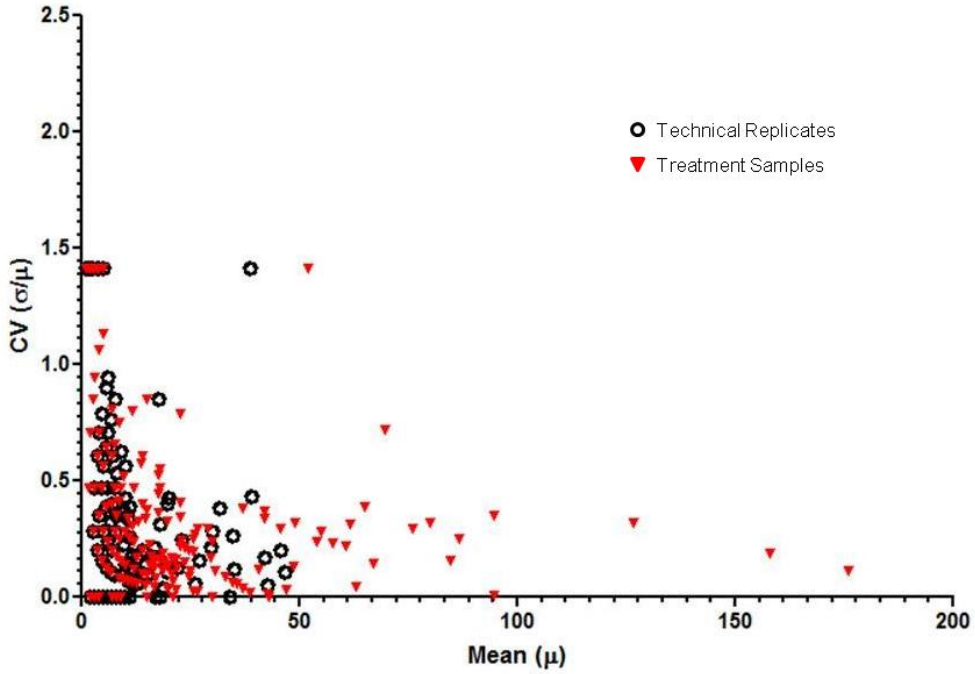

Figure 5.2. Scatter plot of variation for technical replicates and treatment samples. Variation plotted as a function of mean spectra count for proteins identified in both technical replicates (open circles) or treatment groups (red triangles). Data corresponds to transformed data presented in Fig. 2.

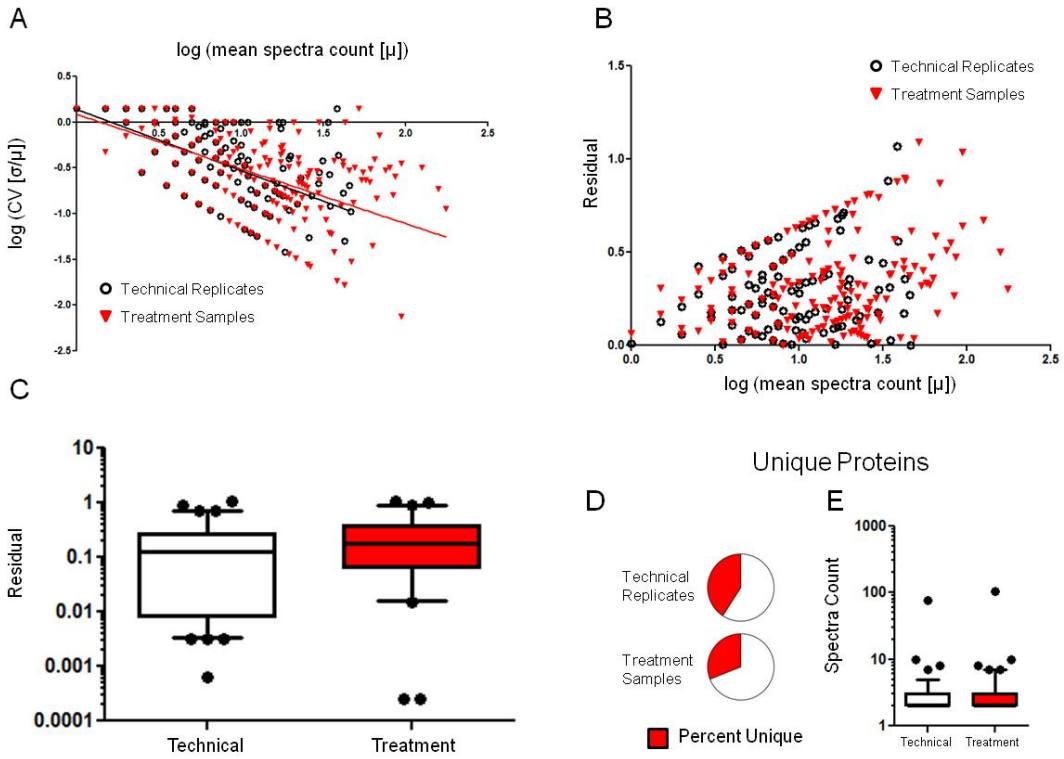

Figure 5.3. Sulforaphane does not alter global protein profile in LNCaP cells. Data from 2D analysis was analyzed for changes in global protein profile. (A) log (CV [σ/μ]) versus log (mean spectra count [μ]) for data separated by technical replicates (open circles) and treatment samples (red triangles). A line was fit to each group for downstream analysis of residuals (Technical Replicates: Y = -0.6694 X + 0.1427; Treatment Samples: Y = -0.5970 X + 0.08734). (B) Residual plot for Technical Replicates and Treatment Samples as a function of log (mean spectra count [μ]) for the chart in (A). (C) Box plot of residuals based on group (Technical versus Treatment) (whiskers 1-99 percentile). (D) Percent of proteins identified by 2D analysis that were unique to each group (Technical versus Treatment). (E) Box plot of spectra count for unique proteins identified in the analysis separated by group (Technical versus Treatment) (whiskers 5-95 percentile).

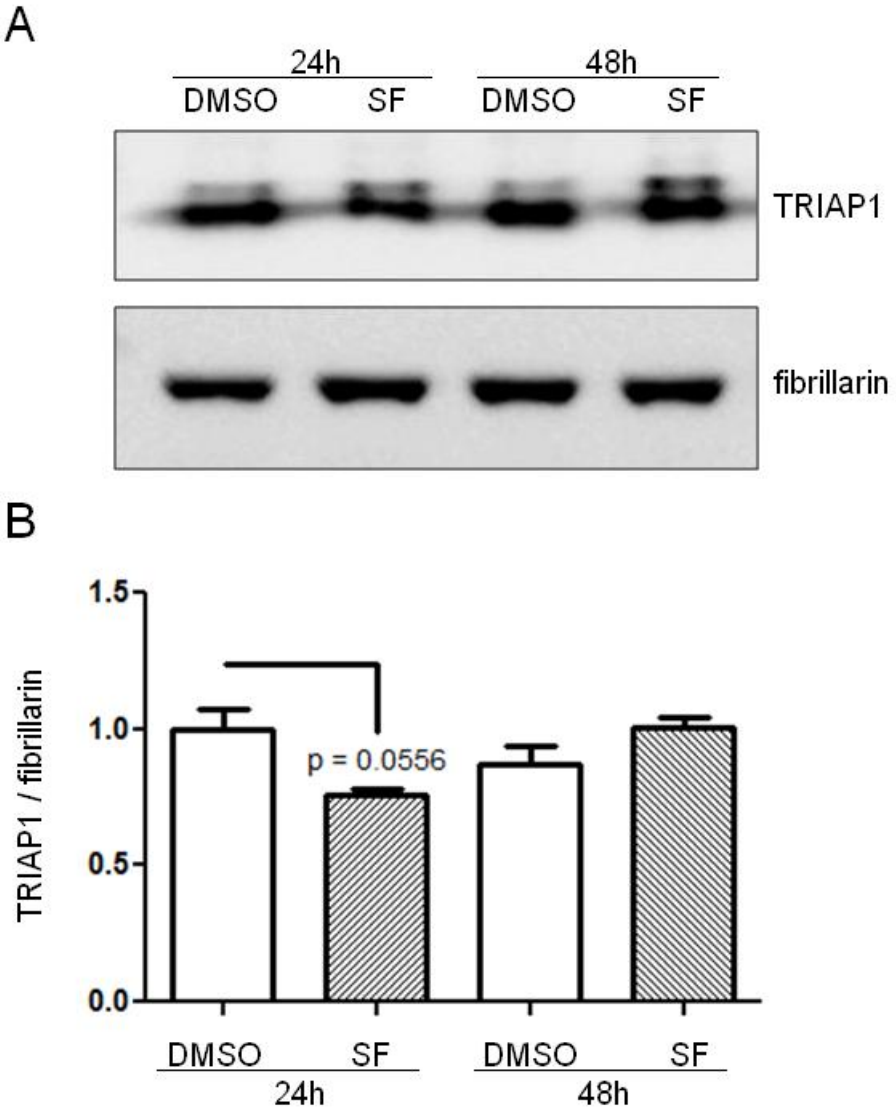

Figure 5.4. Sulforaphane influences TRIAP1 protein level in LNCaP cells. (A) Representative blot of TRIAP1 protein at 24 hours and 48 hours after sulforaphane treatment. The nuclear protein fibrillarin was probed as a loading control. (B) Sulforaphane causes a transient decrease in TRIAP1 protein in LNCaP cells. Graph represents 2 independent experiments (mean + SEM).

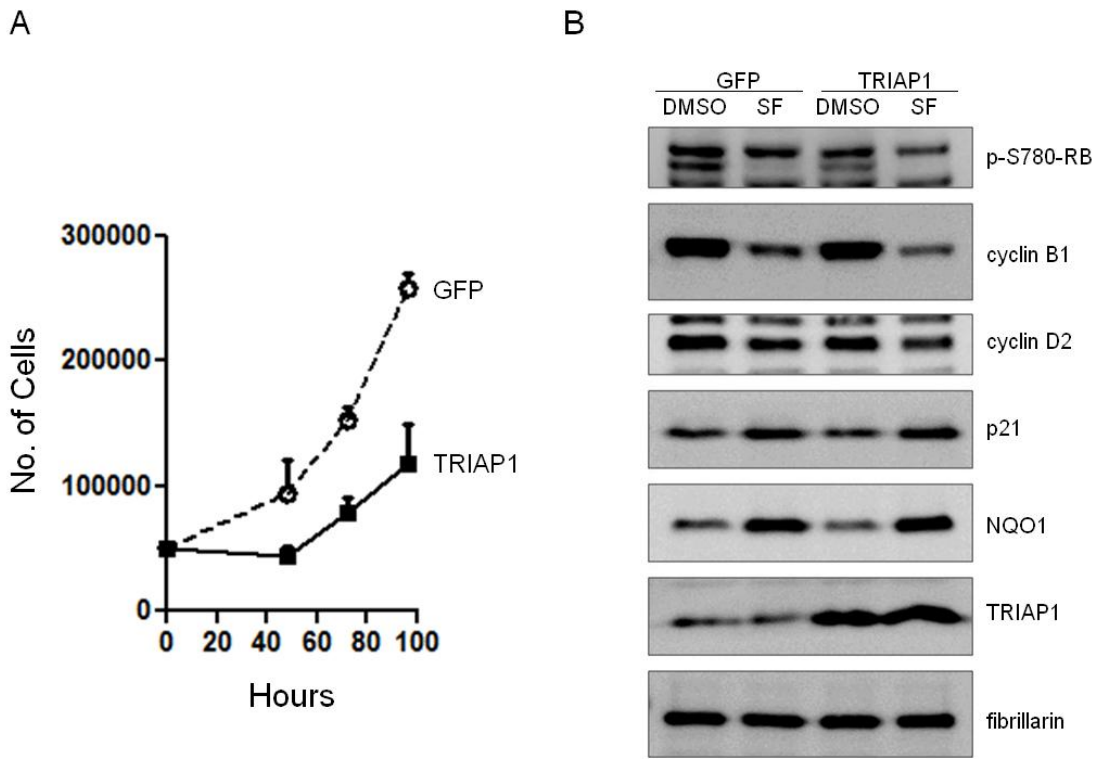

Figure 5.5. TRIAP1 influences cell proliferation in LNCaP cells. (A) Growth curve of LNCaP cells expressing exogenous TRIAP1 or GFP (control). Cells were counted at 48, 72 and 96 hours post-seeding. (B) LNCaP cells expressing exogenous TRIAP1 or GFP (control) were treated with DMSO (control) or sulforaphane for 48 hours and analyzed for the indicated proteins. p-S780-RB, cyclin B1, cyclin D2 and p21 were analyzed to assess the influence of TRIAP1 and sulforaphane on cell cycle regulators. NQO1 was analyzed as a marker for sulforaphane response. The nuclear protein fibrillarin was probed as a loading control.

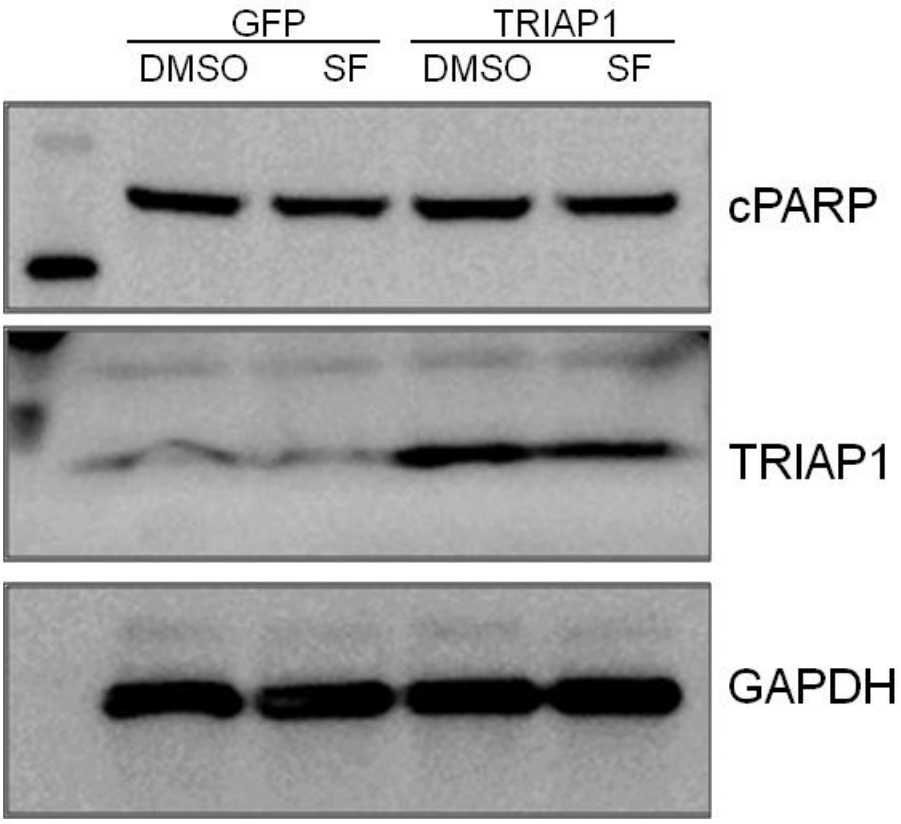

Figure 5.6. TRIAP1 does not influence apoptotic signaling or sensitize LNCaP cells to sulforaphane. LNCaP cells were treated and prepared as described in Fig. 4. Cleaved poly-ADP ribose polymerase (cPARP) was probed to assess apoptotic signaling. GAPDH was probed as a loading control.

Chapter 6.

General Conclusions

Sulforaphane has shown promising results as a cancer chemotherapeutic compound in pre-clinical models of carcinogenesis in tissues such as the lung and colon. *In vitro* work from multiple independent research groups utilizing human prostate cancer cell lines and a pre-clinical model of prostate carcinogenesis has led to the proposal that sulforaphane may also be suitable for development as a prostate cancer chemotherapeutic agent. In these previous studies various modes of suppression have been proposed, but the ultimate intended outcome is prostate cancer growth arrest and apoptosis. In this dissertation we aimed to characterize the response to sulforaphane in metastatic prostate cancer cells at concentrations and exposure times similar to what is expected to be experienced *in vivo*. As part of this dissertation, we identified novel responses to sulforaphane involving chromatin regulation, demonstrated induction of autophagic flux at high concentrations, and identified a previously unrecognized regulator of cellular proliferation in LNCaP cells. In addition, this dissertation work refines our understanding of the response to sulforaphane in prostate cancer cells and opens up the door to the exciting possibility that yet to be identified factors contribute to suppression *in vivo*. Another important aspect of this dissertation is to highlight that the response to sulforaphane at physiological concentrations differs from that of a high-concentration exposure in prostate cancer cells.

In Chapter 2 we characterized a novel response to sulforaphane involving the histone methyltransferase SUV39H1 and demonstrated that SUV39H1 (or H3K9 trimethylation) can be protective in the context of cellular stress. Although we do not yet know the outcome of an early and transient decrease in H3K9me3, one would hypothesize that it is a protective response downstream of a transient increase in oxidative stress. We did observe a transient increase in SUV39H1

protein level, which is consistent with an earlier report characterizing stabilization of SUV39H1 in response to stress. However, increased SUV39H1 did not correlate with increased H3K9me3 levels in our experiments. This suggests that posttranslational control of SUV39H1 is the deciding factor in determining H3K9me3 levels in PC3 cells. We did observe an association between posttranslational modification of SUV39H1 and changes in its interaction with chromatin. Characterization of the specific modifications we observed and of the proposed nuclear localization signal we identified will be important in future work investigating SUV39H1 regulation.

A decrease in global H3K9me3 in PC3 cells despite an increase in SUV39H1 also suggests that sulforaphane influences the activity of ubiquitin-ligases (UBL) and/or deubiquitinases (DUB), which is itself a novel hypothesis. An increase is SUV39H1 ubiquitination despite a global decrease in ubiquitinated proteins further suggests specific, regulated control of SUV39H1 stability as opposed to general protein ubiquitination and turnover. Mouse double minute 2 (MDM2) has been identified as a SUV39H1 UBL, and MDM2 is known to be involved in cytoprotective damage response signaling. However, PC3 cells contain defects in damage response signaling as they are *TP53*-null. Exploring this hypothesis and the effect of sulforaphane on global UBL/DUB activity in general will be an interesting area of future research.

An interesting finding that also came out of this investigation was the novel observation that H3K9me3 decreased apoptotic signaling in PC3 cells under extreme stress. At this time, there is little known concerning how SUV39H1 may influence apoptosis, but our experiment suggests that targeting SUV39H1 may be a viable strategy to sensitize cancer cells to endogenous stressors or enhance the efficacy of chemotherapeutic stressors in cancer cells.

In Chapters 3 and 4 we set out to test the hypothesis that sulforaphane slows autophagic flux in metastatic prostate cancer cells through depletion of HDAC6 protein. Previous investigations have proposed that sulforaphane

stimulates autophagy, a cytoprotective response that is activated when cells are exposed to an array of stressors, in prostate cancer cells. However, these early reports do not provide sufficient data to draw conclusions concerning autophagic activity. Autophagy is a dynamic process which requires multiple markers to be assessed to conclude whether autophagy is up-regulated or inhibited. Specifically addressing flux is therefore required to draw conclusions about autophagy. Previous investigations suggested that depletion of HDAC6 protein following sulforaphane exposure may contribute to decreased cell viability and HDAC6 deacetylase activity has recently been shown to be required for efficient autophagic flux in mouse embryonic fibroblasts. Sulforaphane may therefore decrease cell viability through depletion of HDAC6 and inhibition of autophagic flux. What has been suggested to be a therapeutic concentration of sulforaphane (~15 μM) in a pre-clinical model of prostate carcinogenesis was not found to influence autophagic flux in prostate cancer cells. Sulforaphane did rapidly induce autophagic flux at 150 and 300 μM, but was only able to overcome cytoprotective responses and initiate a durable arrest after a 40 hour recovery period at the 300 μM concentration. HDAC6 inhibition with tubacin also did not inhibit autophagic flux in metastatic prostate cancer cells. This likely reflects cell-specific HDAC6 and autophagy functions in combination with some stimulus-dependence. Exploring how these different inputs influence flux rate will be an important area of future research, particularly in exploring the potential requirement for HDAC6 in autophagic flux where chemotherapeutic stress is the primary stimulus.

Despite recent work showing that HDAC6 may be a viable therapeutic target for some cancers, the role of HDAC6 in prostate cell biology and prostate cancer cell biology is not known. Our assessment of HDAC6-interacting proteins in LNCaP cells in Chapter 4 is a substantial contribution toward addressing this gap in knowledge. A majority of previous investigations focus on HDAC6 deacetylase activity and screen for increased protein acetylation following

HDAC6-inhibition to gain insight into the role of HDAC6 in cell biology. However, HDAC6 is a multi-domain protein with some discrete regions having functions independent of deacetylase activity. This suggests that identifying only HDAC6 enzymatic targets will miss important deacetylase-independent functions. By conducting an unbiased screen for HDAC6-interacting proteins, we will likely identify proteins that are regulated by, or otherwise influenced by, HDAC6 in a deacetylase-dependent and deacetylase-independent manner. This is important in understanding how HDAC6 may be involved in the response to sulforaphane because sulforaphane does not inhibit HDAC6 activity or decrease HDAC6 protein level (unpublished data), which suggests deacetylase-independent effects. Two key areas for further exploration would be in cellular energetics/metabolism and protein synthesis (Chapter 4 Table I). We identified direct interaction between HDAC6 and metabolic enzymes, suggesting a role in energy production or in influencing metabolic substrate generation required for proliferation. HDAC6 was also found to interact with proteins involved in protein synthesis, including ribosomal enzymes and translation-associated proteins. Exploring these various possibilities in future work will contribute to understanding the role of HDAC6 in metastatic prostate cancer cells and in the further development of HDAC6 as a therapeutic target.

In Chapter 5 we applied proteomics to capture a global view of how the proteome responds to sulforaphane in LNCaP metastatic prostate cancer cells. We found that sulforaphane does not stimulate a rapid change in global protein profile in LNCaP cells. This finding is consistent with our observations in Chapter 3 showing no significant increase in autophagic flux (i.e. lysosomal degradation) or ubiquitinated protein levels (i.e. proteasomal degradation, unpublished data) in LNCaP cells treated with sulforaphane. In the future, our proteomic approach can be further refined to increase sensitivity and proteome coverage by using alternative methods. Continuing to pursue a proteomics approach will be important in future discovery work because it directly assess the response to

sulforaphane at the protein level and avoids the caveat of translational regulation or changes in protein stability that can influence conclusions drawn from global gene expression analyses. Taken together, this work suggests sulforaphane can influence global processes in metastatic prostate cancer cells and supports the further exploration of sulforaphane as a prostate cancer therapeutic agent.

Looking forward, the above general conclusions from this dissertation work suggest the field could benefit from a well controlled drug-metabolism-pharmacokinetic (DMPK) analysis exploring higher doses of sulforaphane administered via different routes. The current data suggests higher doses (potentially much higher) are achievable and safe following a single exposure. The safety of repeated high-dose exposure is not known, but this information will be required to establish safe dosing protocols for therapeutic exploration. This will provide important information for the development of sulforaphane as a cancer therapeutic agent.

Bibliography

Chapter 1

1. Richman EL, Carroll PR, Chan JM. Vegetable and fruit intake after diagnosis and risk of prostate cancer progression. Int J Cancer 2011;131(1):201-10.
2. Liu B, Mao Q, Cao M, Xie L. Cruciferous vegetables intake and risk of prostate cancer: a meta-analysis. Int J Urol 2012;19(2):134-41.
3. Steinbrecher A, Nimptsch K, Husing A, Rohrmann S, Linseisen J. Dietary glucosinolate intake and risk of prostate cancer in the EPIC-Heidelberg cohort study. Int J Cancer 2009;125(9):2179-86.
4. Howlader N NA, Krapcho M, Neyman N, Aminou R, Altekruse SF, Kosary CL, Ruhl J, Tatalovich Z, Cho H, Mariotto A, Eisner MP, Lewis DR, Chen HS, Feuer EJ, Cronin KA (eds). SEER Cancer Statistics Review, 1975-2009 (Vintage 2009 Populations). 2012.
5. Ferlay J SH, Bray F, Forman D, Mathers C and Parkin DM. GLOBOCAN 2008 v2.0, Cancer Incidence and Mortality Worldwide: IARC CancerBase No. 10 [Internet]. International Agency for Research on Cancer; 2010 2008 [cited Accessed on 12/11/2012]; Available from: http://globocan.iarc.fr
6. Shimizu H, Ross RK, Bernstein L, Yatani R, Henderson BE, Mack TM. Cancers of the prostate and breast among Japanese and white immigrants in Los Angeles County. Br J Cancer 1991;63(6):963-6.
7. Lee J, Demissie K, Lu SE, Rhoads GG. Cancer incidence among Korean-American immigrants in the United States and native Koreans in South Korea. Cancer Control 2007;14(1):78-85.
8. IARC. IARC: Cruciferous vegetables, isothiocyanates and indoles. Volume 9. Lyon, France; 2004.
9. McNaughton SA, Marks GC. Development of a food composition database for the estimation of dietary intakes of glucosinolates, the biologically active constituents of cruciferous vegetables. Br J Nutr 2003;90(3):687-97.
10. Hanlon N, Coldham N, Gielbert A, Sauer MJ, Ioannides C. Repeated intake of broccoli does not lead to higher plasma levels of sulforaphane in human volunteers. Cancer Lett 2009;284(1):15-20.
11. Hauder J, Winkler S, Bub A, Rufer CE, Pignitter M, Somoza V. LC-MS/MS quantification of sulforaphane and indole-3-carbinol metabolites in human plasma and urine after dietary intake of selenium-fortified broccoli. J Agric Food Chem 2011;59(15):8047-57.
12. Veeranki OL, Bhattacharya A, Marshall JR, Zhang Y. Organ-specific exposure and response to sulforaphane, a key chemopreventive ingredient in broccoli: implications for cancer prevention. Br J Nutr 2012:1-8.

13. Clarke JD, Hsu A, Williams DE, Dashwood RH, Stevens JF, Yamamoto M, et al. Metabolism and tissue distribution of sulforaphane in Nrf2 knockout and wild-type mice. Pharm Res 2011;28(12):3171-9.
14. Keum YS, Khor TO, Lin W, Shen G, Kwon KH, Barve A, et al. Pharmacokinetics and pharmacodynamics of broccoli sprouts on the suppression of prostate cancer in transgenic adenocarcinoma of mouse prostate (TRAMP) mice: implication of induction of Nrf2, HO-1 and apoptosis and the suppression of Akt-dependent kinase pathway. Pharm Res 2009;26(10):2324-31.
15. Traka MH, Spinks CA, Doleman JF, Melchini A, Ball RY, Mills RD, et al. The dietary isothiocyanate sulforaphane modulates gene expression and alternative gene splicing in a PTEN null preclinical murine model of prostate cancer. Mol Cancer 2010;9:189.
16. Traka M, Gasper AV, Melchini A, Bacon JR, Needs PW, Frost V, et al. Broccoli consumption interacts with GSTM1 to perturb oncogenic signalling pathways in the prostate. PLoS One 2008;3(7):e2568.
17. Grose KR, Bjeldanes LF. Oligomerization of indole-3-carbinol in aqueous acid. Chem Res Toxicol 1992;5(2):188-93.
18. Anderton MJ, Manson MM, Verschoyle RD, Gescher A, Lamb JH, Farmer PB, et al. Pharmacokinetics and tissue disposition of indole-3-carbinol and its acid condensation products after oral administration to mice. Clin Cancer Res 2004;10(15):5233-41.
19. Reed GA, Arneson DW, Putnam WC, Smith HJ, Gray JC, Sullivan DK, et al. Single-dose and multiple-dose administration of indole-3-carbinol to women: pharmacokinetics based on 3,3'-diindolylmethane. Cancer Epidemiol Biomarkers Prev 2006;15(12):2477-81.
20. Souli E, Machluf M, Morgenstern A, Sabo E, Yannai S. Indole-3-carbinol (I3C) exhibits inhibitory and preventive effects on prostate tumors in mice. Food Chem Toxicol 2008;46(3):863-70.
21. Bradlow HL, Zeligs MA. Diindolylmethane (DIM) spontaneously forms from indole-3-carbinol (I3C) during cell culture experiments. In Vivo 2010;24(4):387-91.
22. Bradlow HL. Review. Indole-3-carbinol as a chemoprotective agent in breast and prostate cancer. In Vivo 2008;22(4):441-5.
23. Cho HJ, Park SY, Kim EJ, Kim JK, Park JH. 3,3'-Diindolylmethane inhibits prostate cancer development in the transgenic adenocarcinoma mouse prostate model. Mol Carcinog 2011;50(2):100-12.
24. Gasper AV, Al-Janobi A, Smith JA, Bacon JR, Fortun P, Atherton C, et al. Glutathione S-transferase M1 polymorphism and metabolism of sulforaphane from standard and high-glucosinolate broccoli. Am J Clin Nutr 2005;82(6):1283-91.
25. Heath EI, Heilbrun LK, Li J, Vaishampayan U, Harper F, Pemberton P, et al. A phase I dose-escalation study of oral BR-DIM (BioResponse 3,3'-

Diindolylmethane) in castrate-resistant, non-metastatic prostate cancer. Am J Transl Res 2010;2(4):402-11.
26. Brooks JD, Paton VG, Vidanes G. Potent induction of phase 2 enzymes in human prostate cells by sulforaphane. Cancer Epidemiol Biomarkers Prev 2001;10(9):949-54.
27. Fahey JW, Talalay P. Antioxidant functions of sulforaphane: a potent inducer of Phase II detoxication enzymes. Food Chem Toxicol 1999;37(9-10):973-9.
28. Guerrero-Beltran CE, Calderon-Oliver M, Pedraza-Chaverri J, Chirino YI. Protective effect of sulforaphane against oxidative stress: recent advances. Exp Toxicol Pathol 2012;64(5):503-8.
29. Wang TT, Schoene NW, Milner JA, Kim YS. Broccoli-derived phytochemicals indole-3-carbinol and 3,3'-diindolylmethane exerts concentration-dependent pleiotropic effects on prostate cancer cells: comparison with other cancer preventive phytochemicals. Mol Carcinog;51(3):244-56.
30. Ernst IM, Schuemann C, Wagner AE, Rimbach G. 3,3'-Diindolylmethane but not indole-3-carbinol activates Nrf2 and induces Nrf2 target gene expression in cultured murine fibroblasts. Free Radic Res 2011;45(8):941-9.
31. Saw CL, Cintron M, Wu TY, Guo Y, Huang Y, Jeong WS, et al. Pharmacodynamics of dietary phytochemical indoles I3C and DIM: Induction of Nrf2-mediated phase II drug metabolizing and antioxidant genes and synergism with isothiocyanates. Biopharm Drug Dispos 2011;32(5):289-300.
32. Reed GA, Peterson KS, Smith HJ, Gray JC, Sullivan DK, Mayo MS, et al. A phase I study of indole-3-carbinol in women: tolerability and effects. Cancer Epidemiol Biomarkers Prev 2005;14(8):1953-60.
33. Dalessandri KM, Firestone GL, Fitch MD, Bradlow HL, Bjeldanes LF. Pilot study: effect of 3,3'-diindolylmethane supplements on urinary hormone metabolites in postmenopausal women with a history of early-stage breast cancer. Nutr Cancer 2004;50(2):161-7.
34. Michnovicz JJ, Adlercreutz H, Bradlow HL. Changes in levels of urinary estrogen metabolites after oral indole-3-carbinol treatment in humans. J Natl Cancer Inst 1997;89(10):718-23.
35. Michnovicz JJ, Bradlow HL. Altered estrogen metabolism and excretion in humans following consumption of indole-3-carbinol. Nutr Cancer 1991;16(1):59-66.
36. Fowke JH, Longcope C, Hebert JR. Brassica vegetable consumption shifts estrogen metabolism in healthy postmenopausal women. Cancer Epidemiol Biomarkers Prev 2000;9(8):773-9.
37. Castagnetta LA, Miceli MD, Sorci CM, Pfeffer U, Farruggio R, Oliveri G, et al. Growth of LNCaP human prostate cancer cells is stimulated by estradiol via its own receptor. Endocrinology 1995;136(5):2309-19.
38. Dubrovska A, Kim S, Salamone RJ, Walker JR, Maira SM, Garcia-Echeverria C, et al. The role of PTEN/Akt/PI3K signaling in the maintenance and

viability of prostate cancer stem-like cell populations. Proc Natl Acad Sci U S A 2009;106(1):268-73.
39. Majumder PK, Sellers WR. Akt-regulated pathways in prostate cancer. Oncogene 2005;24(50):7465-74.
40. Sarker D, Reid AH, Yap TA, de Bono JS. Targeting the PI3K/AKT pathway for the treatment of prostate cancer. Clin Cancer Res 2009;15(15):4799-805.
41. Kinkade CW, Castillo-Martin M, Puzio-Kuter A, Yan J, Foster TH, Gao H, et al. Targeting AKT/mTOR and ERK MAPK signaling inhibits hormone-refractory prostate cancer in a preclinical mouse model. J Clin Invest 2008;118(9):3051-64.
42. Morgan TM, Koreckij TD, Corey E. Targeted therapy for advanced prostate cancer: inhibition of the PI3K/Akt/mTOR pathway. Curr Cancer Drug Targets 2009;9(2):237-49.
43. Wiczk A, Hofman D, Konopa G, Herman-Antosiewicz A. Sulforaphane, a cruciferous vegetable-derived isothiocyanate, inhibits protein synthesis in human prostate cancer cells. Biochim Biophys Acta 2012;1823(8):1295-305.
44. Martelli AM, Tabellini G, Bressanin D, Ognibene A, Goto K, Cocco L, et al. The emerging multiple roles of nuclear Akt. Biochim Biophys Acta 2012;1823(12):2168-78.
45. Song G, Ouyang G, Bao S. The activation of Akt/PKB signaling pathway and cell survival. J Cell Mol Med 2005;9(1):59-71.
46. Xu C, Shen G, Chen C, Gelinas C, Kong AN. Suppression of NF-kappaB and NF-kappaB-regulated gene expression by sulforaphane and PEITC through IkappaBalpha, IKK pathway in human prostate cancer PC-3 cells. Oncogene 2005;24(28):4486-95.
47. Kennedy SG, Wagner AJ, Conzen SD, Jordan J, Bellacosa A, Tsichlis PN, et al. The PI 3-kinase/Akt signaling pathway delivers an anti-apoptotic signal. Genes Dev 1997;11(6):701-13.
48. Xu C, Shen G, Yuan X, Kim JH, Gopalkrishnan A, Keum YS, et al. ERK and JNK signaling pathways are involved in the regulation of activator protein 1 and cell death elicited by three isothiocyanates in human prostate cancer PC-3 cells. Carcinogenesis 2006;27(3):437-45.
49. Choi S, Lew KL, Xiao H, Herman-Antosiewicz A, Xiao D, Brown CK, et al. D,L-Sulforaphane-induced cell death in human prostate cancer cells is regulated by inhibitor of apoptosis family proteins and Apaf-1. Carcinogenesis 2007;28(1):151-62.
50. Dan HC, Cooper MJ, Cogswell PC, Duncan JA, Ting JP, Baldwin AS. Akt-dependent regulation of NF-{kappa}B is controlled by mTOR and Raptor in association with IKK. Genes Dev 2008;22(11):1490-500.
51. Choi S, Singh SV. Bax and Bak are required for apoptosis induction by sulforaphane, a cruciferous vegetable-derived cancer chemopreventive agent. Cancer Res 2005;65(5):2035-43.
52. Chu ZL, McKinsey TA, Liu L, Gentry JJ, Malim MH, Ballard DW. Suppression of tumor necrosis factor-induced cell death by inhibitor of apoptosis

c-IAP2 is under NF-kappaB control. Proc Natl Acad Sci U S A 1997;94(19):10057-62.
53. Stehlik C, de Martin R, Kumabashiri I, Schmid JA, Binder BR, Lipp J. Nuclear factor (NF)-kappaB-regulated X-chromosome-linked iap gene expression protects endothelial cells from tumor necrosis factor alpha-induced apoptosis. J Exp Med 1998;188(1):211-6.
54. McEleny K, Coffey R, Morrissey C, Williamson K, Zangemeister-Wittke U, Fitzpatrick JM, et al. An antisense oligonucleotide to cIAP-1 sensitizes prostate cancer cells to fas and TNFalpha mediated apoptosis. Prostate 2004;59(4):419-25.
55. Xiao D, Powolny AA, Antosiewicz J, Hahm ER, Bommareddy A, Zeng Y, et al. Cellular responses to cancer chemopreventive agent D,L-sulforaphane in human prostate cancer cells are initiated by mitochondrial reactive oxygen species. Pharm Res 2009;26(7):1729-38.
56. Singh AV, Xiao D, Lew KL, Dhir R, Singh SV. Sulforaphane induces caspase-mediated apoptosis in cultured PC-3 human prostate cancer cells and retards growth of PC-3 xenografts in vivo. Carcinogenesis 2004;25(1):83-90.
57. Singh SV, Warin R, Xiao D, Powolny AA, Stan SD, Arlotti JA, et al. Sulforaphane inhibits prostate carcinogenesis and pulmonary metastasis in TRAMP mice in association with increased cytotoxicity of natural killer cells. Cancer Res 2009;69(5):2117-25.
58. Clarke JD, Dashwood RH, Ho E. Multi-targeted prevention of cancer by sulforaphane. Cancer Lett 2008;269(2):291-304.
59. Juge N, Mithen RF, Traka M. Molecular basis for chemoprevention by sulforaphane: a comprehensive review. Cell Mol Life Sci 2007;64(9):1105-27.
60. Chinni SR, Li Y, Upadhyay S, Koppolu PK, Sarkar FH. Indole-3-carbinol (I3C) induced cell growth inhibition, G1 cell cycle arrest and apoptosis in prostate cancer cells. Oncogene 2001;20(23):2927-36.
61. Nachshon-Kedmi M, Yannai S, Haj A, Fares FA. Indole-3-carbinol and 3,3'-diindolylmethane induce apoptosis in human prostate cancer cells. Food Chem Toxicol 2003;41(6):745-52.
62. Vivar OI, Lin CL, Firestone GL, Bjeldanes LF. 3,3'-Diindolylmethane induces a G(1) arrest in human prostate cancer cells irrespective of androgen receptor and p53 status. Biochem Pharmacol 2009;78(5):469-76.
63. Nachshon-Kedmi M, Yannai S, Fares FA. Induction of apoptosis in human prostate cancer cell line, PC3, by 3,3'-diindolylmethane through the mitochondrial pathway. Br J Cancer 2004;91(7):1358-63.
64. Garikapaty VP, Ashok BT, Tadi K, Mittelman A, Tiwari RK. 3,3'-Diindolylmethane downregulates pro-survival pathway in hormone independent prostate cancer. Biochem Biophys Res Commun 2006;340(2):718-25.
65. Bhuiyan MM, Li Y, Banerjee S, Ahmed F, Wang Z, Ali S, et al. Down-regulation of androgen receptor by 3,3'-diindolylmethane contributes to inhibition

of cell proliferation and induction of apoptosis in both hormone-sensitive LNCaP and insensitive C4-2B prostate cancer cells. Cancer Res 2006;66(20):10064-72.
66. Kong D, Banerjee S, Huang W, Li Y, Wang Z, Kim HR, et al. Mammalian target of rapamycin repression by 3,3'-diindolylmethane inhibits invasion and angiogenesis in platelet-derived growth factor-D-overexpressing PC3 cells. Cancer Res 2008;68(6):1927-34.
67. Kong D, Li Y, Wang Z, Banerjee S, Sarkar FH. Inhibition of angiogenesis and invasion by 3,3'-diindolylmethane is mediated by the nuclear factor-kappaB downstream target genes MMP-9 and uPA that regulated bioavailability of vascular endothelial growth factor in prostate cancer. Cancer Res 2007;67(7):3310-9.
68. Li Y, Chinni SR, Sarkar FH. Selective growth regulatory and pro-apoptotic effects of DIM is mediated by AKT and NF-kappaB pathways in prostate cancer cells. Front Biosci 2005;10:236-43.
69. Chen D, Banerjee S, Cui QC, Kong D, Sarkar FH, Dou QP. Activation of AMP-Activated Protein Kinase by 3,3'-Diindolylmethane (DIM) Is Associated with Human Prostate Cancer Cell Death In Vitro and In Vivo. PLoS One 2012;7(10):e47186.
70. Le HT, Schaldach CM, Firestone GL, Bjeldanes LF. Plant-derived 3,3'-Diindolylmethane is a strong androgen antagonist in human prostate cancer cells. J Biol Chem 2003;278(23):21136-45.
71. Baylin SB, Jones PA. A decade of exploring the cancer epigenome - biological and translational implications. Nat Rev Cancer 2011;11(10):726-34.
72. Sharma S, Kelly TK, Jones PA. Epigenetics in cancer. Carcinogenesis 2010;31(1):27-36.
73. Kim HJ, Bae SC. Histone deacetylase inhibitors: molecular mechanisms of action and clinical trials as anti-cancer drugs. Am J Transl Res 2011;3(2):166-79.
74. Dashwood RH, Myzak MC, Ho E. Dietary HDAC inhibitors: time to rethink weak ligands in cancer chemoprevention? Carcinogenesis 2006;27(2):344-9.
75. Weichert W, Roske A, Gekeler V, Beckers T, Stephan C, Jung K, et al. Histone deacetylases 1, 2 and 3 are highly expressed in prostate cancer and HDAC2 expression is associated with shorter PSA relapse time after radical prostatectomy. Br J Cancer 2008;98(3):604-10.
76. Gibbs A, Schwartzman J, Deng V, Alumkal J. Sulforaphane destabilizes the androgen receptor in prostate cancer cells by inactivating histone deacetylase 6. Proc Natl Acad Sci U S A 2009;106(39):16663-8.
77. Noonan EJ, Place RF, Pookot D, Basak S, Whitson JM, Hirata H, et al. miR-449a targets HDAC-1 and induces growth arrest in prostate cancer. Oncogene 2009;28(14):1714-24.
78. Myzak MC, Hardin K, Wang R, Dashwood RH, Ho E. Sulforaphane inhibits histone deacetylase activity in BPH-1, LnCaP and PC-3 prostate epithelial cells. Carcinogenesis 2006;27(4):811-9.

79. Myzak MC, Tong P, Dashwood WM, Dashwood RH, Ho E. Sulforaphane retards the growth of human PC-3 xenografts and inhibits HDAC activity in human subjects. Exp Biol Med (Maywood) 2007;232(2):227-34.
80. Clarke JD, Hsu A, Yu Z, Dashwood RH, Ho E. Differential effects of sulforaphane on histone deacetylases, cell cycle arrest and apoptosis in normal prostate cells versus hyperplastic and cancerous prostate cells. Mol Nutr Food Res 2011;55(7):999-1009.
81. Hsu A, Wong CP, Yu Z, Williams DE, Dashwood RH, Ho E. Promoter de-methylation of cyclin D2 by sulforaphane in prostate cancer cells. Clin Epigenetics 2011;3:3.
82. Padar A, Sathyanarayana UG, Suzuki M, Maruyama R, Hsieh JT, Frenkel EP, et al. Inactivation of cyclin D2 gene in prostate cancers by aberrant promoter methylation. Clin Cancer Res 2003;9(13):4730-4.
83. Meeran SM, Patel SN, Tollefsbol TO. Sulforaphane causes epigenetic repression of hTERT expression in human breast cancer cell lines. PLoS One 2010;5(7):e11457.
84. Valenzuela-Fernandez A, Cabrero JR, Serrador JM, Sanchez-Madrid F. HDAC6: a key regulator of cytoskeleton, cell migration and cell-cell interactions. Trends Cell Biol 2008;18(6):291-7.
85. Azarenko O, Okouneva T, Singletary KW, Jordan MA, Wilson L. Suppression of microtubule dynamic instability and turnover in MCF7 breast cancer cells by sulforaphane. Carcinogenesis 2008;29(12):2360-8.
86. Mi L, Xiao Z, Hood BL, Dakshanamurthy S, Wang X, Govind S, et al. Covalent binding to tubulin by isothiocyanates. A mechanism of cell growth arrest and apoptosis. J Biol Chem 2008;283(32):22136-46.
87. Xiao Z, Mi L, Chung FL, Veenstra TD. Proteomic analysis of covalent modifications of tubulins by isothiocyanates. J Nutr 2012;142(7):1377S-81S.
88. Shankar S, Ganapathy S, Srivastava RK. Sulforaphane enhances the therapeutic potential of TRAIL in prostate cancer orthotopic model through regulation of apoptosis, metastasis, and angiogenesis. Clin Cancer Res 2008;14(21):6855-66.
89. Ai J, Wang Y, Dar JA, Liu J, Liu L, Nelson JB, et al. HDAC6 regulates androgen receptor hypersensitivity and nuclear localization via modulating Hsp90 acetylation in castration-resistant prostate cancer. Mol Endocrinol 2009;23(12):1963-72.
90. Beaver LM, Yu TW, Sokolowski EI, Williams DE, Dashwood RH, Ho E. 3,3'-Diindolylmethane, but not indole-3-carbinol, inhibits histone deacetylase activity in prostate cancer cells. Toxicol Appl Pharmacol 2012;263(3):345-51.
91. Li Y, Li X, Guo B. Chemopreventive agent 3,3'-diindolylmethane selectively induces proteasomal degradation of class I histone deacetylases. Cancer Res 2010;70(2):646-54.
92. Kong D, Heath E, Chen W, Cher ML, Powell I, Heilbrun L, et al. Loss of let-7 up-regulates EZH2 in prostate cancer consistent with the acquisition of

cancer stem cell signatures that are attenuated by BR-DIM. PLoS One 2012;7(3):e33729.
93. Bachmann IM, Halvorsen OJ, Collett K, Stefansson IM, Straume O, Haukaas SA, et al. EZH2 expression is associated with high proliferation rate and aggressive tumor subgroups in cutaneous melanoma and cancers of the endometrium, prostate, and breast. J Clin Oncol 2006;24(2):268-73.
94. van Leenders GJ, Dukers D, Hessels D, van den Kieboom SW, Hulsbergen CA, Witjes JA, et al. Polycomb-group oncogenes EZH2, BMI1, and RING1 are overexpressed in prostate cancer with adverse pathologic and clinical features. Eur Urol 2007;52(2):455-63.
95. Kong D, Heath E, Chen W, Cher M, Powell I, Heilbrun L, et al. Epigenetic silencing of miR-34a in human prostate cancer cells and tumor tissue specimens can be reversed by BR-DIM treatment. Am J Transl Res 2012;4(1):14-23.
96. Fimognari C, Hrelia P. Sulforaphane as a promising molecule for fighting cancer. Mutat Res 2007;635(2-3):90-104.
97. Weng JR, Tsai CH, Kulp SK, Chen CS. Indole-3-carbinol as a chemopreventive and anti-cancer agent. Cancer Lett 2008;262(2):153-63.
98. Yu S, Khor TO, Cheung KL, Li W, Wu TY, Huang Y, et al. Nrf2 expression is regulated by epigenetic mechanisms in prostate cancer of TRAMP mice. PLoS One 2010;5(1):e8579.
99. Choudhary C, Kumar C, Gnad F, Nielsen ML, Rehman M, Walther TC, et al. Lysine acetylation targets protein complexes and co-regulates major cellular functions. Science 2009;325(5942):834-40.
100. Bantscheff M, Hopf C, Savitski MM, Dittmann A, Grandi P, Michon AM, et al. Chemoproteomics profiling of HDAC inhibitors reveals selective targeting of HDAC complexes. Nat Biotechnol 2011;29(3):255-65.

Chapter 2

1. Karantanos T, Corn PG, Thompson TC. Prostate cancer progression after androgen deprivation therapy: mechanisms of castrate resistance and novel therapeutic approaches. Oncogene 2013;32(49):5501-11.
2. Juge N, Mithen RF, Traka M. Molecular basis for chemoprevention by sulforaphane: a comprehensive review. Cell Mol Life Sci 2007;64(9):1105-27.
3. Clarke JD, Hsu A, Yu Z, Dashwood RH, Ho E. Differential effects of sulforaphane on histone deacetylases, cell cycle arrest and apoptosis in normal prostate cells versus hyperplastic and cancerous prostate cells. Mol Nutr Food Res 2011;55(7):999-1009.
4. Pledgie-Tracy A, Sobolewski MD, Davidson NE. Sulforaphane induces cell type-specific apoptosis in human breast cancer cell lines. Mol Cancer Ther 2007;6(3):1013-21.

5. Chaudhuri D, Orsulic S, Ashok BT. Antiproliferative activity of sulforaphane in Akt-overexpressing ovarian cancer cells. Mol Cancer Ther 2007;6(1):334-45.
6. Chuang LT, Moqattash ST, Gretz HF, Nezhat F, Rahaman J, Chiao JW. Sulforaphane induces growth arrest and apoptosis in human ovarian cancer cells. Acta Obstet Gynecol Scand 2007;86(10):1263-8.
7. Gamet-Payrastre L, Li P, Lumeau S, Cassar G, Dupont MA, Chevolleau S, et al. Sulforaphane, a naturally occurring isothiocyanate, induces cell cycle arrest and apoptosis in HT29 human colon cancer cells. Cancer Res 2000;60(5):1426-33.
8. Pham NA, Jacobberger JW, Schimmer AD, Cao P, Gronda M, Hedley DW. The dietary isothiocyanate sulforaphane targets pathways of apoptosis, cell cycle arrest, and oxidative stress in human pancreatic cancer cells and inhibits tumor growth in severe combined immunodeficient mice. Mol Cancer Ther 2004;3(10):1239-48.
9. Hu R, Khor TO, Shen G, Jeong WS, Hebbar V, Chen C, et al. Cancer chemoprevention of intestinal polyposis in ApcMin/+ mice by sulforaphane, a natural product derived from cruciferous vegetable. Carcinogenesis 2006;27(10):2038-46.
10. Singh SV, Warin R, Xiao D, Powolny AA, Stan SD, Arlotti JA, et al. Sulforaphane inhibits prostate carcinogenesis and pulmonary metastasis in TRAMP mice in association with increased cytotoxicity of natural killer cells. Cancer Res 2009;69(5):2117-25.
11. Wang H, Lin W, Shen G, Khor TO, Nomeir AA, Kong AN. Development and validation of an LC-MS-MS method for the simultaneous determination of sulforaphane and its metabolites in rat plasma and its application in pharmacokinetic studies. J Chromatogr Sci 2011;49(10):801-6.
12. Weichert W, Roske A, Gekeler V, Beckers T, Stephan C, Jung K, et al. Histone deacetylases 1, 2 and 3 are highly expressed in prostate cancer and HDAC2 expression is associated with shorter PSA relapse time after radical prostatectomy. Br J Cancer 2008;98(3):604-10.
13. Ellinger J, Kahl P, von der Gathen J, Rogenhofer S, Heukamp LC, Gutgemann I, et al. Global levels of histone modifications predict prostate cancer recurrence. Prostate 2010;70(1):61-9.
14. Seligson DB, Horvath S, Shi T, Yu H, Tze S, Grunstein M, et al. Global histone modification patterns predict risk of prostate cancer recurrence. Nature 2005;435(7046):1262-6.
15. van Leenders GJ, Dukers D, Hessels D, van den Kieboom SW, Hulsbergen CA, Witjes JA, et al. Polycomb-group oncogenes EZH2, BMI1, and RING1 are overexpressed in prostate cancer with adverse pathologic and clinical features. Eur Urol 2007;52(2):455-63.
16. Kelly TK, De Carvalho DD, Jones PA. Epigenetic modifications as therapeutic targets. Nat Biotechnol 2010;28(10):1069-1078.

17. Hsu A, Wong CP, Yu Z, Williams DE, Dashwood RH, Ho E. Promoter de-methylation of cyclin D2 by sulforaphane in prostate cancer cells. Clin Epigenetics 2011;3:3.
18. Balasubramanian S, Chew YC, Eckert RL. Sulforaphane suppresses polycomb group protein level via a proteasome-dependent mechanism in skin cancer cells. Mol Pharmacol 2011;80(5):870-8.
19. Bantscheff M, Hopf C, Savitski MM, Dittmann A, Grandi P, Michon AM, et al. Chemoproteomics profiling of HDAC inhibitors reveals selective targeting of HDAC complexes. Nat Biotechnol 2011;29(3):255-65.
20. Esteve PO, Chin HG, Smallwood A, Feehery GR, Gangisetty O, Karpf AR, et al. Direct interaction between DNMT1 and G9a coordinates DNA and histone methylation during replication. Genes Dev 2006;20(22):3089-103.
21. Fritsch L, Robin P, Mathieu JR, Souidi M, Hinaux H, Rougeulle C, et al. A subset of the histone H3 lysine 9 methyltransferases Suv39h1, G9a, GLP, and SETDB1 participate in a multimeric complex. Mol Cell 2010;37(1):46-56.
22. Cedar H, Bergman Y. Linking DNA methylation and histone modification: patterns and paradigms. Nat Rev Genet 2009;10(5):295-304.
23. Lehnertz B, Ueda Y, Derijck AA, Braunschweig U, Perez-Burgos L, Kubicek S, et al. Suv39h-mediated histone H3 lysine 9 methylation directs DNA methylation to major satellite repeats at pericentric heterochromatin. Curr Biol 2003;13(14):1192-200.
24. Vire E, Brenner C, Deplus R, Blanchon L, Fraga M, Didelot C, et al. The Polycomb group protein EZH2 directly controls DNA methylation. Nature 2006;439(7078):871-4.
25. Martin C, Zhang Y. The diverse functions of histone lysine methylation. Nat Rev Mol Cell Biol 2005;6(11):838-49.
26. Kondo Y, Shen L, Ahmed S, Boumber Y, Sekido Y, Haddad BR, et al. Downregulation of histone H3 lysine 9 methyltransferase G9a induces centrosome disruption and chromosome instability in cancer cells. PLoS One 2008;3(4):e2037.
27. Myzak MC, Hardin K, Wang R, Dashwood RH, Ho E. Sulforaphane inhibits histone deacetylase activity in BPH-1, LnCaP and PC-3 prostate epithelial cells. Carcinogenesis 2006;27(4):811-9.
28. Chu L, Zhu T, Liu X, Yu R, Bacanamwo M, Dou Z, et al. SUV39H1 orchestrates temporal dynamics of centromeric methylation essential for faithful chromosome segregation in mitosis. J Mol Cell Biol 2012;4(5):331-40.
29. Frisa PS, Jacobberger JW. Cell cycle-related cyclin b1 quantification. PLoS One 2009;4(9):e7064.
30. Aagaard L, Schmid M, Warburton P, Jenuwein T. Mitotic phosphorylation of SUV39H1, a novel component of active centromeres, coincides with transient accumulation at mammalian centromeres. J Cell Sci 2000;113 (Pt 5):817-29.
31. Kondo Y. Epigenetic cross-talk between DNA methylation and histone modifications in human cancers. Yonsei Med J 2009;50(4):455-63.

32. Fuks F, Hurd PJ, Deplus R, Kouzarides T. The DNA methyltransferases associate with HP1 and the SUV39H1 histone methyltransferase. Nucleic Acids Res 2003;31(9):2305-12.
33. Vaute O, Nicolas E, Vandel L, Trouche D. Functional and physical interaction between the histone methyl transferase Suv39H1 and histone deacetylases. Nucleic Acids Res 2002;30(2):475-81.
34. Vaquero A, Scher M, Erdjument-Bromage H, Tempst P, Serrano L, Reinberg D. SIRT1 regulates the histone methyl-transferase SUV39H1 during heterochromatin formation. Nature 2007;450(7168):440-4.
35. Bosch-Presegue L, Raurell-Vila H, Marazuela-Duque A, Kane-Goldsmith N, Valle A, Oliver J, et al. Stabilization of Suv39H1 by SirT1 is part of oxidative stress response and ensures genome protection. Mol Cell 2011;42(2):210-23.
36. Wang D, Zhou J, Liu X, Lu D, Shen C, Du Y, et al. Methylation of SUV39H1 by SET7/9 results in heterochromatin relaxation and genome instability. Proc Natl Acad Sci U S A 2013;110(14):5516-21.
37. Rajendran P, Kidane AI, Yu TW, Dashwood WM, Bisson WH, Lohr CV, et al. HDAC turnover, CtIP acetylation and dysregulated DNA damage signaling in colon cancer cells treated with sulforaphane and related dietary isothiocyanates. Epigenetics 2013;8(6):612-23.
38. Ye L, Zhang Y. Total intracellular accumulation levels of dietary isothiocyanates determine their activity in elevation of cellular glutathione and induction of Phase 2 detoxification enzymes. Carcinogenesis 2001;22(12):1987-92.
39. Zhang Y, Callaway EC. High cellular accumulation of sulphoraphane, a dietary anticarcinogen, is followed by rapid transporter-mediated export as a glutathione conjugate. Biochem J 2002;364(Pt 1):301-7.
40. Kosugi S, Hasebe M, Tomita M, Yanagawa H. Systematic identification of cell cycle-dependent yeast nucleocytoplasmic shuttling proteins by prediction of composite motifs. Proc Natl Acad Sci U S A 2009;106(25):10171-6.
41. Lin JR, Hu J. SeqNLS: nuclear localization signal prediction based on frequent pattern mining and linear motif scoring. PLoS One 2013;8(10):e76864.
42. Dinkel H, Van Roey K, Michael S, Davey NE, Weatheritt RJ, Born D, et al. The eukaryotic linear motif resource ELM: 10 years and counting. Nucleic Acids Res 2014;42(1):D259-66.
43. Singh AV, Xiao D, Lew KL, Dhir R, Singh SV. Sulforaphane induces caspase-mediated apoptosis in cultured PC-3 human prostate cancer cells and retards growth of PC-3 xenografts in vivo. Carcinogenesis 2004;25(1):83-90.
44. Peters AH, O'Carroll D, Scherthan H, Mechtler K, Sauer S, Schofer C, et al. Loss of the Suv39h histone methyltransferases impairs mammalian heterochromatin and genome stability. Cell 2001;107(3):323-37.
45. Czvitkovich S, Sauer S, Peters AH, Deiner E, Wolf A, Laible G, et al. Over-expression of the SUV39H1 histone methyltransferase induces altered

proliferation and differentiation in transgenic mice. Mech Dev 2001;107(1-2):141-53.
46. Fan DN, Tsang FH, Tam AH, Au SL, Wong CC, Wei L, et al. Histone lysine methyltransferase, suppressor of variegation 3-9 homolog 1, promotes hepatocellular carcinoma progression and is negatively regulated by microRNA-125b. Hepatology 2013;57(2):637-47.
47. Chaib H, Nebbioso A, Prebet T, Castellano R, Garbit S, Restouin A, et al. Anti-leukemia activity of chaetocin via death receptor-dependent apoptosis and dual modulation of the histone methyl-transferase SUV39H1. Leukemia 2012;26(4):662-74.
48. Cherblanc FL, Chapman KL, Brown R, Fuchter MJ. Chaetocin is a nonspecific inhibitor of histone lysine methyltransferases. Nat Chem Biol 2013;9(3):136-7.
49. Greiner D, Bonaldi T, Eskeland R, Roemer E, Imhof A. Identification of a specific inhibitor of the histone methyltransferase SU(VAR)3-9. Nat Chem Biol 2005;1(3):143-5.
50. Tibodeau JD, Benson LM, Isham CR, Owen WG, Bible KC. The anticancer agent chaetocin is a competitive substrate and inhibitor of thioredoxin reductase. Antioxid Redox Signal 2009;11(5):1097-106.
51. Wade M, Li YC, Wahl GM. MDM2, MDMX and p53 in oncogenesis and cancer therapy. Nat Rev Cancer 2013;13(2):83-96.
52. Gan N, Wu YC, Brunet M, Garrido C, Chung FL, Dai C, et al. Sulforaphane activates heat shock response and enhances proteasome activity through up-regulation of Hsp27. J Biol Chem 2010;285(46):35528-36.
53. Herman-Antosiewicz A, Johnson DE, Singh SV. Sulforaphane causes autophagy to inhibit release of cytochrome C and apoptosis in human prostate cancer cells. Cancer Res 2006;66(11):5828-35.
54. Zhang X, Tamaru H, Khan SI, Horton JR, Keefe LJ, Selker EU, et al. Structure of the Neurospora SET domain protein DIM-5, a histone H3 lysine methyltransferase. Cell 2002;111(1):117-27.
55. Chin HG, Patnaik D, Esteve PO, Jacobsen SE, Pradhan S. Catalytic properties and kinetic mechanism of human recombinant Lys-9 histone H3 methyltransferase SUV39H1: participation of the chromodomain in enzymatic catalysis. Biochemistry 2006;45(10):3272-84.
56. Rea S, Eisenhaber F, O'Carroll D, Strahl BD, Sun ZW, Schmid M, et al. Regulation of chromatin structure by site-specific histone H3 methyltransferases. Nature 2000;406(6796):593-9.
57. Park SH, Yu SE, Chai YG, Jang YK. CDK2-dependent phosphorylation of Suv39H1 is involved in control of heterochromatin replication during cell cycle progression. Nucleic Acids Res 2014.
58. Hanlon N, Coldham N, Gielbert A, Sauer MJ, Ioannides C. Repeated intake of broccoli does not lead to higher plasma levels of sulforaphane in human volunteers. Cancer Lett 2009;284(1):15-20.

59. Clarke JD, Hsu A, Riedl K, Bella D, Schwartz SJ, Stevens JF, et al. Bioavailability and inter-conversion of sulforaphane and erucin in human subjects consuming broccoli sprouts or broccoli supplement in a cross-over study design. Pharmacol Res 2011;64(5):456-63.

Chapter 3

1. Juge N, Mithen RF, Traka M. Molecular basis for chemoprevention by sulforaphane: a comprehensive review. Cell Mol Life Sci 2007;64(9):1105-27.
2. Wattenberg LW. Chemoprevention of cancer. Cancer Res 1985;45(1):1-8.
3. Thimmulappa RK, Mai KH, Srisuma S, Kensler TW, Yamamoto M, Biswal S. Identification of Nrf2-regulated genes induced by the chemopreventive agent sulforaphane by oligonucleotide microarray. Cancer Res 2002;62(18):5196-203.
4. Clarke JD, Hsu A, Yu Z, Dashwood RH, Ho E. Differential effects of sulforaphane on histone deacetylases, cell cycle arrest and apoptosis in normal prostate cells versus hyperplastic and cancerous prostate cells. Mol Nutr Food Res 2011;55(7):999-1009.
5. Bao Y, Wang W, Zhou Z, Sun C. Benefits and risks of the hormetic effects of dietary isothiocyanates on cancer prevention. PLoS One 2014;9(12):e114764.
6. Gan N, Wu YC, Brunet M, Garrido C, Chung FL, Dai C, et al. Sulforaphane activates heat shock response and enhances proteasome activity through up-regulation of Hsp27. J Biol Chem 2010;285(46):35528-36.
7. Herman-Antosiewicz A, Johnson DE, Singh SV. Sulforaphane causes autophagy to inhibit release of cytochrome C and apoptosis in human prostate cancer cells. Cancer Res 2006;66(11):5828-35.
8. Rajendran P, Kidane AI, Yu TW, Dashwood WM, Bisson WH, Lohr CV, et al. HDAC turnover, CtIP acetylation and dysregulated DNA damage signaling in colon cancer cells treated with sulforaphane and related dietary isothiocyanates. Epigenetics 2013;8(6):612-23.
9. White E. Deconvoluting the context-dependent role for autophagy in cancer. Nat Rev Cancer 2012;12(6):401-10.
10. He C, Klionsky DJ. Regulation mechanisms and signaling pathways of autophagy. Annu Rev Genet 2009;43:67-93.
11. Klionsky DJ, Abeliovich H, Agostinis P, Agrawal DK, Aliev G, Askew DS, et al. Guidelines for the use and interpretation of assays for monitoring autophagy in higher eukaryotes. Autophagy 2008;4(2):151-75.
12. Mizushima N, Yoshimori T, Levine B. Methods in mammalian autophagy research. Cell 2010;140(3):313-26.
13. Vyas AR, Hahm ER, Arlotti JA, Watkins S, Beer-Stolz D, Desai D, et al. Chemoprevention of Prostate Cancer by D,L-Sulforaphane Is Augmented by Pharmacological Inhibition of Autophagy. Cancer Res 2013.
14. Gump JM, Thorburn A. Autophagy and apoptosis: what is the connection? Trends Cell Biol 2011;21(7):387-92.

15. Lee CH, Jeong SJ, Yun SM, Kim JH, Lee HJ, Ahn KS, et al. Down-regulation of phosphoglucomutase 3 mediates sulforaphane-induced cell death in LNCaP prostate cancer cells. Proteome Sci 2010;8:67.
16. Shankar S, Ganapathy S, Srivastava RK. Sulforaphane enhances the therapeutic potential of TRAIL in prostate cancer orthotopic model through regulation of apoptosis, metastasis, and angiogenesis. Clin Cancer Res 2008;14(21):6855-66.
17. Herman-Antosiewicz A, Xiao H, Lew KL, Singh SV. Induction of p21 protein protects against sulforaphane-induced mitotic arrest in LNCaP human prostate cancer cell line. Mol Cancer Ther 2007;6(5):1673-81.
18. Myzak MC, Hardin K, Wang R, Dashwood RH, Ho E. Sulforaphane inhibits histone deacetylase activity in BPH-1, LnCaP and PC-3 prostate epithelial cells. Carcinogenesis 2006;27(4):811-9.
19. Xiao D, Powolny AA, Antosiewicz J, Hahm ER, Bommareddy A, Zeng Y, et al. Cellular responses to cancer chemopreventive agent D,L-sulforaphane in human prostate cancer cells are initiated by mitochondrial reactive oxygen species. Pharm Res 2009;26(7):1729-38.
20. Choi S, Lew KL, Xiao H, Herman-Antosiewicz A, Xiao D, Brown CK, et al. D,L-Sulforaphane-induced cell death in human prostate cancer cells is regulated by inhibitor of apoptosis family proteins and Apaf-1. Carcinogenesis 2007;28(1):151-62.
21. Singh AV, Xiao D, Lew KL, Dhir R, Singh SV. Sulforaphane induces caspase-mediated apoptosis in cultured PC-3 human prostate cancer cells and retards growth of PC-3 xenografts in vivo. Carcinogenesis 2004;25(1):83-90.
22. Singh SV, Srivastava SK, Choi S, Lew KL, Antosiewicz J, Xiao D, et al. Sulforaphane-induced cell death in human prostate cancer cells is initiated by reactive oxygen species. J Biol Chem 2005;280(20):19911-24.
23. Veeranki OL, Bhattacharya A, Marshall JR, Zhang Y. Organ-specific exposure and response to sulforaphane, a key chemopreventive ingredient in broccoli: implications for cancer prevention. Br J Nutr 2013;109(1):25-32.
24. Clarke JD, Hsu A, Williams DE, Dashwood RH, Stevens JF, Yamamoto M, et al. Metabolism and tissue distribution of sulforaphane in Nrf2 knockout and wild-type mice. Pharm Res 2011;28(12):3171-9.
25. Cornblatt BS, Ye L, Dinkova-Kostova AT, Erb M, Fahey JW, Singh NK, et al. Preclinical and clinical evaluation of sulforaphane for chemoprevention in the breast. Carcinogenesis 2007;28(7):1485-90.
26. Hanlon N, Coldham N, Gielbert A, Kuhnert N, Sauer MJ, King LJ, et al. Absolute bioavailability and dose-dependent pharmacokinetic behaviour of dietary doses of the chemopreventive isothiocyanate sulforaphane in rat. Br J Nutr 2008;99(3):559-64.
27. Hu R, Hebbar V, Kim BR, Chen C, Winnik B, Buckley B, et al. In vivo pharmacokinetics and regulation of gene expression profiles by isothiocyanate sulforaphane in the rat. J Pharmacol Exp Ther 2004;310(1):263-71.

28. Wang H, Lin W, Shen G, Khor TO, Nomeir AA, Kong AN. Development and validation of an LC-MS-MS method for the simultaneous determination of sulforaphane and its metabolites in rat plasma and its application in pharmacokinetic studies. J Chromatogr Sci 2011;49(10):801-6.
29. Singh SV, Warin R, Xiao D, Powolny AA, Stan SD, Arlotti JA, et al. Sulforaphane inhibits prostate carcinogenesis and pulmonary metastasis in TRAMP mice in association with increased cytotoxicity of natural killer cells. Cancer Res 2009;69(5):2117-25.
30. Cho SD, Li G, Hu H, Jiang C, Kang KS, Lee YS, et al. Involvement of c-Jun N-terminal kinase in G2/M arrest and caspase-mediated apoptosis induced by sulforaphane in DU145 prostate cancer cells. Nutr Cancer 2005;52(2):213-24.
31. Scherz-Shouval R, Elazar Z. Regulation of autophagy by ROS: physiology and pathology. Trends Biochem Sci 2011;36(1):30-8.
32. Carracedo A, Cantley LC, Pandolfi PP. Cancer metabolism: fatty acid oxidation in the limelight. Nat Rev Cancer 2013;13(4):227-32.
33. Pizer ES, Jackisch C, Wood FD, Pasternack GR, Davidson NE, Kuhajda FP. Inhibition of fatty acid synthesis induces programmed cell death in human breast cancer cells. Cancer Res 1996;56(12):2745-7.
34. Singh R, Cuervo AM. Lipophagy: connecting autophagy and lipid metabolism. Int J Cell Biol 2012;2012:282041.
35. Kanematsu S, Uehara N, Miki H, Yoshizawa K, Kawanaka A, Yuri T, et al. Autophagy inhibition enhances sulforaphane-induced apoptosis in human breast cancer cells. Anticancer Res 2010;30(9):3381-90.
36. Chaib H, Nebbioso A, Prebet T, Castellano R, Garbit S, Restouin A, et al. Anti-leukemia activity of chaetocin via death receptor-dependent apoptosis and dual modulation of the histone methyl-transferase SUV39H1. Leukemia 2012;26(4):662-74.
37. Naumann P, Fortunato F, Zentgraf H, Buchler MW, Herr I, Werner J. Autophagy and cell death signaling following dietary sulforaphane act independently of each other and require oxidative stress in pancreatic cancer. Int J Oncol 2011;39(1):101-9.
38. Wang M, Zhu JY, Chen S, Qing Y, Wu D, Lin YM, et al. Effects of co-treatment with sulforaphane and autophagy modulators on uridine 5'-diphospho-glucuronosyltransferase 1A isoforms and cytochrome P450 3A4 expression in Caco-2 human colon cancer cells. Oncol Lett 2014;8(6):2407-2416.
39. Rajendran P, Delage B, Dashwood WM, Yu TW, Wuth B, Williams DE, et al. Histone deacetylase turnover and recovery in sulforaphane-treated colon cancer cells: competing actions of 14-3-3 and Pin1 in HDAC3/SMRT corepressor complex dissociation/reassembly. Mol Cancer 2011;10:68.
40. Pappa G, Bartsch H, Gerhauser C. Biphasic modulation of cell proliferation by sulforaphane at physiologically relevant exposure times in a human colon cancer cell line. Mol Nutr Food Res 2007;51(8):977-84.

41. Bergstrom P, Andersson HC, Gao Y, Karlsson JO, Nodin C, Anderson MF, et al. Repeated transient sulforaphane stimulation in astrocytes leads to prolonged Nrf2-mediated gene expression and protection from superoxide-induced damage. Neuropharmacology 2011;60(2-3):343-53.
42. Brooks JD, Paton VG, Vidanes G. Potent induction of phase 2 enzymes in human prostate cells by sulforaphane. Cancer Epidemiol Biomarkers Prev 2001;10(9):949-54.
43. Thejass P, Kuttan G. Modulation of cell-mediated immune response in B16F-10 melanoma-induced metastatic tumor-bearing C57BL/6 mice by sulforaphane. Immunopharmacol Immunotoxicol 2007;29(2):173-86.

Chapter 4

1. Matthias P, Yoshida M, Khochbin S. HDAC6 a new cellular stress surveillance factor. Cell Cycle 2008;7(1):7-10.
2. Kawaguchi Y, Kovacs JJ, McLaurin A, Vance JM, Ito A, Yao TP. The deacetylase HDAC6 regulates aggresome formation and cell viability in response to misfolded protein stress. Cell 2003;115(6):727-38.
3. Iwata A, Riley BE, Johnston JA, Kopito RR. HDAC6 and microtubules are required for autophagic degradation of aggregated huntingtin. J Biol Chem 2005;280(48):40282-92.
4. Boyault C, Zhang Y, Fritah S, Caron C, Gilquin B, Kwon SH, et al. HDAC6 controls major cell response pathways to cytotoxic accumulation of protein aggregates. Genes Dev 2007;21(17):2172-81.
5. Lee JY, Koga H, Kawaguchi Y, Tang W, Wong E, Gao YS, et al. HDAC6 controls autophagosome maturation essential for ubiquitin-selective quality-control autophagy. Embo J 2010;29(5):969-80.
6. Kwon S, Zhang Y, Matthias P. The deacetylase HDAC6 is a novel critical component of stress granules involved in the stress response. Genes Dev 2007;21(24):3381-94.
7. Zhang L, Liu S, Liu N, Zhang Y, Liu M, Li D, et al. Proteomic identification and functional characterization of MYH9, Hsc70, and DNAJA1 as novel substrates of HDAC6 deacetylase activity. Protein Cell 2014.
8. Dompierre JP, Godin JD, Charrin BC, Cordelieres FP, King SJ, Humbert S, et al. Histone deacetylase 6 inhibition compensates for the transport deficit in Huntington's disease by increasing tubulin acetylation. J Neurosci 2007;27(13):3571-83.
9. Fung C, Lock R, Gao S, Salas E, Debnath J. Induction of autophagy during extracellular matrix detachment promotes cell survival. Mol Biol Cell 2008;19(3):797-806.
10. Kim JK, Jung Y, Wang J, Joseph J, Mishra A, Hill EE, et al. TBK1 regulates prostate cancer dormancy through mTOR inhibition. Neoplasia 2013;15(9):1064-74.

11. Kenific CM, Thorburn A, Debnath J. Autophagy and metastasis: another double-edged sword. Curr Opin Cell Biol 2009;22(2):241-5.
12. Yang ZJ, Chee CE, Huang S, Sinicrope FA. The role of autophagy in cancer: therapeutic implications. Mol Cancer Ther 2011;10(9):1533-41.
13. White E. Deconvoluting the context-dependent role for autophagy in cancer. Nat Rev Cancer 2012;12(6):401-10.
14. Namdar M, Perez G, Ngo L, Marks PA. Selective inhibition of histone deacetylase 6 (HDAC6) induces DNA damage and sensitizes transformed cells to anticancer agents. Proc Natl Acad Sci U S A 2010;107(46):20003-8.
15. Rao R, Fiskus W, Yang Y, Lee P, Joshi R, Fernandez P, et al. HDAC6 inhibition enhances 17-AAG--mediated abrogation of hsp90 chaperone function in human leukemia cells. Blood 2008;112(5):1886-93.
16. Aldana-Masangkay GI, Rodriguez-Gonzalez A, Lin T, Ikeda AK, Hsieh YT, Kim YM, et al. Tubacin suppresses proliferation and induces apoptosis of acute lymphoblastic leukemia cells. Leuk Lymphoma 2011;52(8):1544-55.
17. Aldana-Masangkay GI, Sakamoto KM. The role of HDAC6 in cancer. J Biomed Biotechnol 2010;2011:875824.
18. Gao J, Aksoy BA, Dogrusoz U, Dresdner G, Gross B, Sumer SO, et al. Integrative analysis of complex cancer genomics and clinical profiles using the cBioPortal. Sci Signal 2013;6(269):pl1.
19. Cerami E, Gao J, Dogrusoz U, Gross BE, Sumer SO, Aksoy BA, et al. The cBio cancer genomics portal: an open platform for exploring multidimensional cancer genomics data. Cancer Discov 2012;2(5):401-4.
20. Haggarty SJ, Koeller KM, Wong JC, Grozinger CM, Schreiber SL. Domain-selective small-molecule inhibitor of histone deacetylase 6 (HDAC6)-mediated tubulin deacetylation. Proc Natl Acad Sci U S A 2003;100(8):4389-94.
21. Klionsky DJ, Abeliovich H, Agostinis P, Agrawal DK, Aliev G, Askew DS, et al. Guidelines for the use and interpretation of assays for monitoring autophagy in higher eukaryotes. Autophagy 2008;4(2):151-75.
22. Schindelin J, Arganda-Carreras I, Frise E, Kaynig V, Longair M, Pietzsch T, et al. Fiji: an open-source platform for biological-image analysis. Nat Methods 2012;9(7):676-82.
23. Watson GW, Wickramasekara S, Palomera-Sanchez Z, Black C, Maier CS, Williams DE, et al. SUV39H1/H3K9me3 attenuates sulforaphane-induced apoptotic signaling in PC3 prostate cancer cells. Oncogenesis 2014;3:e131.
24. Boyault C, Sadoul K, Pabion M, Khochbin S. HDAC6, at the crossroads between cytoskeleton and cell signaling by acetylation and ubiquitination. Oncogene 2007;26(37):5468-76.
25. Valenzuela-Fernandez A, Cabrero JR, Serrador JM, Sanchez-Madrid F. HDAC6: a key regulator of cytoskeleton, cell migration and cell-cell interactions. Trends Cell Biol 2008;18(6):291-7.
26. Hubbert C, Guardiola A, Shao R, Kawaguchi Y, Ito A, Nixon A, et al. HDAC6 is a microtubule-associated deacetylase. Nature 2002;417(6887):455-8.

27. Zhang X, Yuan Z, Zhang Y, Yong S, Salas-Burgos A, Koomen J, et al. HDAC6 modulates cell motility by altering the acetylation level of cortactin. Mol Cell 2007;27(2):197-213.
28. Kovacs JJ, Murphy PJ, Gaillard S, Zhao X, Wu JT, Nicchitta CV, et al. HDAC6 regulates Hsp90 acetylation and chaperone-dependent activation of glucocorticoid receptor. Mol Cell 2005;18(5):601-7.
29. Randow F, Youle RJ. Self and nonself: how autophagy targets mitochondria and bacteria. Cell Host Microbe 2014;15(4):403-11.
30. Lee JY, Nagano Y, Taylor JP, Lim KL, Yao TP. Disease-causing mutations in parkin impair mitochondrial ubiquitination, aggregation, and HDAC6-dependent mitophagy. J Cell Biol 2010;189(4):671-9.
31. Kundu M, Lindsten T, Yang CY, Wu J, Zhao F, Zhang J, et al. Ulk1 plays a critical role in the autophagic clearance of mitochondria and ribosomes during reticulocyte maturation. Blood 2008;112(4):1493-502.
32. Pagliarini DJ, Calvo SE, Chang B, Sheth SA, Vafai SB, Ong SE, et al. A mitochondrial protein compendium elucidates complex I disease biology. Cell 2008;134(1):112-23.
33. Cuervo AM, Wong E. Chaperone-mediated autophagy: roles in disease and aging. Cell Res 2013;24(1):92-104.
34. Lv L, Li D, Zhao D, Lin R, Chu Y, Zhang H, et al. Acetylation targets the M2 isoform of pyruvate kinase for degradation through chaperone-mediated autophagy and promotes tumor growth. Mol Cell 2011;42(6):719-30.
35. Schneider JL, Suh Y, Cuervo AM. Deficient chaperone-mediated autophagy in liver leads to metabolic dysregulation. Cell Metab 2014;20(3):417-32.
36. Mizushima N, Yoshimori T, Levine B. Methods in mammalian autophagy research. Cell 2010;140(3):313-26.
37. Yan J, Seibenhener ML, Calderilla-Barbosa L, Diaz-Meco MT, Moscat J, Jiang J, et al. SQSTM1/p62 interacts with HDAC6 and regulates deacetylase activity. PLoS One 2013;8(9):e76016.
38. Hanahan D, Weinberg RA. Hallmarks of cancer: the next generation. Cell 2011;144(5):646-74.
39. Altomare DA, Testa JR. Perturbations of the AKT signaling pathway in human cancer. Oncogene 2005;24(50):7455-64.
40. Majumder PK, Sellers WR. Akt-regulated pathways in prostate cancer. Oncogene 2005;24(50):7465-74.
41. Jung CH, Ro SH, Cao J, Otto NM, Kim DH. mTOR regulation of autophagy. FEBS Lett 2010;584(7):1287-95.
42. Vlietstra RJ, van Alewijk DC, Hermans KG, van Steenbrugge GJ, Trapman J. Frequent inactivation of PTEN in prostate cancer cell lines and xenografts. Cancer Res 1998;58(13):2720-3.
43. Wu X, Senechal K, Neshat MS, Whang YE, Sawyers CL. The PTEN/MMAC1 tumor suppressor phosphatase functions as a negative regulator

of the phosphoinositide 3-kinase/Akt pathway. Proc Natl Acad Sci U S A 1998;95(26):15587-91.
44. Duran A, Amanchy R, Linares JF, Joshi J, Abu-Baker S, Porollo A, et al. p62 is a key regulator of nutrient sensing in the mTORC1 pathway. Mol Cell 2011;44(1):134-46.
45. Moscat J, Diaz-Meco MT. p62 at the crossroads of autophagy, apoptosis, and cancer. Cell 2009;137(6):1001-4.
46. Moscat J, Diaz-Meco MT. p62: a versatile multitasker takes on cancer. Trends Biochem Sci 2012;37(6):230-6.
47. Kirkin V, Lamark T, Sou YS, Bjorkoy G, Nunn JL, Bruun JA, et al. A role for NBR1 in autophagosomal degradation of ubiquitinated substrates. Mol Cell 2009;33(4):505-16.
48. Wong YC, Holzbaur EL. Optineurin is an autophagy receptor for damaged mitochondria in parkin-mediated mitophagy that is disrupted by an ALS-linked mutation. Proc Natl Acad Sci U S A 2014;111(42):E4439-48.
49. Pandey UB, Nie Z, Batlevi Y, McCray BA, Ritson GP, Nedelsky NB, et al. HDAC6 rescues neurodegeneration and provides an essential link between autophagy and the UPS. Nature 2007;447(7146):859-63.
50. Hao R, Nanduri P, Rao Y, Panichelli RS, Ito A, Yoshida M, et al. Proteasomes activate aggresome disassembly and clearance by producing unanchored ubiquitin chains. Mol Cell 2013;51(6):819-28.
51. Myeku N, Figueiredo-Pereira ME. Dynamics of the degradation of ubiquitinated proteins by proteasomes and autophagy: association with sequestosome 1/p62. J Biol Chem 2011;286(25):22426-40.
52. Reed NA, Cai D, Blasius TL, Jih GT, Meyhofer E, Gaertig J, et al. Microtubule acetylation promotes kinesin-1 binding and transport. Curr Biol 2006;16(21):2166-72.
53. Chen S, Owens GC, Makarenkova H, Edelman DB. HDAC6 regulates mitochondrial transport in hippocampal neurons. PLoS One 2010;5(5):e10848.
54. Gao YS, Hubbert CC, Yao TP. The microtubule-associated histone deacetylase 6 (HDAC6) regulates epidermal growth factor receptor (EGFR) endocytic trafficking and degradation. J Biol Chem 2010;285(15):11219-26.
55. Watanabe Y, Tanaka M. p62/SQSTM1 in autophagic clearance of a non-ubiquitylated substrate. J Cell Sci 2011;124(Pt 16):2692-701.
56. Kroemer G, Marino G, Levine B. Autophagy and the integrated stress response. Mol Cell 2010;40(2):280-93.

Chapter 5

1. Clarke JD, Hsu A, Yu Z, Dashwood RH, Ho E. Differential effects of sulforaphane on histone deacetylases, cell cycle arrest and apoptosis in normal prostate cells versus hyperplastic and cancerous prostate cells. Mol Nutr Food Res 2011;55(7):999-1009.

2. Beaver LM, Buchanan A, Sokolowski EI, Riscoe AN, Wong CP, Chang JH, et al. Transcriptome analysis reveals a dynamic and differential transcriptional response to sulforaphane in normal and prostate cancer cells and suggests a role for Sp1 in chemoprevention. Mol Nutr Food Res 2014;58(10):2001-13.
3. Chambers KF, Bacon JR, Kemsley EK, Mills RD, Ball RY, Mithen RF, et al. Gene expression profile of primary prostate epithelial and stromal cells in response to sulforaphane or iberin exposure. Prostate 2009;69(13):1411-21.
4. Varambally S, Yu J, Laxman B, Rhodes DR, Mehra R, Tomlins SA, et al. Integrative genomic and proteomic analysis of prostate cancer reveals signatures of metastatic progression. Cancer Cell 2005;8(5):393-406.
5. Gebauer F, Hentze MW. Molecular mechanisms of translational control. Nat Rev Mol Cell Biol 2004;5(10):827-35.
6. Ma XM, Blenis J. Molecular mechanisms of mTOR-mediated translational control. Nat Rev Mol Cell Biol 2009;10(5):307-18.
7. Wang X, Proud CG. The mTOR pathway in the control of protein synthesis. Physiology (Bethesda) 2006;21:362-9.
8. Wiczk A, Hofman D, Konopa G, Herman-Antosiewicz A. Sulforaphane, a cruciferous vegetable-derived isothiocyanate, inhibits protein synthesis in human prostate cancer cells. Biochim Biophys Acta 2012;1823(8):1295-305.
9. Agyeman AS, Chaerkady R, Shaw PG, Davidson NE, Visvanathan K, Pandey A, et al. Transcriptomic and proteomic profiling of KEAP1 disrupted and sulforaphane-treated human breast epithelial cells reveals common expression profiles. Breast Cancer Res Treat 2012;132(1):175-87.
10. Mastrangelo L, Cassidy A, Mulholland F, Wang W, Bao Y. Serotonin receptors, novel targets of sulforaphane identified by proteomic analysis in Caco-2 cells. Cancer Res 2008;68(13):5487-91.
11. Lee CH, Jeong SJ, Yun SM, Kim JH, Lee HJ, Ahn KS, et al. Down-regulation of phosphoglucomutase 3 mediates sulforaphane-induced cell death in LNCaP prostate cancer cells. Proteome Sci 2010;8:67.
12. Angeloni C, Turroni S, Bianchi L, Fabbri D, Motori E, Malaguti M, et al. Novel targets of sulforaphane in primary cardiomyocytes identified by proteomic analysis. PLoS One 2013;8(12):e83283.
13. Nakamura T, Kuromitsu J, Oda Y. Evaluation of comprehensive multidimensional separations using reversed-phase, reversed-phase liquid chromatography/mass spectrometry for shotgun proteomics. J Proteome Res 2008;7(3):1007-11.
14. Zhang X, Fang A, Riley CP, Wang M, Regnier FE, Buck C. Multi-dimensional liquid chromatography in proteomics--a review. Anal Chim Acta 2010;664(2):101-13.
15. Gilar M, Olivova P, Daly AE, Gebler JC. Two-dimensional separation of peptides using RP-RP-HPLC system with different pH in first and second separation dimensions. J Sep Sci 2005;28(14):1694-703.

16. Gilar M, Olivova P, Daly AE, Gebler JC. Orthogonality of separation in two-dimensional liquid chromatography. Anal Chem 2005;77(19):6426-34.
17. Manadas B, English JA, Wynne KJ, Cotter DR, Dunn MJ. Comparative analysis of OFFGel, strong cation exchange with pH gradient, and RP at high pH for first-dimensional separation of peptides from a membrane-enriched protein fraction. Proteomics 2009;9(22):5194-8.
18. Yang F, Shen Y, Camp DG, 2nd, Smith RD. High-pH reversed-phase chromatography with fraction concatenation for 2D proteomic analysis. Expert Rev Proteomics 2012;9(2):129-34.
19. Watson GW, Wickramasekara S, Palomera-Sanchez Z, Black C, Maier CS, Williams DE, et al. SUV39H1/H3K9me3 attenuates sulforaphane-induced apoptotic signaling in PC3 prostate cancer cells. Oncogenesis 2014;3:e131.
20. Juge N, Mithen RF, Traka M. Molecular basis for chemoprevention by sulforaphane: a comprehensive review. Cell Mol Life Sci 2007;64(9):1105-27.
21. Herman-Antosiewicz A, Xiao H, Lew KL, Singh SV. Induction of p21 protein protects against sulforaphane-induced mitotic arrest in LNCaP human prostate cancer cell line. Mol Cancer Ther 2007;6(5):1673-81.
22. Myzak MC, Hardin K, Wang R, Dashwood RH, Ho E. Sulforaphane inhibits histone deacetylase activity in BPH-1, LnCaP and PC-3 prostate epithelial cells. Carcinogenesis 2006;27(4):811-9.
23. Park WR, Nakamura Y. p53CSV, a novel p53-inducible gene involved in the p53-dependent cell-survival pathway. Cancer Res 2005;65(4):1197-206.
24. Sionov RV, Haupt Y. The cellular response to p53: the decision between life and death. Oncogene 1999;18(45):6145-57.
25. Hu R, Xu C, Shen G, Jain MR, Khor TO, Gopalkrishnan A, et al. Gene expression profiles induced by cancer chemopreventive isothiocyanate sulforaphane in the liver of C57BL/6J mice and C57BL/6J/Nrf2 (-/-) mice. Cancer Lett 2006;243(2):170-92.
26. Kwak MK, Cho JM, Huang B, Shin S, Kensler TW. Role of increased expression of the proteasome in the protective effects of sulforaphane against hydrogen peroxide-mediated cytotoxicity in murine neuroblastoma cells. Free Radic Biol Med 2007;43(5):809-17.
27. Gan N, Wu YC, Brunet M, Garrido C, Chung FL, Dai C, et al. Sulforaphane activates heat shock response and enhances proteasome activity through up-regulation of Hsp27. J Biol Chem 2010;285(46):35528-36.
28. Bhamre S, Sahoo D, Tibshirani R, Dill DL, Brooks JD. Temporal changes in gene expression induced by sulforaphane in human prostate cancer cells. Prostate 2009;69(2):181-90.
29. Thimmulappa RK, Mai KH, Srisuma S, Kensler TW, Yamamoto M, Biswal S. Identification of Nrf2-regulated genes induced by the chemopreventive agent sulforaphane by oligonucleotide microarray. Cancer Res 2002;62(18):5196-203.
30. Gillet LC, Navarro P, Tate S, Rost H, Selevsek N, Reiter L, et al. Targeted data extraction of the MS/MS spectra generated by data-independent acquisition:

a new concept for consistent and accurate proteome analysis. Mol Cell Proteomics 2012;11(6):O111 016717.
31. Andrysik Z, Kim J, Tan AC, Espinosa JM. A genetic screen identifies TCF3/E2A and TRIAP1 as pathway-specific regulators of the cellular response to p53 activation. Cell Rep 2013;3(5):1346-54.
32. Potting C, Tatsuta T, Konig T, Haag M, Wai T, Aaltonen MJ, et al. TRIAP1/PRELI complexes prevent apoptosis by mediating intramitochondrial transport of phosphatidic acid. Cell Metab 2013;18(2):287-95.